Doctoral theses at NTNU, 2013:145

Mari Kirkebøen Næss

Mechanisms and kinetics of liquid silicon oxidation

Doctoral Thesis

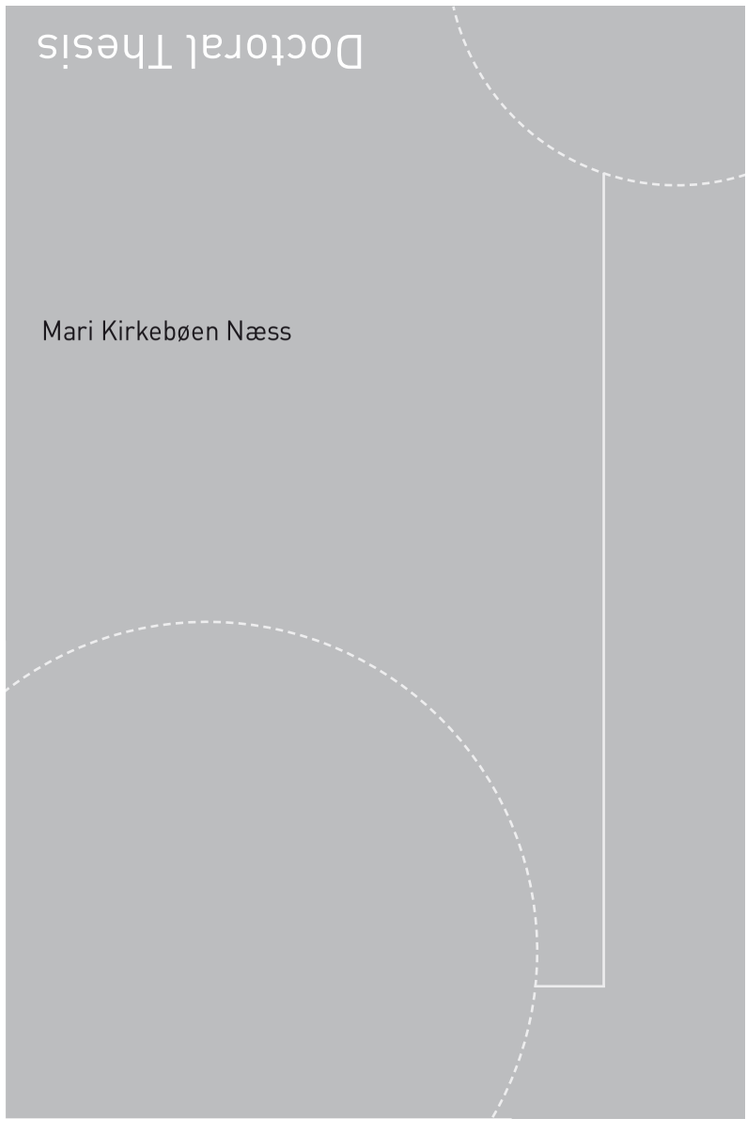

ISBN 978-82-471-4394-0 (printed version)
ISBN 978-82-471-4396-4 (electronic version)
ISSN 1503-8181

Doctoral theses at NTNU, 2013:145

NTNU – Trondheim
Norwegian University of
Science and Technology

NTNU

NTNU – Trondheim
Norwegian University of
Science and Technology

NTNU
Norwegian University of Science and Technology
Thesis for the degree of Philosophiae Doctor
Faculty of Natural Sciences and Technology
Department of Materials Science and Engineering

Mari Kirkebøen Næss

Mechanisms and kinetics of liquid silicon oxidation

Thesis for the degree of Philosophiae Doctor

Trondheim, June 2013

Norwegian University of Science and Technology
Faculty of Natural Sciences and Technology
Department of Materials Science and Engineering

NTNU – Trondheim
Norwegian University of
Science and Technology

NTNU
Norwegian University of Science and Technology

Thesis for the degree of Philosophiae Doctor

Faculty of Natural Sciences and Technology
Department of Materials Science and Engineering

ISBN 978-82-471-4394-0 (printed version)
ISBN 978-82-471-4396-4 (electronic version)
ISSN 1503-8181

IMT-Report 2013:176

Doctoral theses at NTNU, 2013:145

Printed by Skipnes Kommunikasjon as

Preface

The work presented in this thesis was carried out at the Department of Materials Science and Engineering at the Norwegian University of Science and Technology (NTNU). The project was funded by the Norwegian Research Council and FFF (Norwegian Ferroalloy Producers Research Association) through the FUME project (Fugitive emissions of Materials and Energy). A part of the experimental work was performed at the School of Materials Science and Engineering at The University of New South Wales in Sydney, Australia. The funding for the research exchange stay was provided by UNIFOR, the Elkem research fund and Norsk Hydro's research fund.

Acknowledgements

There are several people I would like to express my thanks and deep appreciation to. First of all is my supervisor, Gabriella Tranell. You have challenged me, and inspired me to do my best. There has literally been blood, sweat and tears along the way (for me), and you have always been there to cheer me up and give advice. Thank you for (nearly) four great years.

I would like to thank my co-supervisor, Merete Tangstad. Your commitment to the SiManTiAl-group is unique, and I have enjoyed many good discussions both with you and the group. Our trips to China, DisneyWorld and San Antonio have been great experiences. Thank you for taking me in and for being the glue in the group (even when you have not been present).

To each and every current and former member of the SiManTiAl-group: Thank you for giving me feedback on presentations, for engaging in discussions about results, and for discussing experimental challenges. Thank you for many, many great memories from trips, Gingerbread competitions, salary beers and other social events. It's been a blast :)

I have been to several measurement campaigns, and I have not been alone. There are some friendly and skilled people I would like to thank for good times and a lot of advice and help; Helge Midtdal, Svend Grådal, Nils Eivind Kamfjord, Lars Brøndbo, Håkon Skistad, Bendik Sægrov and Vegar Andersen.

Several of the industrial partners in FFF have engaged in discussions about my research. I am very thankful for all the help you have given me, and I would especially like to thank Halvard Tveit and Edin Myrhaug for good discussions.

I would like to thank Professor David Young from UNSW for everything that he taught me during the three months I stayed in Sydney. Thank you for taking me in and for giving me the opportunity to work with and learn from you. A big thanks also goes to Dr. Jianqiang Zhang, for all the help with the practical work, everything from cutting samples and ordering gas, to writing SJA's and our paper.

A big thank you to Jan Erik Olsen for a very fruitful cooperation, which I think we both have learned a lot from. I want to thank Kai Tang for always being enthusiastic and having time for my endless questions.

There are some colleagues, who I am also proud to call my friends; Maria, Ida, Marit and Delphine. Thank you for good conversations about everything between heaven and earth, and for great fun at trips and other occasions. Special thanks to Ida, for a very good cooperation. I hope we get the opportunity to work together in the future as well.

Of course, I want to thank my family for always being supportive and curious about my work. I want to thank all my friends for letting me be me and talk about everything other than work sometimes, and just have fun and drink beer. The names I want to mention are numerous, and the space is small, but you all know who you are!

Lastly I would like to thank Irvin, this would not have been possible without you.

Trondheim, April 2013

Mari K. Næss

Abstract

The formation of silica fume when liquid metal is in contact with air during refining of metallurgical grade silicon leads to a direct loss of silicon. Apart from this yield loss the associated fume may be harmful to the workers in the plant. During tapping, refining and casting of silicon, the fume formation makes up 40 – 80 % of the fugitive emissions from the plant. In this work, the kinetics and mechanisms of fume formation during refining of metallurgical grade silicon were studied.

Active oxidation is defined as the partial oxidation of Si to the gaseous product SiO. This type of oxidation does not protect the surface from further attack (passivation).When reviewing relevant literature, the majority of the research on active oxidation of silicon is done on solid silicon Research to date on liquid silicon oxidation on the other hand is primarily theoretical. As such, there is a knowledge gap concerning a mechanistic understanding of the active oxidation of liquid silicon. Boundary conditions, rate-controlling factors and flux dependencies on oxygen partial pressure and gas flow rate have not been systematically studied experimentally for active oxidation of liquid silicon. The amount of fume on an industrial scale and the characteristics of the fume such as elemental content, particle size and shape have not been adequately explored.

In this project, the active oxidation of liquid silicon was investigated at three different scales; industrial measurements (~7 tonne Si); small-scale experiments 10 g Si); and medium-scale induction furnace experiments (1750 g Si). An experimental element distribution analysis of both main and trace-elements in the industrial refining ladle was performed. It was found that the amount of fume formed during industrial refining is in the range 0.7 – 1.8 kg of SiO_2 per tonne silicon produced. The main mechanism of SiO_2-fume formation is oxidation of the surface, so that the exposed surface area is a main parameter controlling the fume formation in the industry. The boundary conditions for the oxidation of a still Si surface were determined from the small-scale experiments. The measurements confirmed an approximated theoretical mass transfer rate of oxygen and a maximum bulk oxygen pressure for active oxidation. From the induction furnace

experiments it was found that the primary factor determining the rate of fume formation is the rate of transport of oxygen to the surface, which in turn is given by the velocity of the gas above the surface.

This work is the first qualitative and quantitative study containing experimental investigations from small-scale to industrial scale on the kinetic and mechanistic nature of silicon oxidation. The industrial work has also contributes to a better understanding of distribution of elements in the silicon refining process, and it gives implications for emission estimation of toxic and other trace elements to the environment.

List of papers

Paper 1

Næss, M.K., Tranell, G., and Kamfjord, N.E., *Fugitive emissions related to oxidation of liquid silicon during ladle refining,* 2nd International Symposium on High-Temperature Metallurgical Processing, *TMS* Annual Meeting & Exhibition February 27 - March 3, 2011. DOI: 10.10029781118062081.ch11

Statement of contribution

Næss: Experimental work, data analysis, discussion of results, writing the paper.
Tranell: Discussion of results, writing the paper.
Kamfjord: Data analysis, discussion of results.

Paper 2

Næss, M.K., Tranell, G., Olsen, J.E., Kamfjord, N.E., and Tang, K. (2012) *Mechanisms and Kinetics of Liquid Silicon Oxidation During Industrial Refining*, Oxidation of Metals, Vol. 78, pp. 239-251. DOI: 10.1007/s11085-012-9303-9

Statement of contribution

Næss: Experimental work, data analysis, discussion of results, writing the paper.
Tranell: Discussion of results, writing the paper.
Olsen: CFD modeling, writing the paper.
Kamfjord: Data analysis, discussion of results.
Tang: Discussion of results.

Paper 3

Næss, M.K., Young, D.J., Zhang, J., Olsen, J.E., and Tranell, G., (2012) *Active Oxidation of Liquid Silicon: Experimental Investigation of Kinetics*, Oxidation of Metals, Vol. 78, pp. 363-376. DOI: 10.1007/s11085-012-9312-8

Statement of contribution

Næss: Experimental work, data analysis, discussion of results, writing the paper.
Young: Data analysis, discussion of results, writing the paper.
Zhang: Experimental work, discussion of results, writing the paper.
Olsen: CFD modeling.
Tranell: Discussion of results, writing the paper.

Paper 4

Næss, M.K., Smith, N., Tranell, G., and Olsen, J.E. (2013) *Experimental study of rate of silica formation from active oxidation of liquid silicon*, Infacon XIII, Almaty, Kazakhstan, 8.-13. June 2013. Accepted for publication.

Statement of contribution

Næss: Experimental work, data analysis, discussion of results, writing the paper.
Smith: Experimental work.
Tranell: Data analysis, discussion of results, writing the paper.
Olsen: CFD modeling, discussion of results.

Paper 5

Næss, M.K., Kero, I. and Tranell, G. (2013), *A new method for estimation of emissions and sources of measurements error in the silicon refining process*. Accepted for publication in The Member Journal of the Minerals, Metals and Materials Society (JOM), DOI: 10.1007/s11837-013-0661-9

Statement of contribution

Næss: Experimental work, data analysis, discussion of results, writing the paper.
Kero: Data analysis, discussion of results, writing the paper.
Tranell: Discussion of results, writing the paper.

Paper 6

Næss, M.K., Kero, I., Tranell, G., Tang, K., and Tveit, H. (2013), *Element distribution in silicon refining – Thermodynamic model and industrial measurements*, Submitted.

Statement of contribution

Næss: Experimental work, data analysis, discussion of results, writing the paper.
Kero: Data analysis, discussion of results, writing the paper.
Tranell: Discussion of results, writing the paper.
Tang: Thermochemical modeling, writing the paper.
Tveit: Discussion of results.

Co-authored papers

Olsen, J.E., Næss, M. and Tranell, G., *CFD modeling of silica fume formation during refining of silicon metal*, Proceedings of the 8th International Conference on CFD in Oil & Gas, Metallurgical and Process Industries, Trondheim, 2011

Kamfjord, N.E., Tveit, H., Næss, M.K., and Myrhaug, E.H., *Mechanisms of NO formation during SiO combustion*, 3rd International Symposium on High-Temperature Metallurgical Processing, *TMS* Annual Meeting & Exhibition March 3-7, 2012. DOI: 10.1002/9781118364987.ch49

Olsen, J.E., Næss, M. & Tranell, G., *Understanding fuming during metal refining by CFD,* CFD Modeling and Simulation in Materials Processing, *TMS* Annual Meeting & Exhibition March 3-7, 2012. DOI: 10.1002/9781118364697.ch4

Kero., I., Næss, M.K., Tranell, G., (2013) *Fume characterization in the ferroalloy industry*, Infacon XIII, Almaty, Kazakhstan, 8.-13. June 2013. (Accepted for publication).

Contents

List of abbreviations and symbols

Abbreviations

BET – Brunauer, Emmett and Teller. Method for measuring specific surface area
bp – boiling point, (°C)
CFD – Computational Fluid Dynamics
EPMA – Element Probe Micro Analyzer
HR-ICP-MS – High Resolution Inductively Coupled Mass Spectroscopy
OLR – Oxidative Ladle Refining
ppm – Parts per million
Re – Reynolds number
Sc – Schmidt number
SEM – Scanning Electron Microscopy
Sh – Sherwood number
TEM – Transmission Electron Microscopy
TGA – Thermo Gravimetric Analysis
XRD – X-ray Diffraction

Latin letters

A - Area, (m^2)
c - Diameter of spherical segment,(m), or sticking coefficient
C_0 - Concentration of molecules, (m^{-3})
d - Diameter, (m)
D - Diffusion coefficient, (m^2/s)
G - Gibb's free energy, (kJ)
h - Height of spherical segment, (m)
J - Flux, ($moles/m^2 \cdot s$)
k - Mass transfer coefficient, (m/s)
k_B - Boltzmann constant, (J/K, erg/K)
l – Characteristic length, (m)
m - Mass, (g)
M - Molar mass, (g/mol)
N - Number of moles, or concentration of particles, (m^{-3})
n - Number of atoms of metal per molecule of oxide
N_A - Avogadro's number, $6.022 \cdot 10^{23}$ mol^{-1}
p_i - Partial pressure of species i, (atm)
r - Radius, (m)

R - Universal gas constant, value depends on units used
SA - Specific surface area, (m^2/g)
T - Temperature, Kelvins (K)
t - Time, (s)
V - Volume, (L or m^3)
v_g - Linear gas velocity, (m/s)
x_i - Molar fraction of species i

Greek letters

α - Stoichiometric number
γ – Activity coefficient
Δ - Difference, or boundary layer thickness, (m)
δ - Boundary layer thickness, (m)
ε - Characteristic energy of interaction
ζ - Relative distance from Si surface
λ - Mean free path, (m)
μ - Viscosity, (kg/m·s)
ν - Kinematic viscosity, (m^2/s)
π - The number pi
ϱ - Density, (kg/m^3)
σ – Surface tension (mN/m), or collision diameter (Å)
Σ – Sum
Φ - Dimensionless quantity used in calculation of mixed viscosity
Ω - Collision integral

Superscripts

* at the surface
° in the bulk

Subscripts

(s) Solid state
(l) Liquid state
(g) Gaseous state

1 Introduction

In the ferroalloy industry, fugitive emissions have become an increasing concern over the past few years[1]. Fugitive emissions are both a threat to health and environment, and represent loss of valuable resources. In 2006, after 94 days with outdoor air dust levels exceeding the daily mean limit (50 $\mu g/m^3$ for PM_{10}) in Mo i Rana in Norway, the Climate and Pollution Agency (KLIF) initiated a large investigation aiming at monitoring of dust concentration, characterization of the dust and a mapping of their origin[1]. Several of the ferroalloy plants in the industry park in Mo i Rana were forced to periodically shut down parts of the production in order to reduce emissions[1]. Following this incident, the governmental restrictions on emission limits for selected elements and compounds that the plants release have become stricter, and thus the industry needs to present solutions to reduce their emissions. The Norwegian Research Council funded "FUME" project (Fugitive Emissions of Materials and Energy) is one of the projects addressing this issue. This project is a collaboration between the Norwegian Ferroalloy Producers Research Association (FFF), NTNU and SINTEF, where the overall aim is to reduce the fugitive emissions in the ferroalloy industry. The FUME-project is divided into three sub-projects; Emissions of Materials, Emissions of Energy and Measurements and Tools. The present work has been a part of the first sub-project, where both gases and fumes are considered material emissions. The last FUME-subproject has focused on developing simple measurement techniques and tools which make online monitoring possible. This is important to implement at the plants as a path to documentation and reporting of all their emissions.

Regarding human exposure of dust, three size-dependent fractions are defined: Inhalable (aerodynamic diameter, $d_{ae} < 100$ μm), thoracic ($d_{ae} < 10$ μm) and respirable ($d_{ae} < 4$ μm) dust. The inhalable fraction is all particles that may enter the body through the mouth and nose during breathing. Most of it will deposit high up in the respiratory system and is not harmful. The thoracic fraction is a fraction of the inhalable dust that may go past the larynx, and the respirable fraction may penetrate all the way into the unciliated airways (the alveolar region) where the gas exchange takes place[2], see Figure 1-1**.** Research has shown association between the indoor working environment in the Norwegian ferroalloy industry and lung conditions such as decreased lung function, chronic cough and chronic obstructive pulmonary disease (COPD)[2].

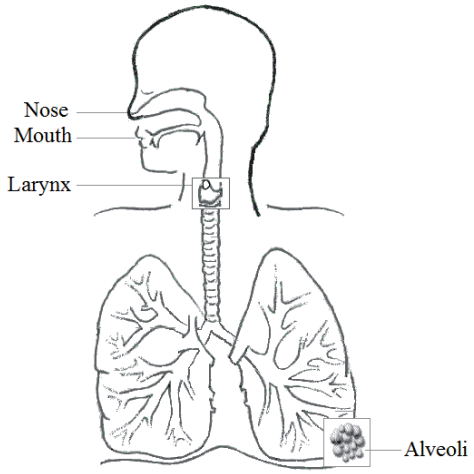

Figure 1-1: Schematic of the human respiratory system. Modified from [3].

Silicon is produced in an electric arc furnace, where quarts and carbon materials are the raw materials. Inside the furnace is a crater where SiO and CO

gas are produced and rise up through the charge. The SiO and CO will burn at the charge top and produce silica (SiO_2) and CO_2. The silica produced at the furnace top is captured in filters and sold as a by-product[4]. A schematic of the process is shown in Figure 1-2.

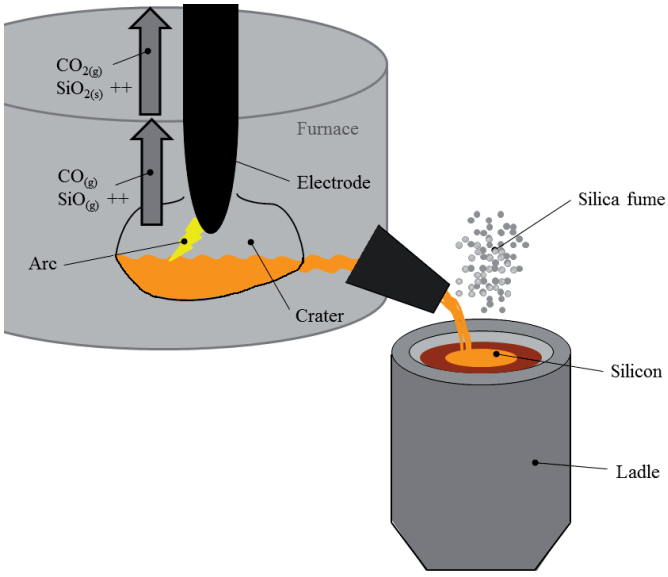

Figure 1-2: Simple, non-proportional schematic of the furnace with crater, furnace gases, electrode, arc, silica fume, silicon and ladle.

The produced silicon is continuously tapped from a hole in the lower part of the furnace into ladles. In the ladle the silicon is typically refined continuously during the tapping process, and when the ladle is full the metal is ready for casting. The refining is a process where oxygen-rich air is bubbled through the melt in order to remove the main impurities; aluminum and calcium. During the tapping and refining, a fume hood over the ladle captures the fumes produced.

Conversely, when the ladle is moved from the tapping area and into the plant hall for casting, there is no capture and the fume produced is emitted to the indoor environment. This is a direct loss of silicon, which has economic consequences, and it is a potential health risk for the workers at the plant.

An overview of the fugitive emissions of fume in the silicon production is given in Table 1-1.

Table 1-1: Overview of sources of fugitive emissions of dust and fume from a silicon plant, estimations of % of total emission from each source and a description of the emissions. From Kamfjord[5] (2012).

Work process	**Share of diffuse emissions**	**Share of internal pollution**	**Description of emission**
Raw material handling from key to storage	0 – 5 %	0 %	Fume generated by transportation, conveyer belts etc.
Raw material transport from storage to furnace	0 – 5 %	5 -10 %	Fume generated by raw material mixing and internal transportation to furnace
Furnace processes	10 – 20 %	5 – 20 %	Smoke and fume escaping the off-gas system and spreading inside the plant
Tapping	20 – 40 %	30 – 50 %	Smoke and fume from tapping process
Casting	20 – 40 %	15 – 25 %	Smoke and fume from liquid metal handling
Crushing screening and packing	5 – 15 %	5 – 15 %	Metal fume from operations
Off-gas system	5 – 10 %	0 – 5 %	Fume and smoke escaping channels, fans, etc.
Product packing of collected fume from off-gas	0 – 5 %	5 - 10 %	Fume into work environment from operations.

The largest sources of total emissions and emissions to the indoor environment are the tapping and casting processes, where liquid metal is in contact with air. The percentages in Table 1-1 are crude estimates, and the amounts of fugitive emissions in kg/year are not known. As such, there is a need for quantification and characterization of the fume in the ferroalloy industry.

There is a lack of knowledge about the fundamental mechanisms and kinetics of the fume formation and an increased understanding is needed. The refining process has not been experimentally characterized in terms of trace-element mass balances and element distributions. When studying fume, it is important not only to know the amount and characteristics of the fume, but also its contents. The fume may contain harmful trace-elements, and a source-to-sink investigation with a broad spectrum of elements is needed. This project has focused on the fugitive emissions from the silicon ladle refining step.

The principal aims of this work were to characterize the fume produced in the tapping and refining of silicon and to obtain a fundamental understanding of the mechanisms and kinetics governing the rate of fume formation. Qualitative and quantitative investigations were conducted in order to obtain a complete understanding from industrial scale through small-scale. In addition, a complete element distribution in the industrial refining ladle, including main and trace-elements, was performed.

This project has resulted in six papers which are enclosed in the back of this thesis. The relevant literature for the work is presented in Chapter 2, and the methods are presented and discussed in Chapter 3. Finally the results are summed up and discussed in Chapter 4. Overall conclusions and suggested future work is presented in Chapter 5.

2 Literature review

The fugitive emissions of silica in the silicon and ferrosilicon industry results in a possibly harmful indoor environment for the workers at the plants[2]. The increasingly strict governmental constraints on the working environment have led to enhanced attention to quantifying and characterization of the fumes the workers are exposed to. However, there is a knowledge gap in terms of the fundamental mechanism of fume formation, and lack of information on the physical and chemical properties of the fume. The objective of this project has been to do qualitative and quantitative investigations of the fume formation, as fundamental knowledge about the mechanisms behind the problem is imperative in order to further evaluate possible solutions.

In this chapter, a general introduction to silicon oxidation is presented, and the published knowledge relevant to this project is presented and discussed. Existing models for the oxidation mechanism of silicon will be presented. The nucleation and growth of the silica particles will be briefly discussed, as the size and shape of the particles is highly important in the discussion of how harmful the fume is. The effect of impurities in the silicon is discussed, and also literature on the mass balance of impurity elements in the silicon production is included. This last subject is important in terms of establishing the fume composition, in addition to silica, in the evaluation the toxicity of the fume to the environment and the human body.

2.1 Oxidation of silicon

Silicon is the second most abundant element in the earth's crust and it is usually found in combination with oxygen as silicates and quartz in nature, in which silicon is in the oxidation state 4+. The production of silicon metal on industrial scale began in the end of the 19th century, and in the 1950's very pure silicon was used to make silicon chips, which started a new era of computer technology[4]. Solid silicon is a semiconductor, not a metal, however many refer to solid silicon as silicon metal due to the metallic appearance and the metallic properties of liquid silicon.

As silicon is most stable in oxidized form in ambient pressure and oxidizing atmosphere, it will easily react with oxygen to form different oxides when in contact with air. At high temperatures these reactions will happen readily[6]. In the silicon production, the molten silicon comes in contact with air during tapping, refining and casting. When liquid silicon is oxidized in these situations, silica fume is formed. An example of the working conditions in the tapping area is shown in Figure 2-1. At the tapping and refining stations, off-gas channels are usually installed to capture the fume, however their efficiency is often not sufficient, and fugitive emissions of silica will spread in the plant.

Figure 2-1: A picture of the tapping area at a silicon production plant shows that the capture of fume formed during tapping is not efficient. Photo: Mari Kirkebøen Næss.

Some oxidation reactions where silicon is oxidized from liquid state are presented in Table 2.1, with their respective thermodynamic driving force. Silicon can either be oxidized directly to become $SiO_{2(l/s)}$, or it may be partially oxidized to become SiO gas. When the partial oxidation occurs, the reaction product, SiO, may escape from the silicon surface, and be further oxidized in the combustion reaction in Eq. 2.6.

In all reactions presented in Table 2-1 where SiO_2 is the product, the gaseous form is used, and the condensation reaction is presented in Eq. 2.10, to show that the condensation of $SiO_{2(g)}$ to $SiO_{2(l)}$ is a highly exothermic reaction itself. It has been

shown that the oxidation and especially the condensation of SiO_2 results in such high local temperatures, that large amounts of thermal NO_x gas is produced[7].

Table 2-1: Reaction equations for different types and stages of oxidation of silicon with thermodynamic driving force for each equation given. The Gibbs free energy of reaction (ΔG) is calculated at 1500°C using the software HSC Chemistry[8].

Description	**Reaction**	**Eq. #**	**ΔG at 1500°C [kJ]**
Direct oxidation of silicon to form silica	$Si_{(l)} + O_{2(g)} \rightarrow SiO_{2(g)}$	(2.1)	-594
Stoichiometric partial oxidation of silicon to form SiO gas	$Si_{(l)} + \frac{1}{2} O_{2(g)} \rightarrow SiO_{(g)}$	(2.2)	-248
Partial oxidation of silicon forming SiO and a radical	$Si_{(l)} + O_{2(g)} \rightarrow SiO_{(g)} + O^*_{(g)}$	(2.3)	-112
Partial oxidation of silicon from a radical, forming SiO	$Si_{(l)} + O^*_{(g)} \rightarrow SiO_{(g)}$	(2.4)	-385
Partial oxidation of silicon with water	$Si_{(l)} + H_2O_{(g)} \rightarrow SiO_{(g)} + H_{2(g)}$	(2.5)	-99
Combustion of SiO gas to form silica gas	$SiO_{(g)} + \frac{1}{2} O_{2(g)} \rightarrow SiO_{2(g)}$	(2.6)	-73
Combustion of SiO gas to form silica gas and a radical	$SiO_{(g)} + O_{2(g)} \rightarrow SiO_{2(g)} + O^*_{(g)}$	(2.7)	64
Combustion of SiO gas from a radical to form silica gas	$SiO_{(g)} + O^*_{(g)} \rightarrow SiO_{2(g)}$	(2.8)	-210
Condensation of SiO to form silicon and silica	$2SiO_{(g)} \rightarrow Si_{(l)} + SiO_{2(s)}$	(2.9)	-99
Condensation of silica from gas to liquid phase	$SiO_{2(g)} \rightarrow SiO_{2(l)}$	(2.10)	-273

2.1.1 Thermodynamic and kinetic calculation of boundary conditions

A simple schematic of the active oxidation of liquid silicon is shown in Figure 2-2. Diffusion of gaseous species both inward towards the surface and outward to the bulk gas are expected. Oxygen from the bulk, with partial pressure $p^{\circ}_{O_2}$, diffuses

through a boundary layer of thickness δ, and meets the liquid silicon surface with a partial pressure $p^*_{O_2}$. This value is very low as a result of the rapid consumption of oxygen via the reaction in Eq. 2.2 (Table 2.1). The resulting $SiO_{(g)}$, with surface partial pressure p^*_{SiO}, diffuses out of the boundary layer. Its bulk partial pressure is $p^\circ_{SiO} \approx 0$, due to the instability of $SiO_{(g)}$ and its prompt oxidation presented in Eq. 2.6 (Table 2-1).

These processes generate the concentration gradients of gaseous species within the boundary layer shown schematically in Figure 2-2. The diffusion of $SiO_{(g)}$ out to the bulk will be a counter flux to the oxygen coming in, and the production of $SiO_{(g)}$ is controlled by the rate of the oxygen flux. In this discussion, it is assumed that $SiO_{(g)}$ oxidizes to SiO_2 outside the boundary layer.

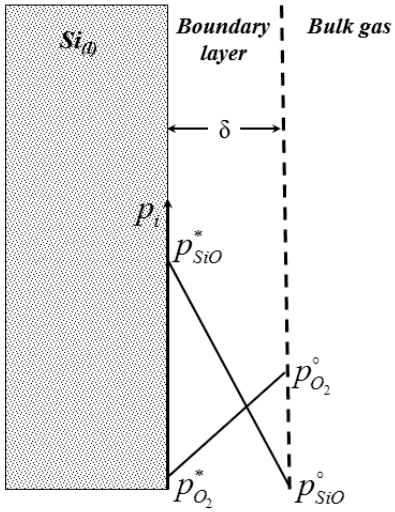

Figure 2-2: Schematic of active oxidation in the Si-O system, where oxygen diffuses in to the surface and reacts with liquid silicon to form $SiO_{(g)}$, which diffuses out through the boundary layer of thickness δ.

Thermodynamic equilibrium calculations using HSC Chemistry[8] were used to establish the partial pressure of Si-bearing species at 1500°C. The results are shown in Figure 2-3, which illustrates the principal features of the Si-O system. The partial pressure of SiO is controlled by the equilibrium of Equation 2.2 (Table 2.1) at oxygen activities too low for solid silica formation.

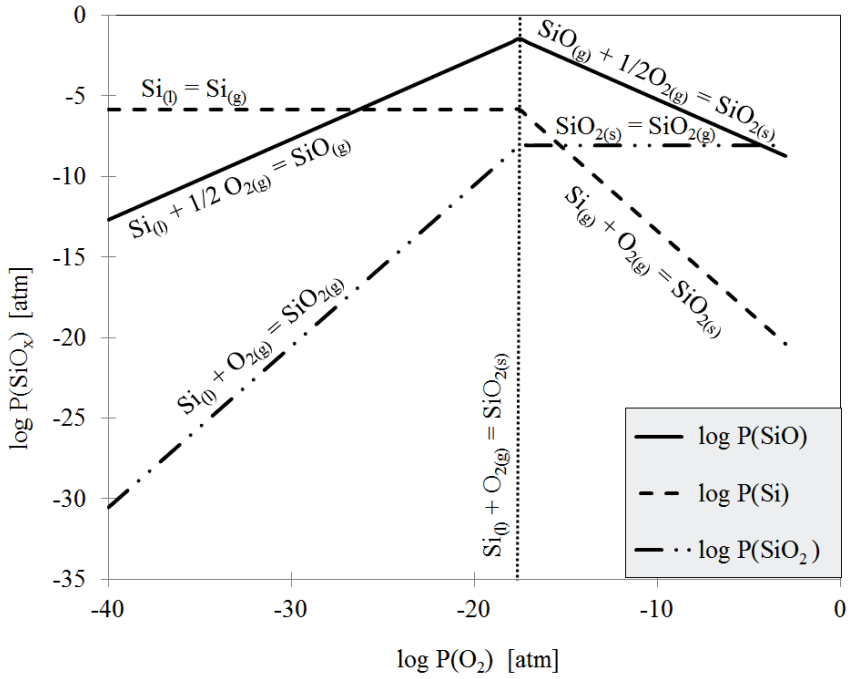

Figure 2-3: Thermodynamically calculated partial pressures of $Si_{(g)}$, $SiO_{(g)}$ and $SiO_{2(g)}$ as a function of $P(O_2)$ at 1500°C.

The variation of p^*_{SiO} with $p^*_{O_2}$ is represented by the solid line in Figure 2-3, and reaches a maximum at a surface oxygen pressure of $p^*_{O_2}$ (max) = $2.86 \cdot 10^{-18}$ atm, where SiO_2 becomes stable. At higher $p^*_{O_2}$ values, the equilibrium in Equation (2.1) leads to formation of a stable SiO_2 phase, and passivation of the silicon surface.

The maximum oxygen partial pressure in the bulk gas permitting active oxidation, $p^{\circ}_{O_2}$ (max), may now be calculated.

Boundary value gas partial pressures are related to the rate of mass transport across the hydrodynamic boundary layer. Assuming that the melt surface is clean, and $Si_{(l)}$ freely available, then if chemical reaction at the liquid-gas interface is fast enough to establish local equilibrium, the molar flux of $SiO_{(g)}$, J_{SiO}, from the silicon surface can be calculated with:

$$-2J_{O_2} = -2\frac{k_{O_2}}{RT}p^{\circ}_{O_2} = J_{SiO} = \frac{k_{SiO}}{RT}\cdot p^{*}_{SiO} \tag{2.11}$$

Here k_{SiO} is the mass transfer coefficient for $SiO_{(g)}$ [m/s], R is the gas constant (here: $8.21\cdot10^{-5}$ $m^3atm/K\cdot mole$), T is the absolute temperature [K] and the stoichiometric balance between SiO and O_2 fluxes is recognized.

The mass transfer coefficient, k, is calculated from the relationship[9, 10]

$$k = 0.664\left(\frac{D^4}{\upsilon}\right)^{\frac{1}{4}}\left(\frac{v_g}{l}\right)^{\frac{1}{2}} \tag{2.12}$$

where D is the diffusion coefficient, l is the characteristic length of the surface in the direction of the gas flow, υ is the kinematic viscosity (ratio of viscosity and density, μ/ρ), and v_g is the uniform linear velocity of gas in vicinity of the metal surface. A condition[11] for the applicability for Eq. 2.12 can be expressed in terms of the Schmidt number, Sc,

$$Sc = \frac{\mu}{\rho D}, \qquad 0.6 < Sc < 50 \tag{2.13}$$

The diffusion coefficient and viscosity of the gases are calculated in Chapter 3, according to the Chapman-Enskog method as described by Bird et al.[12] (2002).

For T = 1500°C and $p^*_{O_2}$ = 1·10^{-18} atm (just below the maximum $p^*_{O_2}$), p^*_{SiO} is calculated to be 2.1·10^{-2} atm. This value allows calculation of the outward SiO flux from Eq. 2.11, as 1.47·10^{-3} moles m^{-2} s^{-1} at a linear gas velocity of 0.047 m s^{-1}. The stoichiometric equivalent inward flux of oxygen of 7.34·10^{-4} moles m^{-2} s^{-1} then leads via Eq. 2.11 to an estimated maximum $p^\circ_{O_2}$(max) of 8.6·10^{-3} atm. Higher values of $p^\circ_{O_2}$ are expected to produce faster rates of inward mass transfer and silicon passivation. Lower values of $p^\circ_{O_2}$ would reduce the rate of SiO$_{(g)}$ volatilization. This estimate of the maximum $p^\circ_{O_2}$ is independent of v_g, because both k_{SiO} and k_{O_2} depend in the same way on gas flow rate, and the effects cancel out.

2.1.2 Oxidation models

In 1958, Wagner[6] presented a theoretical derivation on the oxidation mechanism and boundary conditions for the Si-O system, based on the experimental findings of Kaiser and Breslin[13] (1958). He introduced the terms *active* and *passive* oxidation. Passive oxidation is the oxidation mechanism resulting in a protective oxide layer at the surface of the silicon. The stoichiometric reaction is presented in Eq. 2.1. This reaction may also be referred to as passivation of the surface. The silica layer at the surface is protective in the way that it inhibits the transport of oxygen to the silicon surface, and thus stops any further oxidation.

Active oxidation is the oxidation mechanism where the silicon surface is only partially oxidized, resulting in the formation of gaseous SiO which escapes the surface (Eq 2.2). The silicon surface will remain bare and thus the reaction can go on and on, as there is no oxide layer stopping the transport of oxygen to the Si surface.

At low oxygen partial pressures above the silicon surface, the gaseous oxide species SiO will form and a partial pressure p_{SiO} is obtained. If the p^*_{SiO} at the surface is lower than the equilibrium partial pressure, $p_{SiO(eq)}$, from the reaction in Eq. 2.9[6] the surface of the silicon will remain bare. In this state of active oxidation the rate of attack is increasing with increasing oxygen partial pressure. When the partial pressure of SiO reaches $p_{SiO(eq)}$, SiO_2 becomes the stable phase and a layer of oxide may be formed at the surface.

Wagner makes an important assumption prior to the derivation of the equations for the rate of oxidation; the reaction between Si and O_2 has a low activation energy, thus the reaction is fast and the partial pressure of oxygen at the Si surface, $p^*_{O_2}$ is low, - much lower than the bulk partial pressure, $p^\circ_{O_2}$. This assumption simplifies Fick's law, the diffusion equation for the consumption of silicon in moles per unit area per unit time, J_{Si}, during active oxidation to [6]

$$J_{Si} = \frac{2 p^\circ_{O_2} D_{O_2}}{\delta_{O_2} RT} \tag{2.14}$$

where D_{O_2} is the diffusion coefficient of oxygen through the boundary layer with thickness δ_{O_2}, R is the gas constant and T is the absolute temperature. The rate of

oxidation is determined by the supply of oxygen for the formation of SiO, and when $p^{\circ}_{O_2}$ become larger than $p^{\circ}_{O_2}(\max)$, passivation occurs according to Eq. 2.1. Based on the data by Kaiser and Breslin, Wagner calculated the maximum bulk partial pressure of oxygen at 1410°C to be $6.1 \cdot 10^{-3}$ atm*. In Figure 2-4, Wagner's derived partial pressure of SiO as a function of $p^{\circ}_{O_2}$ is shown. The partial pressure of SiO at the surface increases linearly with $p^{\circ}_{O_2}$, and is equal to the equilibrium partial pressure when the oxygen pressure reaches maximum. Now, the SiO pressure drops to a value eight orders of magnitude lower.

In Figure 2-4 there is a clear hysteresis between the point where the SiO_2 layer becomes stable ($6.1 \cdot 10^{-3}$ atm) and the point where the SiO_2 becomes unstable when lowering the oxygen partial pressure ($3 \cdot 10^{-8}$ atm). Thus, it takes a very low oxygen partial pressure to remove an already existing SiO_2 layer from the silicon surface. This hysteresis effect has been confirmed by several authors in later works[14-16]. Wagner does not discuss SiO reacting further with oxygen or the formation of silica fume. However, the theory is important in that it includes the formation of SiO.

* Wagner's work was published in 1958, and was indeed a theoretical work on oxidation of *liquid* silicon, even though the melting point according to today's version of Handbook of Chemistry and Physics is 1414°C[20]. It may be assumed that the techniques for measuring high temperatures may not have been as precise in 1958 as they are today, thus the melting point of silicon was erroneous by 4°C.

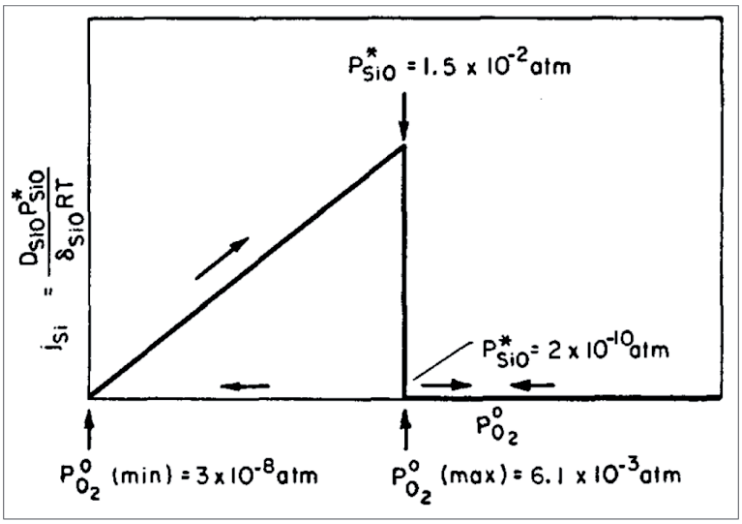

Figure 2-4: Rate of attack of silicon, J_{Si}, as a function of oxygen partial pressure. Constant total pressure of different He-O_2-mixtures, at 1410 °C. From Wagner (1958)[6].

Turkdogan et al.[10] (1963) had a somewhat different approach to the oxidation of liquid metals. They studied the effect of reactive atmospheres on vaporization of metals. The theory was stated to be general for all metals and included the vaporization of the liquid metal and a counter diffusion of oxygen in a gaseous boundary layer. As the two gases meet at a short distance, δ, from the metal surface, a "fog" (condensed fume/aerosol) of oxide is formed and provides a sink for the metal vapor and oxygen. This reaction results in the enhanced counter flux of the gaseous species due to the enhanced driving force for diffusion in terms of a greater concentration gradient. A sketch of the mechanism can be seen in Figure 2-5, with a concentration profile for the metal vapor and the oxygen in Figure 2-6. The oxygen partial pressure affects the vaporization rate of the metal, and in the case of iron the derived equations for the fluxes (moles/cm^{2}s) are [10]

$$J_{Fe} = -2J_{O_2} = \frac{2D_{O_2} p_{O_2}^{\circ}}{\Delta RT} = \frac{2kp_{O_2}^{\circ}}{RT} \qquad (2.15)$$

where J_{Fe} and J_{O_2} are the fluxes of iron vapor and oxygen, respectively, $k = D_0/\Delta$ is the average film mass transfer coefficient for the transport of oxygen through the boundary layer of thickness Δ, $p_{O_2}^{\circ}$ and D_{O_2} are the same as previously stated. Equation 2.15 shows a linear relationship between the flux of iron (vaporization) and the oxygen partial pressure [10].

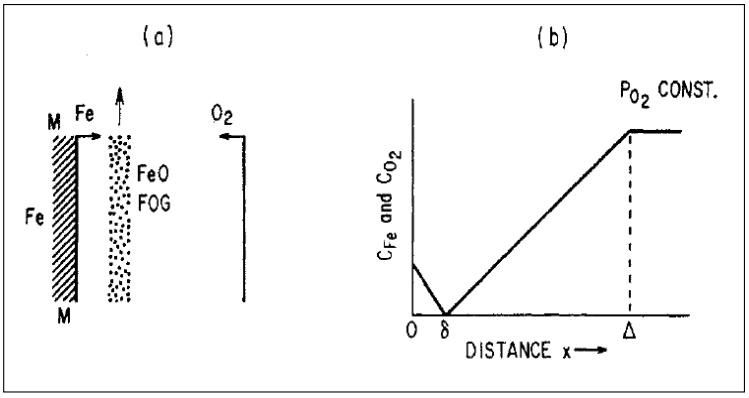

Figure 2-5: (a) Sketch of how the metal vapor and the oxygen forms an oxide "fog" at a distance δ from the metal surface, and (b) the concentration profile for the iron vapor and the oxygen partial pressure in the boundary layer (at steady state and isothermal conditions). From Turkdogan et al. (1963) [10].

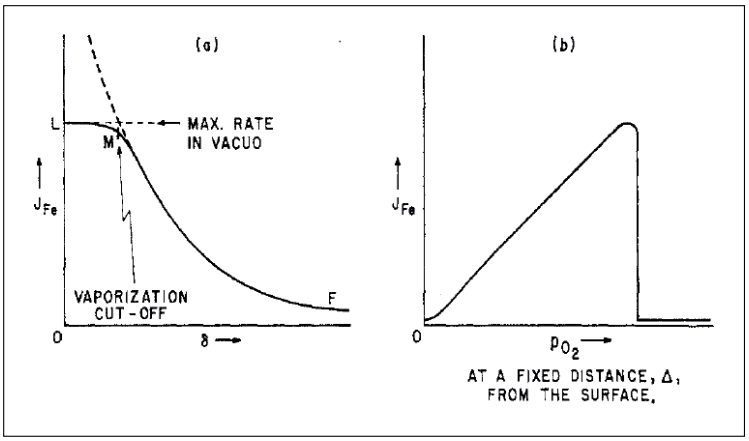

Figure 2-6**:** (a) Flux of iron vapor as a function of the distance δ at which the condensed oxide is formed, and (b) the flux of iron vapor as a function of the oxygen partial pressure in the bulk. From Turkdogan et al. (1963) [10].

In the Turkdogan theory, passivation of the metal surface is explained in a different manner than in the Wagner theory: If the oxygen partial pressure increases, the distance at which the oxide condensate is formed, δ, will decrease (Figure 2-5), and the vaporization is increased. However, the vaporization rate cannot exceed the maximum vaporization rate *in vacuo*. When the oxygen partial pressure exceeds this critical value, δ becomes very small and the flux of oxygen will be greater than the counter flux of iron vapor. An oxide layer will form at the metal surface, which will stop the vaporization (Figure 2-6). In the above calculations it was made an assumption that the formation of the condensed oxide at δ will not interfere with the gas transport processes, but rather be transported away with natural convection. The terms Δ and δ in Turkdogan's theory may be equated with Wagner's boundary layer thickness for oxygen and SiO respectively.

Turkdogan and coworkers also examined the general validity of Eq. 2.15, and did experiments with iron, nickel, copper, cobalt, chromium (solid) and manganese

in streams of argon + oxygen. They measured the rates of vaporization of the liquid metals, and found that the experimental data concurred with their theory. The general form of Eq. 2.15 became

$$J_i = \frac{\alpha k}{RT} p_{O_2} \tag{2.16}$$

where α is the number of gram-atoms of metal vapor required to combine with one mole of oxygen at the distance $x = \delta$ very close to the surface of the metal. The rate J_i is independent of the vapor pressure of the metal, and can be calculated when k is calculated for known boundary conditions by Eq. 2.12. Turkdogan et al. showed that the logarithmic relationship between J_i and p_{O_2} from Eq. 2.16 became a straight line for all the metals they investigated [10].

Turkdogan's theory states that the oxidation reaction happens between metal vapor and oxygen to form an initial condensed oxide, and later an oxide layer on the metal surface when the oxygen partial pressure exceeds a critical maximum value. A consequence of this theory is that the oxygen does not have access to the metal surface as it is consumed by the reaction prior to the surface. Furthermore, the theory does not include the formation of volatile oxide species (like SiO in Wagner's approach). The theory clearly fit with metals that do not form volatile oxides, such as those they examined, however in the case of silicon, the equilibrium SiO pressure will be approximately four orders of magnitude larger than the vapor pressure of $Si_{(g)}$, thus in this particular theory it is more probable that SiO vapor, rather than $Si_{(g)}$, will react to become an oxide aerosol. It is argued that the Turkdogan approach probably is what happens with the SiO formed at the

surface[9]. One evidence of the Wagner theory being correct in terms of the initial oxidation mechanism is the finding of Kaiser and Breslin[13], which showed the oxygen content in silicon to be linearly correlated with the oxygen pressure during active oxidation. This result indicates that the oxygen must have been in contact with the silicon surface, and thus Turkdogan's theory with all oxygen being consumed *prior* to the surface is not suitable in the case of liquid silicon oxidation.

Hinze and Graham[9] (1976) did an extensive experimental and theoretical study of the active oxidation of *solid* silicon, and they also identified experimentally the active-to-passive transition in terms of oxygen partial pressure. They found that there was actually two different active oxidation regimes, with each their own maximum oxygen partial pressure. In the first active oxidation region, they observed a bare silicon surface, as found by Wagner. However, in the second regime, thin whiskers of amorphous silica would grow perpendicular to the surface, and there would still be a very high oxidation rate. At oxygen pressures higher than the second maximum, the entire silicon surface would be covered by silica, and the oxidation rate would decrease significantly. The absolute value of the weight change (loss in the first region and gain in the second region) was linearly correlated with the oxygen partial pressure, and they could extract an experimental mass transfer coefficient from their results. The mass transfer coefficient found by using Wagner's theory on the experimental results $(-2J_{O_2} = J_{Si})$, was very close to the theoretically calculated one, whereas if they used the Turkdogan approach $(-J_{O_2} = J_{Si})$, the mass transfer coefficient did not fit as well. The conclusion was that the Wagner theory is more suitable for the primary oxidation mechanism, but that the Turkdogan theory could account for

the continued oxidation at higher oxygen pressures where the outgoing SiO would consume some of the incoming oxygen in building these silica whickers.

Another theory working from the assumption of an aerosol of oxide forming away from the silicon surface, is the thorough theoretical investigation performed by Ratto et al.[17, 18] (2000, 2001). They made an extended and more general Wagner theory, and they looked at two limiting cases; null reactions in the gas phase, represented by the Wagner theory, and instantaneous reactions in the gas phase. The derivations are applicable to all metal and non-metal systems at high temperature in the presence of gaseous oxygen, and they make an example of the reactions between Si/SiO and O_2 with the subsequent formation of SiO_2 gas and particles in the boundary layer. In the latter case they assumed that chemical equilibrium is reached instantaneously between all species. In both cases an assumption of steady-state was assumed, thus there would be no accumulation. A fundamental result of their study was the derivation of the expression of the curves of the asymptotic behavior of the system. They derived theoretical expressions for the concentration gradients for all gas species in the system (O_2, $Si_{(g)}$, $SiO_{(g)}$, $SiO_{2(g)}$) for both null reactions and instantaneous reactions. The full derivation of Ratto and coworkers' model will not be given here, however parts of their conclusion will be discussed.

In the Ratto model several case studies on silicon were presented, and one of them a case where there was a combined boundary layer; homogeneous close to the silicon surface, then a part with heterogeneous gas phase (condensed phase of $SiO_{2(s)}$ present) and then homogeneous again (bulk gas). When the concentration profiles for oxygen were derived for this particular case study, they could show that the oxygen partial pressure at the Si surface would be independent on the

bulk partial pressure of oxygen. This could be theoretically possible due to the consumption of the incoming oxygen by the reactions with SiO/Si, with the formation of SiO_2 particles inside the boundary layer, which now would make up the heterogeneous part of the boundary layer. This is of course the extreme case of instant reactions and would not be possible in reality. For an intermediately reactive boundary layer (compared to the two limiting cases of instant and zero reactions boundary layers) where some oxide would be present, the oxide formation would not be able to maintain the surface oxygen pressure constant at all bulk oxygen pressures, but the surface oxygen pressure could become much lower than expected from the Wagner theory. The concentration gradients for the gaseous species in this particular mixed boundary layer as calculated by Ratto et al. are illustrated in Figure 2-7.

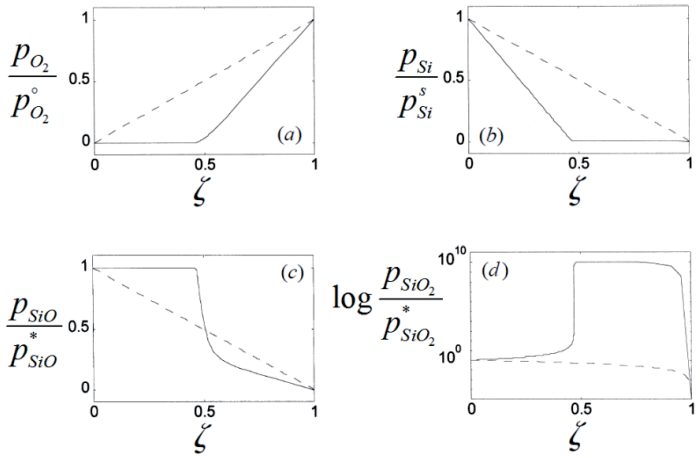

Figure 2-7: Relative pressure profiles for Si, O_2, SiO and SiO_2 at asymptotic behavior at 0.1 Pa and 1750°C, calculated by Ratto et al. (2001). ζ is the relative distance from the silicon surface, where 0 is at the Si surface and 1 is the bulk gas-boundary layer limit [18].

In Figure 2-7 the solid lines are the gradients in a system with instantaneous reactions, and the dashed lines are the gradient according to Wagner's theory. The concentration gradients are strongly nonlinear in the heterogeneous system. The combination of the Si and O_2 concentration profiles are quite similar to those of Turkdogan et al. in Figure 2-5 (b).

Ratto and co-worker's theory is interesting in that it may give an explanation to why it is possible to have active oxidation of liquid silicon in an air atmosphere, as is clearly the case in industry. However, they use $Si_{(g)}$ as the main reactant to form the SiO_2 in the boundary layer, even though the partial pressure of $Si_{(g)}$ at the silicon surface is four orders of magnitude lower that SiO at 1500°C.

A simpler theoretical derivation of the system Ratto presented was published by Arato et al.[19] (2009). They derived simple equations of thermodynamic and kinetic significance which could be used to test if there would be formation of condensed oxide inside the system in question, or not. Arato and co-workers evaluated a system where one can have two oxides present; a volatile oxide C_1 (SiO in our case) and a stable oxide, C_2 (SiO_2 in our case). The evaluation is concerned with both the thermodynamic and kinetic terms in the boundary layer. The first test was to check if the thermodynamics is favoring the formation of the second oxide in gaseous form. In Arato's derivation, the criterion is

$$\frac{p_{SiO_2}}{p_{SiO_2,\ sat}} \leq 1 \geq 0.3849 \left(\frac{p^*_{SiO}}{p^*_{SiO}(\max)} \right) \left(\frac{p^\circ_{O_2}}{p^*_{O_2}(\max)} \right)^{0.5} \tag{2.17}$$

If the right hand side of Eq. 2.17 is more than unity, the thermodynamics favors formation of $SiO_{2(g)}$ under the present conditions. However, even if the

thermodynamics favors the oxidation of $Si_{(g)}$/SiO to $SiO_{2(g)}$, the kinetics of the reaction and/or condensation may still be slow, thus the reaction rates must be evaluated and tested. If the kinetics are overestimated, a conservative limit is set; the collision efficiency is set to 1 (all collisions lead to a successful reaction), and the reaction has no activation energy. Then the reaction constant, *r*, will only be dependent on mean velocity and mean free path (just like the diffusion coefficient). Thus, in the second test, the kinetics of the reaction between $Si_{(g)}$/SiO and O_2 is evaluated. Arato's derivation gives the criterion

$$p_{Si}^{*}, p_{SiO}^{*} \leq 4\left(\frac{\lambda}{\delta}\right)^2 \tag{2.18}$$

where δ is the boundary layer thickness and λ is the mean free path calculated by

$$\lambda = \frac{k_B T}{\sqrt{2}\pi P d^2} \tag{2.19}$$

where k_B is the Boltzmann constant [J/K], T is the absolute temperature [K], P is the total pressure [Pa] and d is the diameter of the molecule, approximated to be a hard sphere[20]. If the criterion in Eq. 2.18 is fulfilled, the reaction between $Si_{(g)}$/SiO and O_2 will not take place inside the boundary layer, thus the kinetics will hinder the thermodynamically favorable reaction path. If however, inequality in Eq. 2.18 is violated, there will be $SiO_{2(g)}$ in the boundary layer. Now, the kinetics of the collision between SiO_2-molecules must be evaluated. The condensation phenomenon may still be slow, and is roughly checked by referring to the

initiation of a dimer reaction (formation of a SiO_2-SiO_2-unit), which gives the criterion:

$$\frac{\left(p_{SiO_2,sat}\right)^2}{p_{SiO}^*} \leq 2\left(\frac{\lambda}{\delta}\right)^2 \tag{2.20}$$

where $p_{SiO_2,sat}$ is the saturated SiO_2 pressure, and the other symbols are as previously stated. If this criterion is fulfilled, the rate of the nucleation is too slow, and will not take place inside the boundary layer. If the inequality in Eq. 2.20 is violated, there will be condensed SiO_2 in the boundary layer.

In the discussion of passive oxidation of solid silicon, Deal and Grove[21] (1965) are the pioneers. They presented a general relationship for the rate of oxide layer growth, and they found that the growth rate is linear at short oxidation times and parabolic at longer oxidation times. They show that the oxidation at the surface is the rate limiting step, and activation energies for diffusion and reaction are presented. They did experiments with both wet and dry oxidation, and found that the wet oxidation is faster than the dry oxidation. The theory is widely used in research where the controlled passive oxidation of silicon for use in microelectronics is in focus[22, 23]. The theory has been used and debated in the field of silicon oxidation; however, in this thesis the theory will not be further elaborated as this is a study of the *active* oxidation of silicon. The main difference between active and passive oxidation is that the rate is linear in active oxidation due to the gas diffusion barrier, as opposed to linear-parabolic in passive oxidation, where the oxygen has to diffuse through an increasingly thicker oxide layer.

Some authors have debated the validity of Deal and Grove's model in the initial stages of oxidation. In their research, Engstrom et al.[24, 25] (1991, 1992) considered the atomic oxidation mechanism for active and passive oxidation of solid silicon. They used supersonic molecular beam techniques and X-ray photoelectron spectroscopy to study the reactions of atomic oxygen with the surface of solid silicon. Their main conclusions are that the reaction is divided into several steps, where the first step is the adsorption of the oxygen atom, and the next step is the reaction with the surface silicon atoms. The Si-O unit can now either desorb and become $SiO_{(g)}$, or the surface coverage of Si-O units is too large, and the favored course of reaction is the nucleation of the Si-O units to become an oxide layer. Engstrom and coworkers suggested that the first step is very fast and practically unactivated (has no activation energy barrier). The step of nucleation of Si-O units into oxide is a very slow reaction, and the nucleation will make islands of oxide at high temperatures, with the islands being surrounded by clean Si surface. At lower temperatures (< 1000 K) the nucleation happens layer by layer. The interesting part with relevance to the present work is the proposed atomic mechanism for the active and passive oxidation, which is illustrated in Figure 2-8.

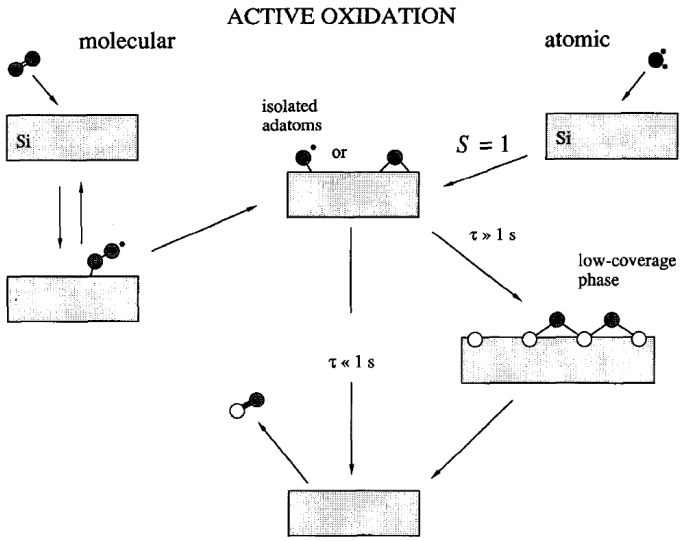

Figure 2-8: Proposed mechanism for active and passive oxidation of silicon by both molecular (left) and atomic (right) oxygen. If the chemisorbed oxygen is next nearest neighbor with one or more oxygen atoms (mid right part of the picture), the residence time for the oxygen becomes longer and the probability for nucleation (passive oxidation) increase. If however the adsorbed oxygen, coming from either molecular or atomic oxygen is alone at the surface, the residence time is short and the SiO is readily vaporized [24].

Even though their main focus was to study the oxidation of silicon by atomic oxygen, they also did experiments with molecular oxygen for comparison. They found that the atomic oxygen reacts with a unit probability with the clean Si surface, independent on the mean kinetic energy and sample temperature. However, for molecular oxygen, the reaction probability was 0.05 at the same conditions. The reaction rate for the "slow" step was the same for both reactants, which in this case is the step from adsorbed O* to adsorbed SiO*. Thus the rate of the reaction is the same, but the probability for the atom/molecule to stick to the

surface is significantly different. The low reaction probability for molecular oxygen is supported by Lander and Morrison[26] (1962), who found a probability as low as 0.01. They also conclude that the adsorption of oxygen is the fast reaction, and that there is a significant energy barrier for the required cooperation of several Si-O units to form a silica layer.

In a more recent study, Choi et al.[27] (2002) presented results found by computational modeling using multi reference wave functions in combination with a hybrid Quantum Mechanics/Molecular Mechanics method. They also studied the oxidation of solid silicon by atomic oxygen, and proposed a new model for how the active oxidation can occur. Their assertion is that desorption of SiO* can only occur if the oxygen is in a "back-bond" configuration. They found that the previously stated weakly bonded silanone does not exist, or if it does, the activation barrier for desorption of such a species is too high. The calculated activation barrier for desorption of SiO* via the backbonded configuration is 90 kcal/mole, which is in good agreement with other studies[24, 25, 28].

Using a molecular modeling method called ReaxFF, Pamungkas et al.[29] (2011) found that in the dry, high temperature oxidation of a Si(100) surface, the kinetic energy of the oxygen molecule is large enough to break the O-O bond before chemisorption of both atoms at the surface, and thus the oxidation of the silicon surface produce O* radicals (Eq. 2.3). Snapshots of the oxidation reaction with two different angles of the incoming oxygen molecule are shown in Figure 2-9.

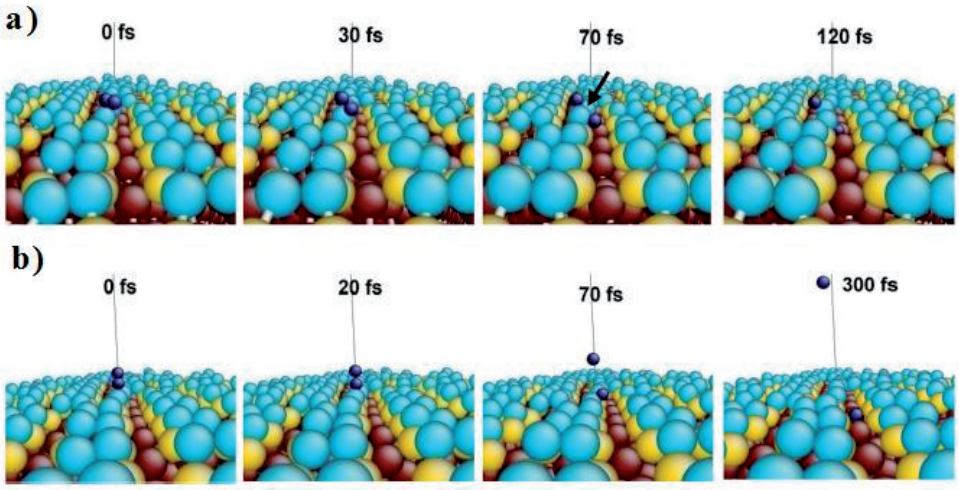

Figure 2-9: Snapshots of the molecular modeling of the early stages of dry oxidation of Si(100) at 1200 K., with the oxygen bond having an angle of a) 90° and b) 0° relative to the normal axis to the surface. The oxygen is represented by dark blue balls. Figure modified from Pamungkas et al. (2011)[29].

They found that the first stage of the surface oxidation happens with spontaneous dissociation of the O_2 molecule and without an energy barrier. When both O-atoms adsorbs to the surface, they will move away from each other due to Columbic repulsion. The oxidation results in an amorphous oxide layer both at room temperature and 1200 K, however with more oxygen in the deeper layers of the silicon structure at higher temperatures.

2.1.3 Nucleation of SiO_2

As we have seen in the previous chapter, the oxidation of liquid silicon involves several steps, and the place and rate of the formation of the silica fume is debated. The presence of a condensed phase inside the boundary layer may affect

the transport of gaseous reactants and products. The boundary conditions of the oxidation in terms of maximum oxygen partial pressure in the bulk gas may also be affected by the formation of silica in the boundary layer. In addition, the size of the silica particles (which is a function of growth parameters) in the fume in industry is an important factor in evaluating how harmful they are to be exposed to[2, 30]. In this section, the nucleation and growth of silica particles is presented.

Ulrich (1971)[31] derived theoretical expressions relating particle concentration and size to residence time and other parameters in a silica synthesis flame. He studied the nucleation and growth of silica in a flame where premixed silicon tetrachloride, hydrogen and air were burned. In such a case, there will be a turbulent velocity field where the particles form, however he argues that the microscopic zones in which individual particles grow are orders of magnitude smaller that the macroscopic turbulent movements, thus they will not be affected. Removing the turbulent gas situation as a parameter, Ulrich argues that the rate of particle growth only depends on the chemical reaction, nucleation and Brownian collisions. In the theoretical study, it is assumed that the chemical reaction occurs instantaneously to produce silica nuclei, or at least this step is faster than the growth step.

In general condensation theory, two opposing forces determine the critical size for nucleation; the thermodynamic free-energy driving force for condensation versus the surface tension force which resists growth of a nuclei. The condensation free energy depends on relative super saturation of the gas mixture, and the surface force is proportional to the square of the particle radius. When the sum of the two opposing forces is zero, one can find the critical radius:

$$r^* = \frac{2\sigma}{\rho \Delta G_{cond}} \tag{2.21}$$

Where r^* is the critical radius, σ is the surface tension, ρ is the density and ΔG_{cond} is the condensation free energy. However, assuming that nanoparticles have the same properties as the bulk of the same substance is a very questionable assumption. Nevertheless, using the bulk properties of silica, Ulrich found the critical radius to be less than the size of a single SiO_2 molecule. This unrealistic result suggests that the super saturation at the temperatures in question (1527°C and 1827°C) reflects the fact that the flames are far below the boiling point of silica (2950°C[20]). This result, in turn, suggests that any silica particle is stable for growth under these conditions.

In arguing that a nuclei of liquid silica is the reaction product, rather that gaseous SiO_2, Ulrich points to the fact that a the reaction between silicon tetrachloride, hydrogen and air is almost thermodynamically neutral when producing $SiO_{2(g)}$ (-29 J/mol), but is highly exothermic when liquid silica is the product (-585 kJ/mol). As a flame needs to be highly exothermic, the latter must be the case, and thus the condensation phenomenon has the heat effect in this reaction.

The main conclusions from Ulrich's theoretical work are that Brownian collisions and coalescence dominates as the growth mechanism, and that nucleation is not a rate limiting factor in the condensation of silica particles. Ultimate particle size is highly dependent on the flame temperature, as a higher temperature will result in higher residence time, and thus a longer time for the

particle to grow before it is quenched to become a rigid sphere. This finding is supported by later studies [32].

In a later work, after testing the theories in the earlier work with experiments, Ulrich and Subramanian (1977)[33] suggest that the rate controlling step in the growth of silica particles is the fusion, rather than the collision rate. Silica has a very high viscosity, thus the fusion and coalescence of the particles is so slow that the small primary particles rather grow into aggregates where the small primary particles keep their shape and can be seen as discrete particles. The particles stick to each other when colliding, but the coalescence is so slow due to high viscosity, thus they quench before they become a new spherical particle. Ulrich and Subramanian propose the collision as the main particle growth mechanism when the particles are still very small (at short residence time), until they become large enough to exhibit macroscopic viscosity. This transition is assumed to be when the particles consists of 1000 SiO_2 molecules, which corresponds to a diameter of 4.4 nm. After this transition point, the coalescence and fusion is the rate controlling process.

In the evaluation of the condensation phenomena, the physical nature of these ultrafine particles/nuclei has to be considered. Preining (1998)[34] describes how the physical state of particles become distinctly different from the larger, bulk material as the particles become smaller and smaller. When a particle of unity density (water) has a diameter of 20 nm, 12 % of the molecules will be at the surface. For a 10 nm diameter particle, 25 % of its molecules are at the surface. When particles are smaller than about 5 nm in diameter, the concept of a “surface” no longer has any meaning, because there is no continuum in the material structure of the particle. The particle can no longer be regarded as solid or liquid

but rather a molecular cluster, an entirely distinct phase which Preining calls the nanophase[34]. Cluster physics will be important to consider when interactions between such ultrafine particles are to be evaluated.

Using Ulrich's equations for particle growth, Kamfjord et al.[7] (2012) calculated the time for the growth of an industrial silica particle with 55 nm diameter at different particle concentrations measured in the off-gas channel in the tapping area at a silicon plant. They found that the formation time of one such particle was 0.014 - 0.028 s, depending on the particle concentration in the off-gas.

2.1.4 Effect of impurities on the oxidation

In his PhD thesis, Hildal[35] (2002) investigated the reaction mechanisms and kinetics for the oxidation of liquid silicon with water, in order to explore the reason for steam explosions associated with water granulation of FeSi and Si in their production processes. He found that oxidation of liquid silicon with water also produce SiO gas in the endothermic reaction in Eq. 2.5, **(**Table 2-1**)**. He found that SiO would either oxidize to SiO_2 in further contact with water, or it would condense (Eq. 2.9, Table 2-1) when the availability of oxidizing agent was low. Reacting pure silicon with water, he found a layer of condensate close to the silicon surface, inside the porous oxide layer. He concluded that the initial reaction when the liquid silicon came in contact with water was formation of SiO, which would either condense or be oxidized. Adding small amounts of Al and Ca to the Si-melt resulted in a mixed oxide layer (slag) closest to the surface, with the same porous silica layer as found in the pure Si experiments further away from the silicon surface. He concluded that the formation of the slag on the surface was slow due to

low concentrations of Al and Ca in the melt, and that the active oxidation would occur first. When the oxide slag had been formed, it would inhibit further active oxidation.

There are several other metals which will react with oxygen at high temperatures to produce gaseous oxides[36]. Aluminum, for example, usually form a thin, dense protective layer of Al_2O_3 very fast in contact with oxygen, but at high temperatures and under high vacuum $Al_2O_{(g)}$ may form due to the reaction[37, 38]

$$4Al_{(l)} + Al_2O_{3(s)} \rightarrow 3Al_2O_{(g)} \tag{2.22}$$

and at 1727°C in vacuum a partial pressure of 0.01 atm of $Al_2O_{(g)}$ may be obtained[37]. In the Al-O-system, at low oxygen pressures, $Al_{(g)}$ and $Al_2O_{(g)}$ will dominate, and at higher oxygen pressures (where α-Al_2O_3 is stable) $O_{(g)}$, $Al_{(g)}$ and $AlO_{(g)}$ will dominate in the gas phase[39].

The Si-O-system is to our knowledge one of the few systems where a very high partial pressure of gaseous oxide may be obtained at ambient pressures. Most other metals will react to form a more or less protective oxide layer, where the degree of protectiveness is determined by the Pilling-Bedworth ratio, R_{PB}[40];

$$R_{PB} = \frac{V_{oxide}}{V_{metal}} = \frac{M_{oxide} \cdot \rho_{metal}}{n \cdot M_{metal} \cdot \rho_{oxide}} \tag{2.23}$$

where $V_{oxide/metal}$ is molar volume of oxide/metal, $M_{oxide/metal}$ is the molar mass of oxide/metal, $\rho_{oxide/metal}$ is density of oxide/metal, n is the number of atoms of metal per molecule of oxide. The rule states that if the volume of the oxide is smaller than

the metal it has consumed/replaced ($R_{PB} < 1$), the oxide layer will not be protective, and if the volume of the oxide layer is larger than the metal it has consumed/replaced ($R_{PB} > 1$), then the oxide layer will be protective and non-porous[40]. If however the ratio is more than 2, then the stress on the oxide scale may make it crack and rupture, and the protective effect will be lost.

When an oxide scale is formed on an alloy, the mixed oxide layer may have characteristics that will deviate from the rule of Pilling and Bedworth, and thus this simple calculation of the ratio may not be sufficient to characterize the protective effect of the oxide layer[41].

2.2 The industrial refining process

2.2.1 The refining

In the oxidative ladle refining process, the method is to bubble oxygen enriched air into the liquid silicon, usually through a nozzle in the bottom of the ladle, with the goal being to remove the main impurities, Al and Ca. The refining processes is illustrated in Figure 2-10, there the flow pattern in the liquid silicon is shown.

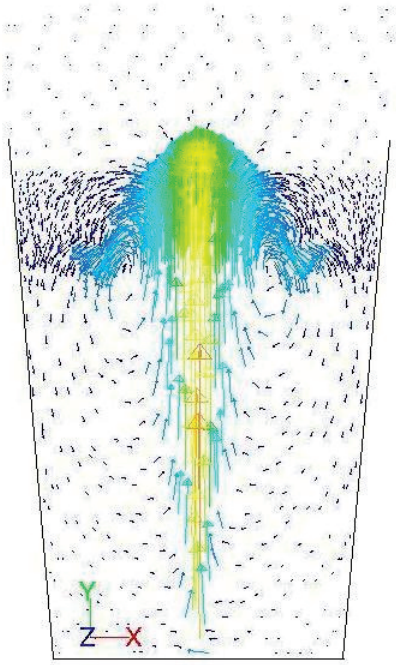

Figure 2-10: Illustration of the flow pattern in the oxidative ladle refining of silicon, where a mixture of air and oxygen in purged through the melt through a nozzle in the bottom of the ladle. Figure by Jan Erik Olsen.

First the oxygen in the bubbles readily reacts with the silicon to form SiO_2 and SiO according to the reactions in Eq. 2.1 and 2.2 (Table 2-1), respectively. Next, exchange reactions between the silica and the dissolved Al and Ca take place,

$$3SiO_{2(s,l)} + 4\underline{Al} \rightarrow 2Al_2O_{3(l)} + Si_{(l)} \tag{2.24}$$

$$SiO_{2(s,l)} + 2\underline{Ca} \rightarrow 2CaO_{(l)} + Si_{(l)} \tag{2.25}$$

where the underlined species designates elemental presence in the metal phase. In the exchange reactions, silicon is recycled back to the melt as the slag is enriched in alumina and calcium oxide. The slag formed at the bubble-melt interface is transported to the surface of the silicon due to uplift of the bubble[4, 42]. In the ladle refining process the reaction rates are only determined by the mass transfer of the reactants to the reaction zone at the interface, as the reaction kinetics are fast due to the high temperatures.

Tang [43](2008) used the equilibrium constants of the reactions in Eq. 2.1 and 2.2 in the derivation of an equation for calculating of the equilibrium partial pressure of SiO in the bubble in the refining process:

$$p_{SiO} \approx P_b \sqrt{\frac{\exp(11.13 + 39464/T)}{\exp(-23.66 + 113623/T)}} \tag{2.26}$$

where P_b is the total pressure in the bubble, usually set to be 1 atm. If the bubble initially contains N_{air} moles of air, with a molar fraction of oxygen x_{O_2}, the molar fractions (x) of SiO and SiO_2 in/at the bubble when the oxygen is consumed completely can be calculated with [42]

$$x_{SiO} = N_{air}(1 - x_{O_2}) \frac{p_{SiO}}{P_b - p_{SiO}} \tag{2.27}$$

$$x_{SiO_2} = N_{air} x_{O_2} - \frac{x_{SiO}}{2} \tag{2.28}$$

In Figure 2-11 the number of moles of SiO and SiO_2 produced is plotted against temperature.

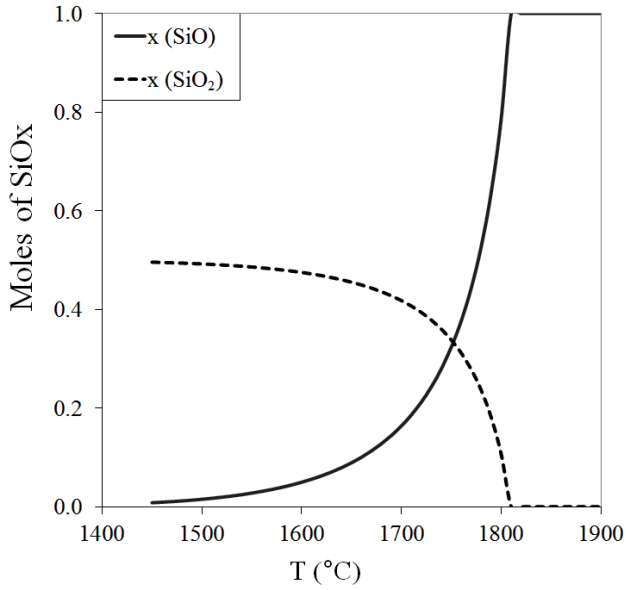

Figure 2-11: One mole of Si reacts with a gas mixture of 0.5 O_2 + 0.5 N_2 at P= 1 atm. Number of moles of SiO and SiO_2 produced plotted against temperature.

The discontinuity in the curve of SiO_2 is where production of silica becomes unstable at a critical temperature

$$T_{crit} = 1874.7 + 88533\ln(x_{O_2}) \tag{2.29}$$

where the temperature is in degrees Celsius. At this critical temperature the production of SiO_2 is terminated. This leads to production of only SiO, which is a condition of pure Si-loss with no refining of Al and Ca[43].

The flow of gas and liquid metal, reactions, and mixing have been extensively investigated in the steel making industry due to the importance of the refining process [44-46]. In a recent study, Xia et al.[47] (2001) compared modeled data to experimentally measured data where gas and liquid flow was analyzed and a sensitivity analysis of different physical constants was performed. As the physical properties of water and mercury (which is often used in such experimental studies) are quite different from molten steel, the use of Wood's metal (a low-melting-point alloy) was used with N_2 as the purge gas. Xia and coworkers found a good agreement between the model and the measured data for the liquid velocity, however the velocities in the plume were overestimated by all modeled cases compared to the experimental data. The experimental radial velocity of the melt was found to be 0-0.13 m/s at the surface of the plume. They found, like several other researchers[46], that the velocity of the bubbles after the initial nozzle zone, and prior to the surface, had a constant upwards velocity in the axial direction, with a Gaussian shape of the velocity distribution in the radial direction.

2.2.2 Distribution of elements in the melt-slag-gas system

In the silicon industry the distribution of the main impurity elements, Al and Ca, between metal and slag is well documented, as the refining process is primarily performed to remove these elements to meet the customer demands on product specifications[4]. In the solar cell industry, the distribution of boron (B) and phosphorous (P) between metal, slag and gas is also well studied[48-51]. Boron and phosphorous are dopants in the solar cells, and thus their content in the silicon has to be very low, < 1 ppmw. Furthermore, B and P are particularly hard to remove

from silicon due to their high segregation coefficients in silicon[52] and are thus unresponsive to directional solidification, which is a widely used method for removing most other elements from silicon. The main methods for removing boron that have been investigated are volatilization by H_2-H_2O purging, with or without plasma, where the compound HBO is by which boron is volatilized[53, 54]. The other main method of boron removal is slag refining, where the slag composition and basicity are the factors determining the efficiency for the boron removal[55]. The methods studied for phosphorous removal have mainly been in the area of vacuum refining, where the high vapor pressure of P_2 is utilized, and some investigation have been done in the area of slag refining of phosphorous [56, 57]. Due to the large interest in B and P removal, the activity of said elements in silicon, slag and gas are well documented in literature.

The distribution of trace-elements in the silicon (Garcia and Myrhaug[58] (2007)) and ferrosilicon (Myrhaug and Tveit[59] (2000)) production furnace has been studied. Samples from all raw material going into the furnace (quarts, reduction material and electrode), and samples of the outgoing phases; silica from furnace top and silicon were collected, and measurements in the purified off-gas was performed. In the material balance in the silicon process, 31 trace-elements were analyzed and given distribution coefficients as to where they go (excluding Al, Ca, Fe, Si and C, as they are main elements in the process). A boiling point model was developed and used to explain the results of where elements end up; in the silicon (bp > 2000°C), microsilica (2000 > bp > 1300°C) or the off-gas (bp < 160°C). The element balance in the outgoing phases in the FeSi-process is shown in Figure 2-12, where the elements are sorted with decreasing boiling point from left to right. From this result, it can be seen that most of the elements follow the boiling point

model. The elements not following the boiling point model are assumed to be present as oxides or sulfides, which will alter the boiling point, or, as in the case of e.g. As and P, they have a high affinity for the Fe present in the ferrosilicon process, and thus stay in the melt. Several stable gaseous compounds around or below 1300°C are discussed in the FeSi-furnace material balance, e.g. SO_3, SeO_3, As_2O_3, MoO_3 and PbS. All these compounds have lower boiling points than their respective pure elements, and will thus behave differently in the furnace than anticipated by looking at only the pure elements' boiling points.

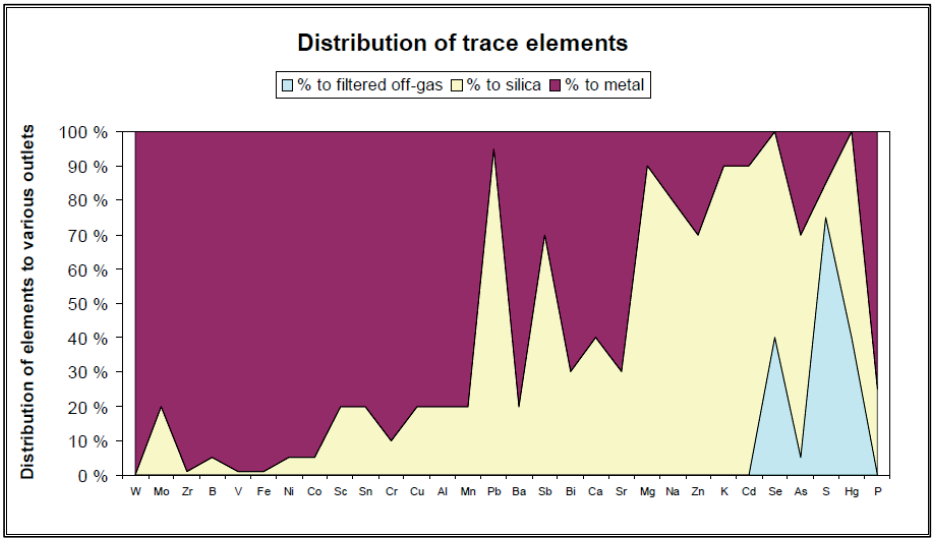

Figure 2-12: Distribution of trace-elements in the FeSi process[59].

Activities of several main and trace-elements in silicon melt have been experimentally determined or modeled [60, 61]. Using well known databases for alloys and slags, like the Fact-database[62], phase diagrams for several binary Si-alloys are well documented and also some binary and ternary silicate slags are well-studied.

For silicon, the Fact-database has limited information, and as such, more specialized database was developed by Tang et al.[63]. The documented activity coefficients of 29 elements in liquid silicon and of 22 associated oxides in a multicomponent 34 % SiO_2 – 25 % Al_2O_3 – 40 % CaO slag are presented in Table 2-2 and Table 2-3, respectively.

Although the databases cover many elements, several alloy-slag systems are not entirely determined thermodynamically. Gaseous compounds are neither well determined. As such, data on the distribution of elements between silicon, slag and fume/gas is challenging to model given limited experimental data. The only references looking at the fume composition are Myrhaug and Tveit (2000) and Garcia and Myrhaug (2007), but both those studies are on the furnace, not the refining ladle, and thus the slag is not a major phase. Furthermore, the conditions are very different in the furnace (up to 2000°C, reducing environment, one liquid phase) than in the refining ladle (1450-1600°C, purging with oxidizing gas, two liquid phases), thus although some fundamental similarities, the results from the furnace are not directly applicable to an oxidative refining system.

Table 2-2: Activity coefficients of elements in dilute solutions in silicon at 1600°C [63]

Element	γ_{Me-Si}
Ag	1.4
Al	0.46
As	4.4
Au	$1.8 \cdot 10^{-3}$
B	2.1
Bi	26
Ca	$4.0 \cdot 10^{-3}$
Co	0.013
Cr	$6.7 \cdot 10^{-4}$
Cu	0.72
Fe	$8.1 \cdot 10^{-4}$
Ga	1.4
Ge	1.5
In	3.9
K	510
Li	0.017
Mg	0.28
Mn	$4.6 \cdot 10^{-3}$
Mo	$1.9 \cdot 10^{-3}$
Na	0.018
Ni	$2.7 \cdot 10^{-7}$
P	3.1
Pb	29
S	0.25
Sb	4.4
Sn	5.5
Ti	$2.5 \cdot 10^{-5}$
V	$3.7 \cdot 10^{-4}$
W	0
Y	$1.1 \cdot 10^{-7}$
Zn	$5.7 \cdot 10^{-47}$
Zr	$6.7 \cdot 10^{-6}$

Table 2-3: Activity coefficients of oxides in a multicomponent 34 % SiO_2 – 25 % Al_2O_3 – 40 % CaO slag system at 1600°C [64]

Oxide	$\gamma_{Me_xO_y-slag}$
Al_2O_3	0.14
As_2O_3	$1.1 \cdot 10^{-16}$
B_2O_3	$1.2 \cdot 10^{-6}$
CaO	0.012
CoO	0.97
CrO	2.69
Cr_2O_3	$8.8 \cdot 10^{-10}$
Cu_2O	$5.2 \cdot 10^{-9}$
FeO	1.78
Fe_2O_3	$4.5 \cdot 10^{-11}$
K_2O	$1.6 \cdot 10^{-10}$
MgO	0.15
MnO	0.28
Mn_2O_3	$2.6 \cdot 10^{-12}$
Na_2O	$2.5 \cdot 10^{-11}$
NiO	2.3
PbO	0.18
SnO	5.2
TiO_2	0.65
Ti_2O_3	$5.8 \cdot 10^{-6}$
ZnO	0.53
ZrO_2	2.7

2.3 Summary of state of the art

2.3.1 Oxidation of silicon

In existing literature, there are two main works which have evaluated the active oxidation of liquid silicon theoretically; Wagner[6] (1958) and Ratto et al.[15, 16] (2000, 2001)[17, 18]. Both theories present theoretical boundary conditions for the active oxidation in terms of oxygen partial pressure in the bulk gas phase. Ratto also presents theories on how the concentration gradients of the four species $O_{2(g)}$, $Si_{(g)}$, $SiO_{(g)}$, $SiO_{2(g/s)}$ in the boundary layer at null reactivity and instant reactivity/equilibrium conditions. However, there is no experimental validation of these theoretical evaluations for liquid silicon.

For solid silicon, there are several experimental investigations presented, with Hinze and Graham[9] being the most thorough. From their experimental results they suggested that the oxidation mechanism of active oxidation of silicon is a combination of Wagner and Turkdogan's suggested mechanisms, where Wagner's theory is what takes place at the surface with the formation of $SiO_{(g)}$, and that Turkdogan's theory is what happens when the SiO meets the incoming oxygen to produce SiO_2 and grow whiskers at the surface. Even though Hinze and Grahams theoretical and experimental investigation is very thorough and well performed, it is for solid silicon, and we cannot assume that the conditions will be exactly the same for liquid silicon. With regards to diffusion and mass transport in the gas phase, the system will likely be similar, if the physical properties of the gases are adjusted for the increased temperature. However the reactions at the surface may be different due to the change in the surface structure, or lack thereof. The silica whiskers Hinze and Graham observed will probably not form on a *liquid* silicon

surface, and very doubtful on a moving liquid surface, however the proposed mechanism with a sink of SiO at some distance away from the surface is interesting to pursue.

The atomic models presented by Engstrom[24, 25] (1991/1992) and Choi[27] (2002) are important to evaluate in the active oxidation of liquid silicon. The explanation for the observed active oxidation of silicon during industrial refining may very well be explained from molecular theory and activation energies and kinetics for desorption versus nucleation of Si-O units at the surface. Maybe the active oxidation of liquid silicon in air atmosphere is possible because there is new fresh, uncovered silicon exposed all the time due to the stirring in the ladle refining. The adsorbed oxygen is in a single state with no neighbors, thus in this particular situation desorption of SiO is more favorable than the nucleation, which is shown to be a slow step. Choi presents the activation energy for SiO desorption of 90 kcal/mole, however no activation energy for nucleation have been found. In addition, Engstrom and other authors have observed a sticking coefficient for molecular oxygen of 0.01 - 0.05, which may be important to take into account when theoretically evaluating the experimental results.

The modeled result presented by Pamungkas et al.[29] (2011) is significant as it shows that the surface oxidation reaction actually may produce oxygen radicals. As the oxygen molecule has large enough kinetic energy to break off the O-atom already at 1200 K, it will most probable have even more probability of breaking off an O-atom at 1800 K, which is the typical working temperature in the industrial situation. What is not clear, however, is to what degree this reaction is energetically preferred. The reason this question is important is due to the high reactivity of the relatively unstable O* radical. Remembering atomic oxygen

having a sticking coefficient of unity in solid silicon oxidation, the radicals produced may readily react with the silicon surface, or, as both oxygen radicals and SiO gas are relatively unstable at lower temperatures, they may readily react to for $SiO_{2(g)}$ (ref Eq. 2.4 and 2.8 in Table 2-1). Which of these two paths for the atomic oxygen are most favorable we cannot be sure.

The literature offers several studies on active oxidation of solid silicon which are not elaborated here, however some of the key information from experimental and theoretical results found in literature are summarized in Table 2-4.

This literature review have shown that, to date, there are no fundamental experimental data on the active oxidation of *liquid* silicon, and no research coupling the fundamental theory of active oxidation of liquid silicon with the industrial observation of active oxidation in air.

Table 2-4: Results from earlier investigation of active oxidation of silicon, with temperature, flow regime, maximum oxygen partial pressure in bulk gas and method of investigation given.

Authors	**T**	**Flow regime**	p_{O_2} (max)	**Method**	**Ref**
Gulbransen et al. (1966/1972)	1300°C	Knudsen	$1.18 \cdot 10^{-5}$ atm	Exp.	15, 65
Gelain et al. (1971)	1060°C	Knudsen	$7.9 \cdot 10^{-6}$ atm	Exp.	14
Kaiser & Breslin (1958)	1410°C	Viscous	0.01 atm	Exp.	13
Hinze & Graham (1976)	1227°C	Viscous	I: $0.385 \cdot 10^{-3}$ atm II: $3.87 \cdot 10^{-3}$ atm	Exp.	9
Wagner (1958)	1410°C	Viscous	$6.1 \cdot 10^{-3}$ atm	Theor.	6
Ratto et al. (2001)	1500°C	Knudsen	~10^{-7} atm	Theor.	18

2.3.2 The industrial refining process

The purging in the refining process leads to a plume of violently stirred silicon, where new silicon surface is exposed to air all the time. If the oxidation of liquid silicon is only determined by the oxygen availability to the Si surface, then the amount of fume must be determined by the exposed silicon surface. In the case of the ladle refining the silicon surface area is large due to the violent stirring, and also constantly renewed. To date, there is a lack of experimental data on the fume formation rate in the industrial silicon refining process. The main mechanism for the fume formation has not been identified, and there are no quantitative or qualitative studies on the fundamental boundary conditions for the fume formation.

The distribution of elements in the Si and FeSi production processes has been established by Garcia and Myrhaug[58] (2007) and Myrhaug and Tveit [59](2000). However, as the present study is on the fume from the refining, there is a lack of information on the distribution of elements between silicon melt, slag and fume in the ladle. The boiling point model is not sufficient to describe the element distribution, as the environment is different at the silicon surface in the ladle, compared to the environment inside the furnace. In addition, the boiling point model uses the boiling point of the elements in their pure systems, thus ideal behavior is assumed. Not taking element activities in the silicon melt into account, this model is more a crude estimation than a thorough thermodynamic analysis.

The distribution of the main elements in the refining ladle are well documented in terms of activities in silicon and slag, however, the number of elements with well-known thermodynamic behavior in both these phases are limited, and as such we know little of what happens to the trace-elements in the

refining process. Additionally, the systems studied are confined to the melt-slag system, without taking the gas phase/fume into account.

2.4 Research questions

In the area of liquid silicon oxidation and refining, there have been several issues to investigate, and the main research questions asked in the present work were:

1. How much silica fume is produced during industrial refining of silicon, and what are the factors determining/limiting the rate of fume formation?
2. What is the main mechanism for fume formation in industrial silicon refining?
3. What are the characteristics of silica fume (particle size, shape, structure, elemental content) and what characterization methods are applicable to determining these properties?
4. What are the boundary conditions for active oxidation of liquid silicon, and how does it vary with oxygen pressure and gas flow rate?
5. Is gas flow rate or amount of oxygen available the most important factor for the fume formation kinetics?
6. When and where does the SiO combust to form SiO_2, and does the silica condense inside or outside the boundary layer?
7. What does the fume from the industrial refining ladle contain other than SiO_2, and where do these impurities come from? A mass balance on the refining ladle is needed.
8. With what level of accuracy can elemental distribution between condensed and gaseous phases in industrial silicon refining be determined for emissions reporting purposes?

3 Methods

3.1 From industrial scale to small-scale

In this work, several different approaches have been used to study the active oxidation of liquid silicon. The main difference between the sub-projects have been the size; industrial measurements (~7 tons of Si), induction furnace experiments (1750 g Si) and small-scale experiments (10 g Si). The experiments are summed up in Table 3-1, where scale, method, conditions and goals are given.

The project began with the industrial scale measurements, where quantification was the main goal. Finding the main macroscopic mechanism for the fume formation in the refining process was also important in order to plan later fundamental experiments. Samples of silica fume were collected and characterized with BET, SEM, TEM and ICP-MS. A particle size distribution was found from the SEM-images. Thermodynamic calculations of the SiO-pressure inside the refining bubbles were done to determine the amount of fume originating from the bubbles, and thereby discussing the main mechanism for fume formation.

In the industrial measurement campaign, samples were also collected from the tapped silicon, the refined silicon, slag and additives (flux material and cooling metal). This was done in order to do a mass balance and an element distribution study of the refining ladle. 105 samples from 8 different ladles were collected during three days. All samples except fume were crushed into a powder prior to the ICP-MS analysis.

Table 3-1: Overview of the three main experiment types used in this work. Scale, conditions and goals are given.

Experiment type	Industrial measurements	Induction furnace experiments	Small-scale experiments
Amount of Si	~7000 kg	1750 g	10 g
Gas flow	Turbulent, natural convection	Laminar, forced impinging jet flow	Laminar, forced flat plate flow
Gas composition	Ambient air	Synthetic air, water saturated synth. air, synth. air + Ar	Ar + O_2
Silicon surface	Gas stirred turbulent, not flat	Induction stirred, moving, flat	Still, flat
Method	Measurements of fume amounts with LaserDust MP (NEO). Sampling of fume, metal, slag and additives. Filming with IR-camera.	75 kW induction furnace run at 10-20 kW. Weight gain of filter and other parts used to measure fume formation rate.	Horizontal, high temperature resistance furnace. Weight loss of sample monitored for measuring oxidation rate.
Measurements done	Amount of fume as a function of gas purge rate and composition. Samples analyzed with ICP-MS (all samples), and SEM, BET and TEM (fume only)	Amount of fume as a function of gas flow, humidity in gas and oxygen pressure. Samples of silica collected and analyzed with SEM and BET.	Amount of Si lost as a function of p_{O_2}, linear gas velocity and time. Samples of silica collected and analyzed with SEM and XRD.
Aim	Quantify and characterize fume in industry. Find distribution of main and trace-elements between the three outgoing phases; refined silicon, slag and fume.	Measure rate of fume formation in air. Investigate the effect of humidity in air. Examine whether the increased oxygen amount per unit time or the increased flow is the main factor determining the rate.	Accurately measure the rate of active oxidation of silicon. Find boundary conditions.

Small-scale experiments were performed to develop a more fundamental understanding of the active oxidation of silicon. The goal was to find boundary conditions for the bulk oxygen partial pressure, and to find the mass transfer coefficient for oxygen. The oxygen partial pressure, gas velocity and oxidation time were varied. The results were compared to theoretical mass transfer calculations based on the laminar flat plate theory, where the mass transfer coefficient is a function of $v_g^{\frac{1}{2}}$.The experimental setup was also modeled with CFD (see section 3.3) to see if it was possible to explain discrepancies between the measured and theoretically calculated mass transfer coefficient and maximum oxygen partial pressure.

When industrial measurements and small-scale experiments were compared it became clear that more investigation was needed. In an attempt to simulate the industrial case in a best possible way, induction furnace experiments were performed. In this setup the surface of the silicon would be dynamic like in the industry, but not as violent and uncontrolled and thus more precise surface area estimations would be possible. The impinging jet would also simulate the gas flow towards the surface in the industry, which is an impinging flow due to the natural convection above the hot ladle, as described in the CFD modeling[68,69]. The setup was made so that laminar impinging jet theory could be used to do theoretical calculations of the mass transfer. In this theory, the mass transfer coefficient is a linear function of $v_g^{\frac{3}{4}}$, thus the flux would be even more dependent on the gas velocity close to the surface than in the small-scale experiments, which is also probably the case in industry. The gas flow of synthetic air was varied, and experiments with wet air were carried out in order to simulate plant conditions on

a rainy day with high humidity. Furthermore, experiments with diluted synthetic air were performed in order to investigate whether the increased amount of oxygen per time unit, or the increased gas velocity itself (i.e. thinner boundary layer) was the governing mechanism for increased silica formation with increased gas flow.

3.2 Experimental control and accuracy

The main difference between the three experimental cases is obviously the scale. With decreased scale, it is easier to control the conditions and thus reduce the uncertainty in the measurements. In the industrial measurements, the only parameter possible to control or change was the purge gas amount and composition, which has a certain degree of inaccuracy given the flow control devices used. The fume measuring equipment was a LaserDust MP, a commercial apparatus from NEO Monitors (Lørenskog, Norway)[66]. The LaserDust measures the transmission of a laser beam and the reduction in the signal will correspond to the amount of fume in the measuring path. This change in signal is dependent on the properties of the particles, primarily the particle size distribution. The LaserDust used was not calibrated particularly for silica fume, however the measurements are evaluated to have a total measuring error of 30 %[67], which is in the same order of magnitude as the typical standard deviations in the measurements. The apparatus had a relative error of 2 % in the measurements, and measured the fume amount in the off-gas channel every 5 s. The frequent measurements gave a large amount of measurements point, which made it possible to obtain a good statistical analysis of the measurements. The

measurements of fume amount had a total uncertainty of ~30 %, which is not too bad, considering the crude nature of the industrial conditions. The laser measurements gave an output of kg/h, which, to be compared to other studies, needed to be converted into flux; mol/m^{2}s. For this a surface area is needed. The surface area of the liquid silicon in the industrial case is not possible to measure or calculate in an accurate manner, however, attempts to estimate it was made. This is described and discussed in the next chapter.

In the small-scale experiments, the control of all parameters was greatly increased, and the uncertainty in the measurements decreased accordingly. The temperature gradient in the furnace and the gas flow rate were calibrated. The scale of the experiments made it possible to use a balance with an accuracy of 0.1 mg, which represents an uncertainty of 0.02 % for the samples with the smallest weight change. Other sources of error may have been leakage of oxygen into the tubing and thus into the furnace. This would be a larger problem at low flow rate and low oxygen partial pressure. Without measurements of the oxygen partial pressure in the ingoing gas it is not possible to quantify the error in gas composition directly. One parallel was performed, and the difference between the two experiments was 3.8 %, reflecting the high level of control in the experiments.

In the induction furnace experiments, the measurement uncertainty was increased compared to the small-scale experiments, however, the control of the gas flow and the surface area was better than in industry. The main points of experimental variation in the induction furnace experiments were temperature and power input, however these variations were in the order of 0.3 % and 6.4 %, respectively. The balance used had an accuracy of 0.01 - 0.1 g (depending on the weight of the item being weighed), which gives a maximum uncertainty of 10 %

for the smallest silica samples (1 – 2 g). The difference between parallels (all experimental conditions were tested twice) varied greatly; 3 – 37 % (one parallel is not included here, where the variation was as high at 49 %. However, one of those experiments is considered an outlier. This is further elaborated in the next chapter). The reason for the large variation in some of the parallels is unknown, but small variations in the height of the lance tip above the silicon surface (i. e. human error) in addition to the mentioned variations may be parameters which have potential for improvement for greater experimental accuracy.

In the element distribution, the sources of error were explored in great detail, and a whole paper was dedicated to calculate the total measurement error for each element in each phase. For more details, see Paper 5.

3.3 Computational Fluid Dynamics (CFD)

In all parts of this project, experimental investigations have been complimented with Computational Fluid Dynamics (CFD) modeling. All the modeling was performed by Jan Erik Olsen at SINTEF Materials and Chemistry and published and to-be-published modeling results and interpretation of these results will be used in order to explain observed phenomena in the present work. The elaborated description of the modeling parameters is found in the published papers[68, 69].

CFD modeling is a tool which can increase the understanding of the flow-patterns in and above the silicon melt. It can be used for qualitative understanding, but also for quantitative modeling. In several cases, the model has been "tuned" to fit the experimental results in terms of measured amounts of silica. An important

function of the CFD modeling has been sensitivity analysis. In especially industrial experiments it is not trivial to change or control all parameters. As such, CFD modeling may be used to get a macro-picture of limiting parameters.

In the industrial measurements, CFD modeling of the flow in the melt was done for a qualitative picture, and it was also found that in the active oxidation of the surface of the silicon, the "supply" of silicon to the surface was not the limiting parameter as the surface velocity is high and hundreds of kilograms of silicon are flowing towards the surface per second. In further modeling it was thus possible to model a wall of silicon with infinite access of silicon. In order to model the fume rate, a sensitivity analysis was done, where several parameters were tested; a flow of nitrogen through the "wall" of Si (from the refining bubbles), temperature in the melt, emissivity of the silicon surface, surface area of exposed silicon and the effect of different lid designs. All these parameters would be impossible to test for or analyze in the industry. Fume rate was plotted as a function of all these parameters, and the flow/natural convection in the air above the melt was modeled to see if the change in parameters had an effect on the flow pattern and gas velocity magnitude.

In the small-scale experiments, the CFD modeling was used to make sure the flow in the tube, and especially above the silicon surface, was indeed laminar. The laminar gas flow was an assumption made in order to use the classical flat plate theory in the theoretical calculations of the mass transfer coefficient. Furthermore, a CFD-modeled mass transfer coefficient for oxygen was found and compared to the theoretical and measured mass transfer coefficients. The modeling was done for all gas flows tested in the experiments, and the results became a very useful tool when it came to analysis of measured data.

In the induction furnace experiments, the only gas velocity we could directly calculate with some certainty was the velocity at the tip of the lance. The overall flow pattern could only be coarsely envisaged from theory on impinging jets. However, when a fundamental understanding of the active oxidation of liquid silicon in air was the goal of these experiments, a better understanding of the flow was imperative for the results. The CFD modeling gave the gas velocity close to the surface, and these data were further used in the laminar impinging jet theory to calculate the theoretical mass transfer coefficient for oxygen.

3.4 Diffusion coefficient and viscosity

In order to evaluate the settings of experimental parameters, and to interpret results by comparing to theoretical calculations, the physical properties of the gases had to be determined for every experimental condition. In this section, the calculations are elaborated and examples are given.

The binary diffusivity of gases at low density is given by the Chapman-Enskog equation:

$$D_{AB} = 0.0018583\sqrt{T^3\left(\frac{1}{M_A}+\frac{1}{M_B}\right)}\frac{1}{p\sigma_{AB}^2\Omega_{D,AB}} \tag{3.1}$$

Where T is temperature [K], M_i is the molecular mass of species i, p is pressure, σ is the collision diameter, and $\Omega_{D,AB}$ is a collision integral, which is a tabular value found by calculating the dimensionless temperature, $k_B T / \varepsilon_{AB}$, where k_B is the

Boltzmann constant and ε_{AB} is the characteristic energy of interaction. The combined values for σ_{AB} and ε_{AB} is calculated from

$$\sigma_{AB} = \tfrac{1}{2}(\sigma_A + \sigma_B) \; ; \quad \varepsilon_{AB} = \sqrt{\varepsilon_A \cdot \varepsilon_B} \tag{3.2}$$

These combining rules predict values for DAB within about 6 % for non-polar gas pairs. Tabular values for σ_A and ε_A for SiO and SiO_2 were found in a NASA report from 1962[70], and are given in Table 3-2 together with the values for oxygen, argon and nitrogen.

Table 3-2: Lennard-Jones parameters for a argon, oxygen, nitrogen, silicon monoxide and silicon dioxide [12, 70]

Species	M_i, **[g/mol]**	σ , **[Å]**	ε/k, **[K]**
Ar	39.948	3.432	122.4
O_2	31.999	3.433	113
N_2	28.013	3.667	99.8
SiO	44.085	3.374	569
SiO_2	60.085	3.706	2954

As an example, the diffusion coefficient and viscosity of 1 % O_2 in Ar is calculated with all details below:

$$\sigma_{O_2-Ar} = \tfrac{1}{2}(3.433 + 3.432) = \underline{3.4325 \ \text{Å}} \; ; \quad \frac{\varepsilon_{O_2-Ar}}{k} = \sqrt{113 \cdot 122.4} = \underline{117.61 \ K} \tag{3.3}$$

In which the ε_{O_2-Ar}/k value is used to calculate kT/ε_{O_2-Ar} that we need to find the tabulated value of Ω_{D,O_2-Ar}. At 1500°C we get kT/ε_{O_2-Ar} = 15, which gives the tabulated value for Ω_{D,O_2-Ar} of 0.69515 (page 865-866 in Bird et al.[12]). Now we have all we need to calculate the diffusion coefficient for oxygen in argon:

$$D_{O_2-Ar} = 0.0018583\sqrt{(1773.15\ K)^3\left(\frac{1}{31.999\ g/mol}+\frac{1}{39.948\ g/mol}\right)} \cdot \frac{1}{1\ atm\cdot(3.4325\ Å)^2\cdot 0.69515} = \underline{\underline{4.02\ cm^2/s}} \tag{3.4}$$

The viscosity of a pure gas is

$$\mu = 2.6693\cdot 10^{-5}\frac{\sqrt{MT}}{\sigma^2\Omega_\mu} \tag{3.5}$$

Also here Ω_μ is a collision integral which is found in the same table as $\Omega_{D,\,AB}$, but with a different value. For pure oxygen at 1500°C we get kT/ε_{O_2} = 16, which gives Ω_μ = 0.7683 [12]. The viscosity of oxygen at 1500°C is then

$$\mu_{O_2} = 2.6693\cdot 10^{-5}\frac{\sqrt{31.999\ g/mol\cdot 1773.15\ K}}{(3.433\ Å)^2\cdot 0.7683} = \underline{0.0007022\ g/cm\cdot s} \tag{3.6}$$

By doing the same calculation for Ar, we get $\mu_{Ar} = 0.0007697\ g/cm\cdot s$ at 1500°C. The viscosity of gas *mixtures* is calculated according to

$$\mu_{mix} = \sum_{A=1}^{N} \frac{x_A \mu_B}{\sum_B x_B \Phi_{AB}} \tag{3.7}$$

Where N is the number of species in the mixture, x_A and x_B are the mole fractions of species A and B, μ_A and μ_B are the viscosities of the pure species A and B at the system temperature and pressure, and the dimensionless quantity Φ_{AB} is

$$\Phi_{AB} = \frac{1}{\sqrt{8}} \left(1 + \frac{M_A}{M_B}\right)^{-\frac{1}{2}} \left[1 + \left(\frac{\mu_A}{\mu_B}\right)^{\frac{1}{2}} \left(\frac{M_B}{M_A}\right)^{\frac{1}{4}}\right]^2 \tag{3.8}$$

where M_A and M_B are the molecular weights of species A and B, respectively. In order to calculate the different values of Φ_{AB} it is useful to set up a table, see Table 3-3.

Table 3-3: Calculation of Eq. (3.8) and the denominator in Eq. (3.7) for a gas mixture of 1 % O_2 in Ar.

A	***B***	M_A/M_B	μ_A/μ_B	Φ_{AB}	$\sum_{B=1}^{2} x_B \Phi_{AB}$
O_2	Ar	0.8010	0.9123	1.064	1.063
Ar	O_2	1.248	1.096	0.9342	0.9993

From this, the viscosity of the mixture may be calculated:

$$\mu_{O_2-Ar} = \left(\frac{0.01 \cdot 0.0007022 \ \ g/cm \cdot s}{1.063}\right) + \left(\frac{0.99 \cdot 0.0007697 \ \ g/cm \cdot s}{0.9993}\right) = \underline{0.00076912 \ \ g/cm \cdot s} \tag{3.9}$$

These methods for calculating diffusion coefficients and viscosities were applied to SiO in Ar, and also O_2, SiO and SiO_2 in N_2 for the cases when the reactions take place in air (industry and induction furnace).

3.5 Other methods

In the chase for finding the answers to our questions in this project, several different techniques have been used in the exploration of the oxidation of liquid silicon. Some were successful, as illustrated by the papers included in this thesis. However, in the early stages of this work, some experiments were performed with disappointing results, and as such, they were never published. However, for documentary reasons, it is believed important to report all results, not only the successful ones, in order to pass on the knowledge about what does *not* work. In this section, the methods used but not mentioned in papers are described.

3.5.1 Wettability experiments

Wettability experiments were performed in a vacuum, sessile drop furnace set-up with a boron nitride (BN) sample holder of 10 mm size. The sessile drop furnace consists of an outer vacuum chamber, a graphite heating element and a sample holder. A camera system at one side allows visual observation of the sample during the experiment as it proceeds. A calibrated pyrometer is mounted on the opposite side of the furnace, which continuously measures the temperature of the sample. The furnace is shown schematically in Figure 3-1.

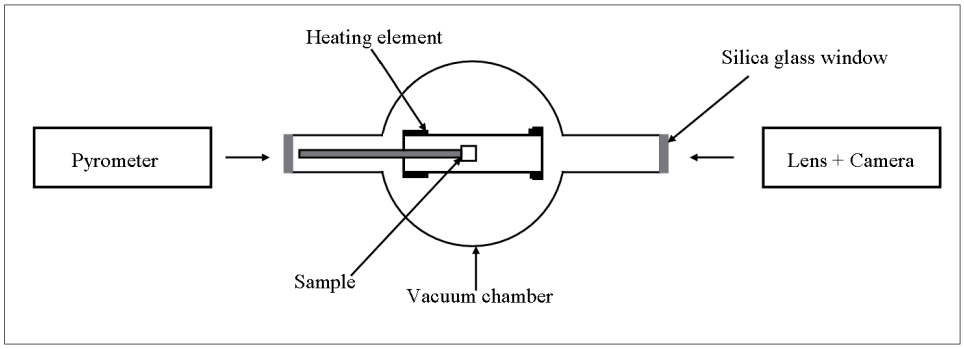

Figure 3-1: Schematic of the sessile drop vacuum furnace.

The vacuum chamber is continuously flushed with argon, and the oxygen partial pressure is typically stable at 10^{-15} atm. This low oxygen partial pressure is obtained by flushing the argon through a separate magnesium furnace kept at 200-300°C prior to the vacuum furnace. One of the reasons to keep such a reducing environment inside the vacuum chamber is because all the parts are made of graphite which readily reacts with oxygen if present at high concentrations at such elevated temperatures.

In the investigation of active oxidation of liquid silicon, this type of apparatus could possibly have provided information about oxidation rate. In the present project, three different samples were tested at two different holding times (1 h and 4 h) and two different temperatures (1450°C and 1650°C). The tested samples were 9N electronic grade silicon, and two alloyed samples; 1 % Al, 0.5 % Ca. The purpose of alloying the electronic grade silicon was to mimic MG-Si and see how the main impurities Ca and Al could affect the oxidation rate.

Cube shaped samples of approximately 3 mm size were placed on the BN substrate and inserted into the furnace. After evacuating the chamber and flushing

with Ar, the heating began. The camera recorded pictures every second. When the goal temperature was reached, the samples were held for either 1 h or 4 h.

After the experiments, the samples were prepared in epoxy and polished for metallographic investigation with EPMA.

3.5.2 Thermo gravimetric analysis (TGA)

In the very beginning of this project, TGA was used to measure the oxidation rate of liquid silicon. Small chips of 9N grade silicon were placed in a BN crucible (ID 5 mm) and heated to 1510 - 1600°C. The crucibles were stored at a constant temperature of 105°C for a minimum of 48 h prior to the experiments to evaporate any water present in the crucible material. Baselines showed that this low temperature baking was necessary to obtain a reproducible mass loss in the crucibles alone. Platinum suspension wires were used to hang the crucible from the balance in the furnace. The samples were held for 1 or 4 hours under air-vacuum, oxygen-vacuum or 20 mL/min flow of Ar under vacuum. The oxygen-vacuum was done to control the oxygen potential in the furnace, thus the chamber was first flushed with pure oxygen and then put under vacuum (1 mbar) before heating. Other parameters that were varied were the crucible type (alumina crucibles were tested) and temperature (it was discovered that 1510°C did not melt the sample, thus 1600°C was used. The furnace temperature was not calibrated).

4 Results and Discussion

4.1 Oxidation of liquid silicon

In the present investigation of active oxidation of liquid silicon, several experimental methods and scales have been applied. The key results from the different studies are presented in Table 4-1, where the scale and experimental conditions are given. The results will be presented in terms of a short summary of the publications they are given in, and then discussed in light of each other and existing literature.

In Paper 1 and 2, the industrial measurements of fume formation are presented. In Paper 2 the overall conclusion is that the surface oxidation of the silicon during refining is the major mechanism for silica formation in the industrial refining process, as opposed to SiO from the bubbles or splashing. Paper 2 also shows the particle size distribution of silica from the refining compared to silica from the furnace top, and it is found that the silica consists of spherical, amorphous and nonporous particles (TEM and BET). In addition to the silica particles, some few large particles 20 - 70 μm in diameter were found (SEM), assumed to originate from splashing of the silicon metal. The amount of silica produced in kg/h is presented and found to increase linearly with the total amount of gas purged through the melt in the refining, which is concluded to be caused by the increased surface area exposed to the air due to more violent stirring with increased gas rate in the purging. An estimate of the flux of silica in moles/m^2s is presented, but because of the difficulty of determining the actual surface area in the industrial case, these values may be overestimates. The amount of silica produces during refining is in the order of 0.8 – 1.7 kg SiO_2 per tonne Si produced.

Table 4-1: Key information and results from the three different scales of experimental investigation of active oxidation of liquid silicon.

Experiment type	**Industrial measurements**	**Induction furnace experiments**	**Small-scale experiments**
Amount of Si	~7000 kg	1750 g	10 g
Gas flow	Turbulent, natural convection	Laminar, forced impinging jet flow	Laminar, forced flat plate flow
Gas composition	Ambient air	Synthetic air, water saturated air, air + Ar	Ar + O_2
Silicon surface	Gas stirred, turbulent, not flat	Induction stirred, flat	Still, flat
Bulk oxygen partial pressure with active oxidation	0.21 atm	0.21 atm, 0.13 atm, 0.07 atm, 0.042 atm.	$0.5 \cdot 10^{-3}$ – $2 \cdot 10^{-3}$ atm
Measured flux of SiO_2	2.5 - 5.1 kg/h ≈ $3.1 \cdot 10^{-2}$ - $7.6 \cdot 10^{-2}$ mole/m²s *	Dry air: $1.2 \cdot 10^{-3}$ - $3.9 \cdot 10^{-3}$ mol/m²s Wet air: $2.8 \cdot 10^{-3}$ mol/m²s Diluted air: $3.5 \cdot 10^{-3}$ - $6.5 \cdot 10^{-3}$ mol/m²s	$2.5 \cdot 10^{-4}$ - $7.5 \cdot 10^{-4}$ mol/m²s
Particle size (silica)	56 – 66 nm (SEM)	40 – 91 nm (BET)	~50 – 200 nm ** (not measured)

* Calculated from estimated surface area. Probably overestimates.
** Samples collected were mixtures from several experiments and polluted with other materials, thus BET was not useful.

In Paper 3, a fundamental oxidation study of a stagnant liquid silicon surface is presented. The experimental mass transfer coefficient was found and compared to the theoretical and CFD-modeled mass transfer coefficient. The maximum bulk oxygen partial pressure for active oxidation was found to be $2 \cdot 10^{-3}$ - $5 \cdot 10^{-3}$ atm. At oxygen pressures above this, a silica film was formed on the silicon surface. The oxidation rate was a linear function of the square root of the linear gas velocity $\left(v_g^{\frac{1}{2}}\right)$, which fits with the flat plate theory for the mass transfer coefficient (see Eq. 2.12). The reaction product from the active oxidation was the same as found in the

industry; small amorphous particles with a spherical shape. Thus, the reaction mechanism from the industry was reproduced, but not the rate (see Table 4-1).

In Paper 4, the results from induction furnace experiments are presented. In this experimental setup, the situation found in the industry was mimicked in terms of having a moving silicon surface (due to induction, as opposed to bubble stirred in industry). Synthetic air was blown towards the silicon surface through a lance. It was found that the flux of silica is a linear function of the linear gas velocity to the power of ¾, which fits with impinging laminar jet theory. In addition to experiments with pure synthetic air, humid and diluted air was also tested. The former was performed to test the effect of water in the gas on the oxidation rate, as most of the silicon plants in Norway are situated in humid environments by the fjords. The dilution experiments were performed in order to determine the dependence of the silica flux with increased gas flow (i.e. thinner boundary layer) and with increased oxygen input per time unit. It was found that the flux of silica increases significantly with flow and only incrementally with oxygen amount, thus the factor determining the oxidation rate is the degree of transport of oxygen to the surface. With a smaller boundary layer to diffuse through, the flux of oxygen and thus silica becomes larger. The experimental SiO pressure at the surface was calculated and found to be principally the same for all gas flow rates (0.0037 - 0.0068 atm), with only 25 % variation. This indicates that SiO will not accumulate, but be transported away from the surface faster than oxygen is transported inwards to the surface. The product in the experiments was the same as was found in the industry, but the rate of silica formation was not reproduced. The oxygen consumption was calculated and plotted as a function of boundary layer thickness extracted from the CFD modeling. The utilization of oxygen increased with

decreased flow rate, i.e. increasing boundary layer thickness. It was found that the delivery of oxygen is not proportional to the gas flow rate. In the pure synthetic air experiments, the oxygen utilization was 4 – 10 % of the total oxygen input depending on the flow rate, but in the diluted experiments, the oxygen utilization increased to 38 % (1:4 air:Ar). This is expected, as the flux of silica was found to be similar for equal flow rates, even though the oxygen pressure is substantially lower for the diluted experiments.

In addition to the one experimental setup with dilution presented in Paper 4 (1:4 air:Ar), two more dilutions were tested after submitting the paper for review, namely 1:2 air:Ar and 3:2 air:Ar. The new results showed the same trend; the gas flow rate is a more important factor in the oxidation rate than the oxygen partial pressure in the bulk gas. The measured flux of silicon as a function of the gas velocity to the power of ¾ is shown in Figure 4-1, where all results are included. While the results suggest that the flux of SiO_2 is *increased* with dilution, experimental variations pertain that the measured results are within experimental error, thus the silica flux is similar for the same flow rates. It is believed that the 3:2 diluted point at $10.7 \cdot 10^{-3}$ mole/m^{2}s is an outlier, and will not be included in the discussion. A third parallel of this particular experimental setup is planned before conclusive results are published.

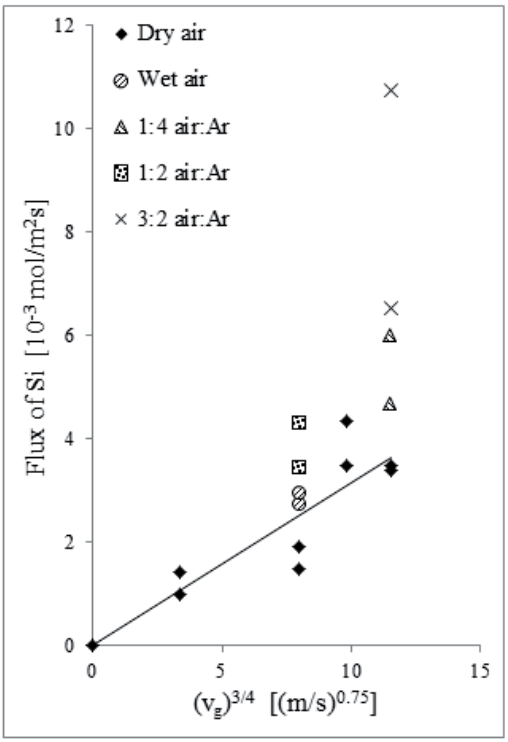

Figure 4-1: Results from induction furnace experiments. Measured flux of Si as a function of gas velocity at lance tip to the power of ¾ ($v_g^{\frac{3}{4}}$). The regression line is for the dry air points only, with an R^2 value of 0.80.

The oxygen utilization in the small-scale and induction furnace experiments are given in Figure 4-2 and Figure 4-3, respectively, plotted as a function of the inverse of the gas velocity close to the surface. The points that are above 100 % in the small-scale experiments are considered as outliers, as they are from the experiments performed at short times and low gas flow rate, and thus the possible effect of contamination of oxygen is higher than at longer experiments. It is clear that the oxygen consumption increases with increased dilution and with lower flow rate. A factor that may be of influence here is the sticking coefficient. The

sticking coefficient was explored to some extent in Paper 4, where the flux calculated from a theoretical mass transfer coefficient from impinging jet theory, and a sticking coefficient of 0.01 gave the same result (in order of magnitude) as the measured results. Thus perhaps it is not only the transport of oxygen, but also the probability of the oxygen close to the surface to actually stick to the surface and react with Si which is a governing factor in the rate of oxidation.

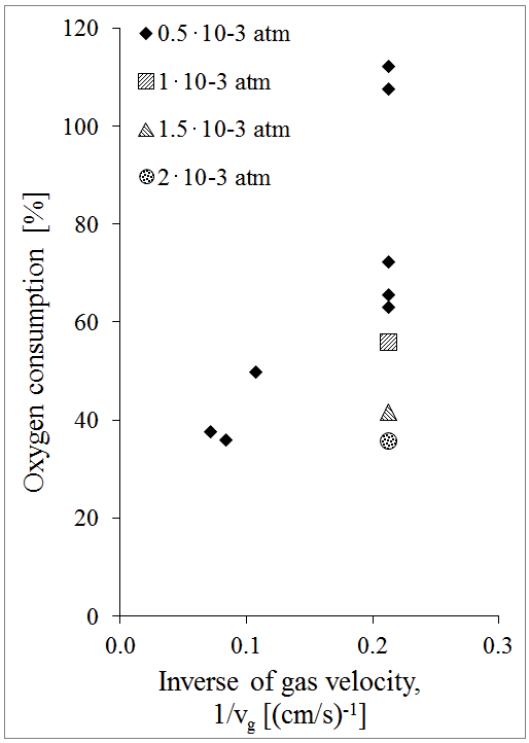

Figure 4-2: Oxygen consumption in the small-scale experiments, plotted as a function of the inverse gas velocity.

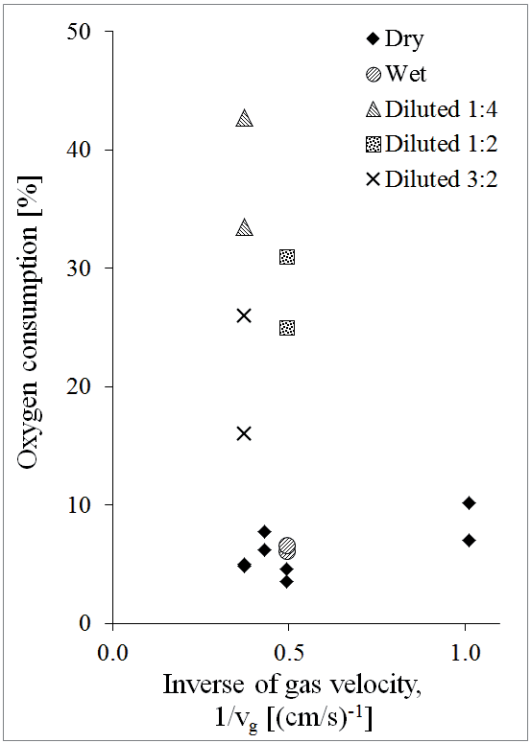

Figure 4-3: Oxygen consumption in the induction furnace experiments plotted as a function of the inverse gas velocity.

As an experiment, the oxygen consumption in the small-scale experiments and the induction furnace experiments was plotted in the same graph. To normalize for the very different oxygen pressures, the x-axis was set to $p^{\circ}_{O_2} / v_g$. The result is shown in Figure 4-4. From the graph it can be seen that at high gas velocity, and/or low oxygen partial pressure, the oxygen utilization is high, whereas at low gas velocity and/or high oxygen pressure, the oxygen utilization is low.

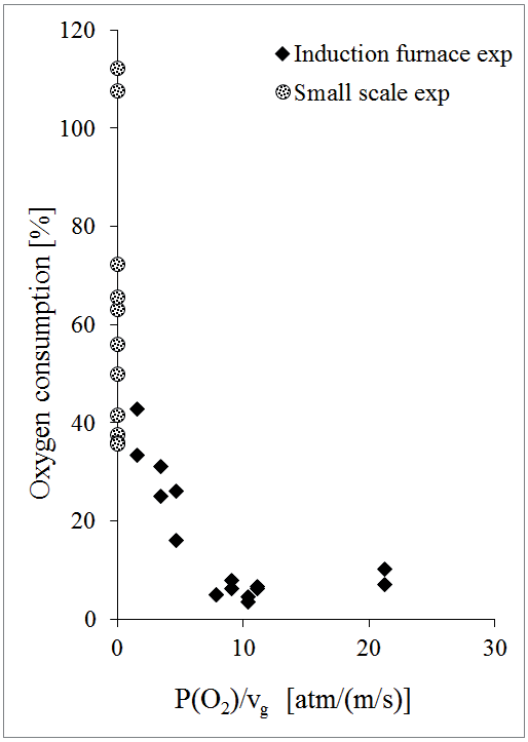

Figure 4-4: Calculated oxygen consumption in small-scale experiments (circle) and induction furnace experiments plotted as a function of $p^{\circ}_{O_2} / v_g$.

The flux measured in the induction furnace experiments are one order of magnitude lower than that calculated from measurements in industry. However, we cannot say that we have a good estimate of the surface area from the industry. In order to find out if the industrial measurements and the induction furnace experiments could be more comparable in terms of flux, the surface area needed in the industry to obtain the flux from the induction experiments was calculated. At the two highest flow rates, 21 and 26 m/s, the industrial surface area would have to be 1.8 – 3.3 m^2, and that is calculated from the lowest amount of fume measured in

the industry; 2.5 kg/h. These values for the surface area might not be too far away from what is possible in the industry.

Let us take a look at the estimated surface area in the industry. The estimation of Si surface area from a spherical segment is shown in Figure 4-5, where the case of a smooth surface (a) and a bubbled surface (b) are indicated. The surface of the smooth surface may be directly calculated with Eq. 4.1:

$$A_{seg} = \pi\left(\frac{c^2}{4} + h^2\right) \tag{4.1}$$

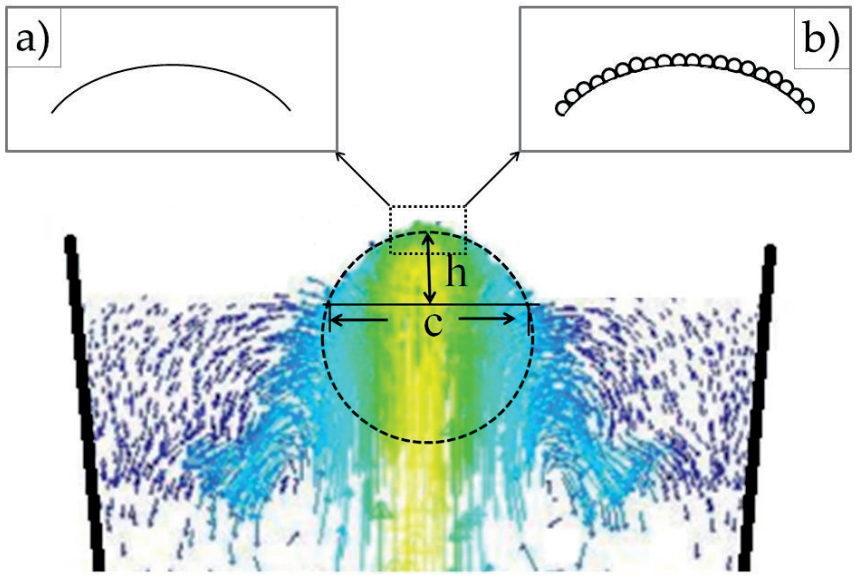

Figure 4-5: Schematic of a spherical segment at the surface used to calculate the surface area of the plume of silicon in the industrial refining. Inset a) represents the smooth surface and b) the bubbled surface due to the refining gas arriving at the surface and thereby increasing the surface area.

When the width of the plume is 0.65 m and the height of the plume is 0.15 m we get a smooth surface area of 0.4 m^2. These values were used in Paper 2 for the calculation of the industrial flux. To mimic the bubbles arriving at the surface (Figure 4-5 b), we can divide this smooth surface into small bubbles of width and height 0.0065 m and 0.003 m, respectively (typical modeled bubble diameters are 1 - 10 mm[71, 72]). The area of the plume is now 0.75 m^2, which is an 82 % increase in the surface area. As we do not know how big the bubbles arriving at the surface really are, we can comfortably guess the surface area to increase with 100 % (to 0.8 m^2) due to the bubbles. Moreover, as we do not know the exact height of the plume (the width was measured from pictures), we can assume for example h = 0.25 m, and thus the doubled surface area (100 % increase) due to bubbles would be 1.1 m^2. With this area and the smallest measured amount of silica of 2.5 kg/h, the flux becomes 0.011 mol/m^2s. This flux is still much higher than the flux found in the small-scale experiments ($2.5 \cdot 10^{-4}$ - $7.5 \cdot 10^{-4}$ mol/m^2s), but is only approximately half an order of magnitude larger than the measurements obtained in the induction furnace at the highest flow rates ($3.5 \cdot 10^{-3}$ - $6.5 \cdot 10^{-3}$ mol/m^2s). Furthermore, taking the measurement uncertainty in the LaserDust MP into account (30 %), the values may be even closer.

Assuming that the conclusion in Paper 2 is correct; that the measured increase in silica production is mainly due to increased surface area of exposed silicon, then the actual physical flux in mol/m^2s should be the same for all the measurements in the industry (assuming that the gas flow rate above the surface is the same). This implies that when the measured amount of silica was 5.1 kg/h, the surface area of the silicon would have to be 2.2 m^2. This is not an unimaginably large surface area for such a dynamic surface as the one observed in industry. In fact, looking at

videos recorded with an infra-red camera, the liquid metal is flowing onto the peripheral slag-layer and back into the "plume hole", thus a much larger surface area than initially estimated is easily visualized. A snapshot-from one of the IR-films is given in Figure 4-6, where the liquid silicon is indicated.

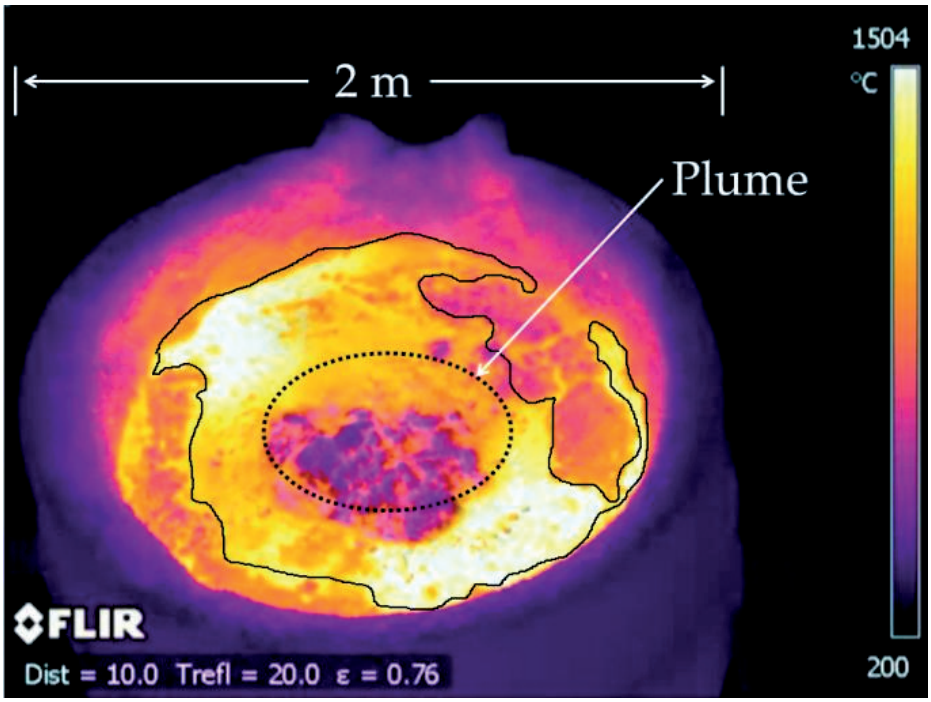

Figure 4-6: Snapshot from an infrared video of the refining ladle. Temperature scale to the right. The plume is indicated with a dotted line, and the area of the actually moving liquid silicon is indicated with a solid line.

The snapshot in Figure 4-6 shows that the actual surface area of moving, exposed liquid silicon may be significantly bigger than if only the plume is included in the estimation of the surface area. It is thus believed that the fluxes

measured in the induction furnace and the actual flux in the industry is most likely in the same order of magnitude.

There is a certain contradiction in the results found in the small-scale experiments and the induction furnace experiments/industry: The boundary condition for active oxidation of liquid silicon at 1500°C in terms of oxygen partial pressure is in the order of $2 \cdot 10^{-3}$ atm, but active oxidation is clearly happening in air atmosphere ($p^{\circ}_{O_2} = 0.21$ atm) in the industry and the induction furnace experiments. This is a 100 times higher oxygen pressure than the maximum oxygen partial pressure found by small-scale experiments and thermodynamically calculated (theoretical $p^{\circ}_{O_2}(\max) = 8.6 \cdot 10^{-3}$ atm). However, in reference to the result found by Engstrom et al.[24, 25] (1991, 1992) and Lander and Morrison (1962)[26]; at low coverage of adsorbed O-atoms at the silicon surface, the kinetically favorable path for the Si-O units is to desorb as $SiO_{(g)}$ rather than migrating together (slow) to form an oxide layer. For a still silicon surface, like in the small-scale experiments, the O-coverage can accumulate and become high, and thus there is a lower limit for the oxygen partial pressure before the most favorable path for the Si-O units becomes the migrating and oxide forming. Conversely, in the industrial refining and the induction furnace experiments, the surface is moving with constantly fresh silicon surface being exposed. It is easily imaginable that the O-coverage of this dynamic surface is constantly low, and that the kinetically favorable path for the Si-O units is to go off as $SiO_{(g)}$, even though the oxygen pressure is very high. The $SiO_{(g)}$ is a counter flux to the incoming oxygen and is readily oxidized to $SiO_{2(g)}$, which condense to become $SiO_{2(s)}$, now known as fume. It is therefore believed that

the combination of the slow kinetics of the oxide forming mechanism and the dynamic surface is what makes the active oxidation of liquid silicon in air possible.

4.1.1 Condensation of SiO_2

The method presented by Kamfjord et al.[7] (2012), based on Ulrich's[31] equations (1971) may be used to calculate the formation time for a particle of a specific size.

$$N = \left(X \cdot C_0^{\frac{1}{6}} \cdot t \right)^{-\frac{6}{5}} \tag{4.2}$$

$$SA = \frac{Y}{\left(X \cdot t \right)^{\frac{6}{5}}} \cdot C_0^{-\frac{2}{5}} \tag{4.3}$$

where

$$X = 4c \left(\frac{3k_B T}{\rho} \right)^{\frac{1}{2}} \left(\frac{3M}{4\pi N_A \rho} \right)^{\frac{1}{6}} \tag{4.4}$$

$$Y = \frac{3}{\rho} \left(\frac{4\pi N_A \rho}{3M} \right)^{\frac{1}{3}} \tag{4.5}$$

Here, N is the concentration of particles [cm^{-3}], C_0 is the concentration of SiO_2 molecules [cm^{-3}], t is time [s], c is the sticking coefficient, set to be 0.3 by Ulrich, k_B is the Boltzmann constant [$1.38 \cdot 10^{-16}$ erg/K], T is temperature [K], ρ is density of SiO_2 [2.2 g/cm^3], M is molar mass of SiO_2 [60 g/mol], N_A is Avogadro's number [$6.022 \cdot 10^{23}$ mol^{-1}] and SA is the specific surface area [cm^2/g] (= $3/(\rho \cdot r)$). As C_0 is an

unknown, if both equations Eq. 4.2 and Eq. 4.3 are rearranged to be equal to C_0, they can be set equal to each other, and thus the new equation can be rearranged to find the time, t:

$$t = \frac{SA^{\frac{1}{2}}}{X \cdot Y^{\frac{1}{2}} \cdot N} \tag{4.6}$$

This rather simple equation may be used to calculate the time needed to form a particle with a defined particle size. From the BET measurements, the average particle size in the experiments in Paper 4 was found for the different experimental conditions. If this particle size, together with measured flux, is used to calculate the concentration of silica particles is in the "off gas" (N), all values in Eq. 4.6 are known, and the formation time can be calculated. Using the theoretically calculated mass transfer coefficient for SiO_2, the distance traveled during formation can be calculated and compared to the boundary layer thickness extracted from CFD. The measured particle size, calculated formation time, distance traveled and boundary layer thickness are given in Table 4-2.

Table 4-2: Measured average particle diameter, calculated formation time and distance traveled for the silica collected at different experimental conditions in the induction furnace experiments, and the average boundary layer thickness from CFD modeling. The gas velocities given are at the tip of the lance.

Gas velocity and composition	**5 m/s air**	**16 m/s air**	**21 m/s air**	**26 m/s air**	**16 m/s wet air**	**26 m/s 1:4 air:Ar**
Avg. particle diameter, nm	91	63	72	66	57	40
Calc. formation time, s	0.013	0.011	0.009	0.010	0.005	0.002
Distance traveled, mm	0.5	0.9	0.9	1.2	0.4	0.2
Average boundary layer thickness from CFD, mm	4.6	3.2	3.0	2.5	3.2	2.5

Using the combination of Ulrich's equations, calculated mass transfer coefficient and CFD-modeling, it may be shown that the distance the particles travel during formation is approximately one order of magnitude shorter than the boundary layer thickness. This indicates that the silica particles are formed within the boundary layer and that a heterogeneous boundary layer is the most probable case.

In Chapter 2, thermodynamic and kinetic tests given by Arato et al.[19] were presented. In their paper, Arato and co-workers apply the described tests to the case of tin. To find out if the formation and condensation of SiO_2 happens inside the boundary layer in the case of silicon at 1500°C, we may use the values presented in Table 4-3.

Table 4-3: Values for the parameters needed to evaluate the silicon system according to Arato's tests. The partial pressures are only given in orders of magnitude, as the tests are rough estimations only, thus approximate values are sufficient.

T	1773 K
P	1 atm ≈ 100 000 Pa
$p^{\circ}_{O_2}$	10^{-3} atm
$p^{*}_{O_2,\max}$	10^{-18} atm
p^{*}_{Si}	10^{-6} atm
p^{*}_{SiO}	10^{-2} atm
$p^{*}_{SiO_2,\max}$	10^{-9} atm
λ	10^{-7} m

The equilibrium pressures for the different species are calculated with HSC Chemistry[8] and the method described in Chapter 3.4.1, and the mean free path is calculated from Eq. 2.19. The boundary layer thickness is set to be 0.5 cm, as in Arato's estimations. In this calculation, it is assumed that the maximum partial pressure of SiO_2 is the thermodynamic saturation pressure, as Ulrich suggested that a single SiO_2 molecule is the minimum nucleus for nucleation and growth of SiO_2-particles. Using these values in Equation 2.17, 2.18 and 2.20, we can see that Test 1 is not satisfied, Test 2 is not satisfied, but Test 3 is satisfied. In other words, both the chemical thermodynamics and the kinetics favors formation of $SiO_{2(g)}$ inside the boundary layer, but the kinetics does not favor the condensation. This simple evaluation of the system leads to the assumption that there will *not* be a heterogeneous boundary layer. However, the reaction between SiO and O_2 takes place inside the boundary layer, thus some of the oxygen will be consumed before reaching the silicon surface, according to this model.

From the Ulrich and Arato calculations, we now have two opposing conclusions. However, the Ulrich calculation does not specify where the condensation starts. Thus if the Arato calculation is correct, the condensation may take place outside the boundary layer, and the distance traveled found using Ulrich's formation time and the theoretical mass transfer coefficient may just as well be a distance traveled in the bulk gas. It is not possible to make a clear conclusion from these rather simple and rough estimations, but it may be assumed that while oxidation of SiO to SiO_2-gas happens inside the boundary layer, the condensation takes place outside the boundary layer.

The fume particle sizes from the induction furnace experiments at high gas velocity in dry air are very similar to the measured average particle diameter in the

silica collected during refining in the industry. The industrial average was found from measuring and counting particles from SEM images, as the silica from SiO-combustion were the particles of interest and not the splashing particles. Ulrich suggested SEM particle counting as a subjective and imprecise method, and argues that BET is the best method for determination of average particle size. The BET measurements of the industrial samples gave specific surface areas of 13.2 - 14.9 m^2/g, which corresponds to average diameter of 210 - 180 nm. The average diameters calculated from particle counting however, were 56 - 66 nm, which is a significant difference. However, as mentioned earlier, it was discovered some few very large particles in the SEM images, 20 - 70 μm in size, and these were not counted in the particle size distribution, because they are assumed to come from a different mechanism. By adding six such large particles (which is a typical number of large particles observed in the SEM) with a diameter of 20 μm to the particle size distribution from the SEM, the average particle diameter increased to become 189 - 210 nm, which corresponds to the BET measurements. Thus in the case of industrial samples it can be concluded that the particle counting from SEM images is the better method, rather than BET, to obtain an average particle size for the silica. BET counts in the splashing-particles, which makes the measurements wrong when considering particles from the surface oxidation only.

4.1.2 CFD modeling

As part of the same overall project, CFD modeling has been used in several occasions as a tool to better understand the flow fields in the gas phase above the silicon melt. The industrial refining has been explored in two publications by Jan

Erik Olsen[68, 69] (with the present author as co-author), and a short summary of the results will be given here.

In the paper from 2011[68], a sensitivity analysis of the factors affecting the rate of fume formation in a silicon refining ladle was performed. Effect of temperature in the melt, emissivity of the melt, exposed melt surface area and different lid designs were tested. It was found that the temperature is not a governing factor, as the fuming rate was more or less the same at 1527°C and 1627°C. The emissivity of the silicon surface was found to be a significant factor when the exposed silicon surface is large (>1 m^2), but at lower surface areas the effect is minor. The most significant factor for fume formation was the exposed silicon surface area, confirming the experimental observations in Papers 1 and 2. The flow in the air above the ladle was modeled, and the natural convection driving the air towards the surface along the center axis gave a radial gas velocity of 0.5 - 1.5 m/s close to the surface.

It was found that an edge lid has little effect on the rate of fume formation. This lid design is typically practiced in the silicon industry today, with the main purpose to gather the fume for better capture. A modeled lid situated in the center of the ladle reduced the fume formation significantly. This was explained by the flow pattern, and that the center lid blocks the air driven towards the silicon surface. A center lid would probably not be very practical in the industrial situation, as sampling of the melt and temperature measurements are done in the center where the silicon is open to the air (the plume).

In the second CFD-paper concerning the industrial fume formation[69], another sensitivity analysis was made. The tested parameters were surface area, temperature, nitrogen flux through the melt (from refining bubbles), silicon

emissivity, adsorption coefficient of the gas/fume and reaction rate of the reactions included in the model. All parameters were increased with 10 %, and the response in fuming rate was found. Again, by far the most important parameter was the surface area. A 10 % increase in the nitrogen flux through the surface reduced the fume formation by 5 %, thus it is not a major factor, but it cannot be left out in the modeling of fume formation. All the other parameters were found to have a minor effect on the fume formation.

The output parameters of interest in the CFD modeling of the industrial refining and the induction furnace experiments were the amounts of fume from measurements/experiments compared directly to the model. Early attempts on modeling the fuming rates yielded an overestimate of the fume formation. This was due to an incomplete description of the reaction scheme at the interface between gas and silicon. Thus proper mass balances needs to be incorporated into the model. The new model accounts for oxygen penetrating into the metal and reacting with silicon to form SiO gas. The stoichiometry of this reaction needs to be reflected in the model stating that $J_{SiO} = -2J_{O_2}$ in conservation of molar flux at the interface. Together with the general expressions for fluxes in gas and metal, this leads to an appropriate mass balance model at the interface. Results based on this model display good correlation to the measured flux of silica in the induction furnace experiments, shown in Figure 4-7.

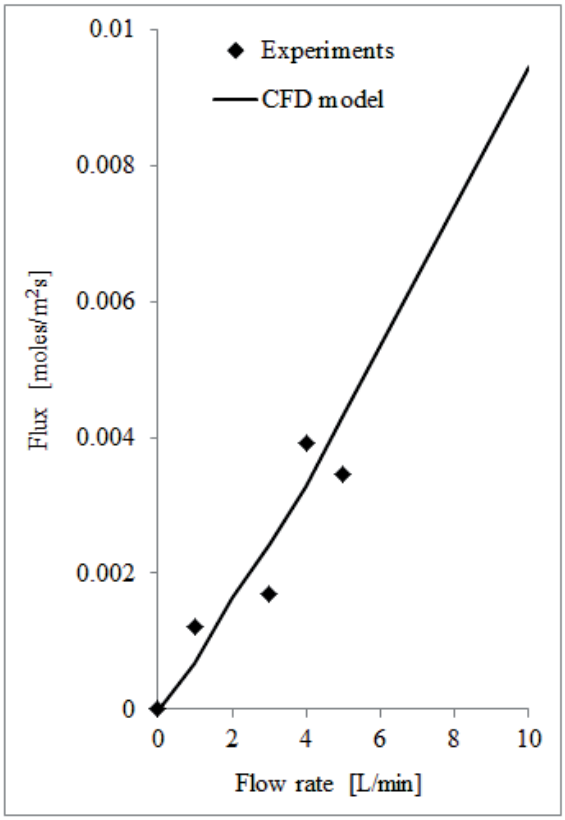

Figure 4-7: Comparison between the experimentally measured fluxes (♦) with varying gas flow (L/min) of synthetic air, and the CFD modeled flux (solid line).

It is planned to use the new and more complex model in the modeling of the ladle refining to obtain a more accurate model of the industrial fume formation rate.

4.2 Element distribution

A large measurement campaign was performed at a silicon production plant where the results presented in Papers 1 and 2 concern the quantification and characterization of the fume. Simultaneously, we sampled all ingoing and outgoing phases of the refining ladle, in order to obtain a complete element mass balance and distribution analysis of the refining ladle, similar to the one developed by Myrhaug and Tveit/Garcia and Myrhaug for the production furnace. From eight ladles, a total of 105 samples were collected. The samples were crushed and analyzed with HR-ICP-MS for 62 elements, both main elements and trace-elements were studied. These results are presented in papers 5 and 6.

Paper 5 mainly focuses on measurement errors in the sampling, and estimation of emissions via the fume. Sample treatment processes were also assessed. The goal was to obtain a total measurement error for estimating annual emissions of elements via the fume. Several sources of error involved in the sampling process and sample treatment were estimated. The main parameter of variation was found to be the production process itself. In addition, the measurement of amount of fume involved a rather large source of error due to variations in fume amount during tapping and thus a large standard deviation. For the distribution analysis, the major source of error was found to be lack of homogeneity in the slag samples. It was found that ICP-MS is not suitable for all elements, especially those present in concentrations lower than the instrumental detection limit (IDL). However, it is argued that the analysis of all elements with satisfactory detectability and relative standard deviation in the ICP-MS was correct in the order of magnitude. Consequently, the measured amounts of trace-elements in the fume can be used to estimate annual emissions of toxic and environmentally

harmful elements. In Paper 5, lead (Pb) was used as an example, and the estimated loss of Pb via the fume from the ladle was found to be <1.9 kg per year.

In Paper 6, the main focus was the distribution of elements between the three outgoing phases; refined silicon, slag and fume. The distribution was evaluated with respect to the boiling point and thermodynamic properties of the elements. The recovery for all elements was calculated from the measured results, and was found to be satisfactory for all elements when using the minimum-maximum concentration values found in Paper 5. The measured concentrations in the input phases (tapped silicon, flux material and cooling metal) were used in a thermochemical model, where known input amounts of refining gas and additives were used. The modeled end-concentrations of 19 (17 for slag) elements were compared to the measured concentrations in the output phases. The modeled results were in the same order of magnitude for 13 elements in the refined silicon. However, in the slag only Al, Ca and Mg were in the same order of magnitude. All other modeled elements in the slag were far from the measured values. In the fume, none of the 19 modeled elements fit with the measured data. However, the evaporation of impurities from silicon metal is likely controlled by kinetic factors, rather than thermodynamic. Therefore, it is expected that the discrepancies between equilibrium calculations and measured values for fume are relative large. These results show that there is a need for fundamental thermodynamic studies of trace-elements distribution in the silicon refining process, especially for slag and fume/gas.

The elements not included in the model due to lack of thermodynamic data, were discussed with respect to the boiling point and oxidation potential. Most elements with a more negative oxidation potential than silicon was found in the

slag, however some elements (such as Th, Hf, U, and Pr) were present in such low concentrations that they would not be refined from the silicon. It is assumed that the activity coefficients of these elements show negative deviation from ideality. Some elements with high boiling points were found in high concentrations in the fume. These elements (such as Ag, Pb and Zn) were found to have high vapor pressures at 1500°C, and thus they will readily report to the fume.

4.3 Other investigations

4.3.1 Wettability

The results from the experiments performed in the sessile drop furnace showed that there was no significant loss of silicon (the size of the drop did not decrease significantly). Thus active oxidation of the silicon did not occur to a large extent, even though the oxygen pressure inside the chamber designates that the system would be in the active oxidation range. In the EPMA images, a layer of SiC was found on the silicon surface, as can be seen in Figure 4-8. This indicates that the atmosphere inside the furnace is not Ar with O_2 at 10^{-15} atm partial pressure, but rather that the oxygen has reacted with the graphite in the furnace to form CO gas, which further reacted with silicon to form SiC:

$$2Si_{(l)} + CO_{(g)} \rightarrow SiC_{(s)} + SiO_{(g)} \tag{4.7}$$

As a decrease in the drop size was not observed, the production of a SiC layer must have passivated the surface early in the experiment and hindered further reaction between Si and CO, which also forms SiO.

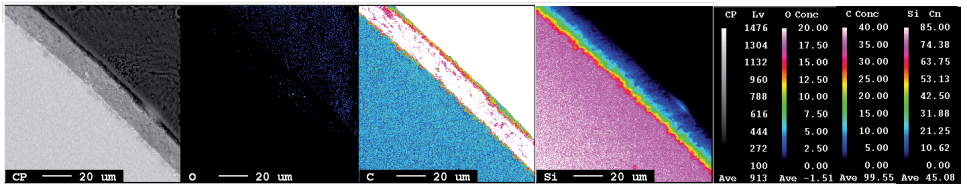

Figure 4-8: EPMA mapping of a typical sample from the wettability experiments. The sample is pure silicon held at 1450°C for 4 hours.

All samples showed the same behavior with the SiC layer, the lack of any significant oxide layer and no reduction in size. Consequently, it was concluded that the sessile drop method in a graphite furnace is not suitable in the investigation of active oxidation of silicon. If the furnace had an alumina interior and a different heating element, the method would probably be more appropriate for this type of investigation.

4.3.2 TGA

The first series of TGA experiments were run with an air-vacuum atmosphere, and a linear decrease in the weight was observed. However, as gases are far from ideal when in vacuum at high temperature, there was no way of knowing or estimating the oxygen potential inside the furnace. As such, the results were not useful to conclude regarding the oxidation rate with respect to the oxygen pressure.

A new experimental setup was used, where pure oxygen was evacuated to a pressure of 10^{-3} atm. This led to failure in the furnace, where the BN crucible and the silicon reacted both with each other and the suspension wire and fell down.

This resulted in an expensive repair of the equipment and three weeks down time for the TGA. A different wire was tested, however with the same result.

The third experimental setup was with pure oxygen under vacuum and an alumina crucible. In this case the crucible cracked and fell down, and the experiment was stopped. The failure of the crucible happened after some time, so some data were recorded, however, glassy silica was found on the suspension wire, which in turn would affect the recorded weight of the sample.

After several runs and different experimental setups, it was concluded that the TGA was not suitable for investigation of active oxidation of liquid silicon. Either the weight loss was good and reproducible, but then with no information on the oxygen concentration, or, the oxygen concentration was known, but reactions between silicon, crucible and/or suspension wires led to expensive failure of the equipment.

5 Conclusions and Future work

5.1 Conclusions

In the investigation of active oxidation of liquid silicon, experiments on three different scales have been performed; industrial measurements, induction furnace experiments, and small-scale experiments. Furthermore, an element balance of 62 elements between gas and condensed phases in the industrial refining ladle has been performed, and the accuracy of the measurements has been evaluated for emission reporting purposes. CFD modeling and thermochemical modeling have been used to complement the experiments and measurements and to increase the understanding of the measured results

The questions asked in this work have been:

1. How much silica fume is produced during industrial refining of silicon, and what are the factors determining/limiting the rate of fume formation?
2. What is the main mechanism for fume formation in industrial silicon refining?
3. What are the characteristics of silica fume (particle size, shape, structure, elemental content) and what characterization methods are applicable to determining these properties?
4. What are the boundary conditions for active oxidation of liquid silicon, and how does it vary with oxygen pressure and gas flow rate?
5. Is gas flow rate or amount of oxygen available the most important factor for the fume formation kinetics?
6. When and where does the SiO combust to form SiO_2, and does the silica condense inside or outside the boundary layer?

7. What does the fume from the industrial refining ladle contain other than SiO_2, and where do these impurities come from? A mass balance on the refining ladle is needed.
8. With what level of accuracy can elemental distribution between condensed and gaseous phases in industrial silicon refining be determined for emissions reporting purposes?

The research questions are answered in the three following sections.

5.1.1 Oxidation mechanism and kinetics

1) In the silicon refining process the amount of fume formed is in the order of 0.8 – 1.7 kg SiO_2 per tonne Si produced, depending on the purging rate. Fume from tapping and refining combined is in the order of 7 – 13 kg SiO_2 per tonne Si.

   Exposed surface area is the major factor determining the rate of fume formation in the industrial refining process. Availability of oxygen is the limiting factor for $SiO_{(g)}$ and subsequent fume formation.

2) The main mechanism of fume formation in the MG-Si refining is active oxidation of the liquid silicon surface in contact with air. Splashing of the metal due to the gas stirring and $SiO_{(g)}$ from the refining bubbles are minor but contributing mechanisms.

3) The silica found in industry, small-scale experiments and induction furnace experiments has the same characteristics; amorphous, spherical and non-porous particles with average particle size in the range 40 – 92 nm. Primary particles with diameters down to 10 nm are found in the industrial fume. The size of particles is concluded to be a function of the temperature and flow condition under which the particle has nucleated and grown.

4) The maximum bulk oxygen partial pressure for active oxidation of a still silicon surface is $2 \cdot 10^{-3}$ atm. The flux of silica is linear with the square root of the gas velocity in the laminar flat plate gas flow regime, and a linear function of the linear gas velocity to the power of ¾ in the impinging laminar jet flow regime. These experimental mass transfer dependencies on the gas velocity are in accordance with the theoretical mass transfer for their respective flow fields. It is believed that the mass transfer in the industry will

be closer to the induction furnace experiments with the impinging jet, due to the gas flow above the silicon surface induced by natural convection in the industrial situation.

5) Gas velocity close to the surface (i.e. the boundary layer thickness) is a more important factor in the rate of fume formation, than the oxygen partial pressure in the bulk. SiO will not accumulate at the surface, but be readily removed and further reacted with incoming oxygen. The transport of oxygen to the surface is the primary factor determining the fume formation.
6) It has been theoretically demonstrated that $SiO_{2(g)}$ may be formed inside the diffusion boundary layer, but that the kinetics of silica gas condensation is slow, and thus the formation of the silica particles by condensation will most probably take place outside the boundary layer.

It is believed that the movement of the surface is the reason why the active oxidation can take place in air. The uncovered silicon surface is constantly renewed, and the kinetically favored path for a Si-O unit is to go off as SiO when the coverage of O-atoms at the Si-surface is low.

5.1.2 Element distribution in the refining ladle

7) The element distribution in the industrial refining ladle has been experimentally determined for both main and trace-elements. The equilibrium concentration of 19 elements in the silicon and fume, and 17 elements in the slag was thermochemically modeled and compared to the industrial measurements.

   For 13 of 19 elements with known activity coefficients in silicon, their modeled concentration in the silicon phase is in agreement with measured values from industry. The thermochemical model for the slag did not agree with the measured values for 14 of 17 elements (only Al, Ca and Mg were in agreement). For the fume, the thermochemical model did not agree with the measured values for any of the 19 elements modeled.

   For the elements with no thermochemical information, most pathways are predicted by looking at the boiling point and oxidation potential. The elements not following these theories either have a high vapor pressure (high boiling point but found mostly in fume) or are believed to exhibit negative deviation from ideality in liquid silicon (found mostly in silicon, but should have gone to the slag).

8) It is possible to predict fugitive emissions of 62 elements for reporting purposes (order of magnitude) using the method presented in Paper 5. However, fundamental investigations are needed for a more accurate thermochemical prediction of trace-elements pathways in the silicon refining ladle.

Elements with measurable higher concentrations in the fume than in slag and silicon are Ag, As, Bi, Cd, Cu, Ga, In, K, Mg, Na, P, Pb, Rb, Sb, Se, Sn, Tl, and Zn, with all being in the ppm range.

5.1.3 Methodology

3) Particle counting from SEM images is, in the case of industrial samples, the better method to obtain an average particle size for the silica, rather than BET. The industrial samples contain splashing-particles, which alter the average particle size measurements greatly and obscure the result when the particles from the surface oxidation are the only particles of interest.

A new CFD model with a complex reaction scheme has been developed. This model may be used to quantitatively model the rate of fume formation in the Si-O system, and thus predict the amount of fume formed in the industrial silicon refining process.

When using measured amounts of fume in the units kg/h to calculate the flux of SiO_2 (mol/m^2s), care must be taken when estimating the surface area of exposed liquid silicon. It has been shown that a simple calculation of the plume surface area from a spherical segment with a smooth surface is not accurate: Both bubbles on the plume surface and secondary surfaces from the flowing of silicon onto the slag layer must be taken into account.

5.2 Future work

There are still several unanswered questions that are recommended to investigate further. Areas suggested for further work are

- ✓ Extend medium scale experiments to get a larger data set in order to develop a more comprehensive empirical model for the fume formation. This empirical model together with the developed CFD model will bring a more accurate basis for predicting the rate of fume formation in the industrial refining of metallurgical grade silicon.
- ✓ Simulate the refining process in the induction furnace to obtain a more controlled environment in order to get a more accurate element distribution model. Results may be used for validation and/or expansion of the thermochemical databases.
- ✓ Include gas measurements in the industrial distribution measurements to detail the gas and fume phase composition in the elements distribution in the refining ladle to get a better consistency towards the thermochemical model.
- ✓ Re-evaluate the gas phases in the thermochemical model.
- ✓ Use molecular modeling to verify that the dynamic surface is the reason for the active oxidation in air by testing the oxidation reaction at varying degree of oxygen coverage.

References

1. Nestaas, I., Hunnes, E.G., (2009), *Sammendrag av undersøkelser av støv i Mo i Rana 2007 - 2008*, Molab AS, Official report for the Climate and Pollution Angency.
2. Johnsen, H.L., *Lung Function, Respiratory Symptoms, and Occupational Exposure*, 2008, PhD-thesis, Faculty Division Akershus University Hospital, Department of Respiratory Medicine, University of Oslo, Oslo.
3. Mikola, Joanne. 2000; Available from: http://www.lessontutor.com/jm_respiratory.html.
4. Schei, A., Tuset, J.K., & Tveit, H., *Production of High Silicon Alloys*. 1st ed. 1998, Trondheim, TAPIR forlag.
5. Kamfjord, N.E., *Mass and energy balances of the silicon process. - Improved emission standards*, 2012, PhD, Department of Materials Science and Engineering, Norwegian University of Science and Technology, Trondheim.
6. Wagner, C. (1958), *Passivity during the oxidation of silicon at elevated temperatures*, Journal of Applied Physics, **29**, pp. 1295-1297.
7. Kamfjord, N.E., Tveit, H., Næss, M.K., Myrhaug, E.H., *Mechanisms of NO formation during SiO combustion*, in *3rd International Symposium on High-Temperature Metallurgical Processing,* . 2012: TMS Annual Meeting & Exhibition, Orlando, FL, March 3-7, 2012. .
8. HSC Chemistry 7.0, Outotec. Research Oy, 2009, Helsinki.
9. Hinze, J.W. & Graham, H.C. (1976), *The active oxidation of Si and SiC in the viscous gas-flow regime*, Journal of the Electrochemical Society: Solid State Science and Technology, **123**, pp. 1066-1073.
10. Turkdogan, E.T. , Grieveson, P., Darken, L.S. (1963), *Enhancement of diffusion-limited rates of vaporization of metals*, Journal of Physical Chemistry, **67**, pp. 1647-1653.
11. Young, D.J., & Pint, B.A. (2006), *Chromium volatilization rates from Cr_2O_3 scales into flowing gases containing water vapor*, Oxidation of Metals, **66**, pp. 137 - 153.
12. Bird, R.B., Stewart, W.E. & Lightfoot, E.N. , *Transport Phenomena*. 2nd ed. 2002 John Wiley & Sons, Inc.
13. Kaiser, W. & Breslin, J. (1958), *Factors determining the oxygen content of liquid silicon at its melting point*, Journal of Applied Physics, **29**, pp. 1292-1294.
14. Gelain, C., Cassuto, A., Le Goff, P. (1971), *Kinetics and mechanism of low-pressure, high-temperature oxidation of silicon*, Oxidation of Metals, **3**, pp. 139 - 151.

15. Gulbransen, E.A. & Jansson, S.A. (1972), *The high-temperature oxidation, reduction, and volatilization reactions of silicon and silicon carbide*, Oxidation of Metals, **4**, pp. 181-201.
16. Jacobson, N.S., Myers, D.L. (2011), *Active oxidation of SiC*, Oxidation of Metals, **75**, pp. 1 - 25.
17. Ratto, M., Ricci, E., Arato, E. (2000), *Mechanism of oxidation/deoxidation of liquid silicon: theoretical analysis and interpretation of experimental surface tension data*, Journal of Crystal Growth, **217**, pp. 233-249.
18. Ratto, M., Ricci, E., Arato, E., Costa, P. (2001), *Oxidation of metals with highly reactive vapors: Extension of Wagner theory* Metallurgical and Materials Transactions B, **32**, pp. 903-911.
19. Arato, E., Ricci, E., Costa, P. (2009), *Analysis of Oxygen−Condensate Interactions in Metal Powder Production: Sprayed Particles in a Carrier Gas Phase*, Industrial & Engineering Chemistry Research, **48**, pp. 3649-3656 DOI: 10.1021/ie800402h.
20. Haynes, W.M, ed., *Handbook of Chemistry and Physics (Internet Version 2013)*. 93rd ed. 2012-2013 CRC Press/Taylor and Francis, Boca Raton, FL.
21. Deal, B.E. & Grove, A.S. (1965), *General relationship for the thermal oxidation of silicon*, Journal of Applied Physics, **36**, pp. 3770-3778.
22. Bongiorno, A., & Pasquarello, A. (2005), *Atomic-scale modelling of kinetic processes occuring during silicon oxidation*, Journal of Physics: Condensed Matter, **17**, pp. 2051-2063.
23. Shalav, A., Kim, T., Elliman, R.G. (2011), *SiO_x nanowires grown via the active oxidation of silicon*, IEEE Journal of Selected Topics in Quantum Electronics, **17**, pp. 785 - 793.
24. Engstrom, J.R., Bonser, D.J., Nelson, M.M., Engel, T. (1991), *The reaction of atomic oxygen with Si(100) and Si(111). I: Oxide decomposition, active oxidation and the transition to passive oxidation.*, Surface Science, **256**, pp. 317-343.
25. Engstrom, J.R., Bonser, D.J., Engel, T. (1992), *The reaction of atomic oxygen with Si(100) ans Si(111). II: Adsorption, apssive oxidation and the effect of coincident ion bombardment*, Surface Science, **268**, pp. 238-264.
26. Lander, J.J. & Morrison, J. (1962), *Low voltage electron diffraction study of the oxidation and reduction of silicon*, Journal of Applied Physics, **33**, pp. 2089-2092.
27. Choi, C.H., Liu, D.-J., Evans, J.W., Gordon, M.S. (2002), *Passive and active oxidation of Si(100) by atomic oxygen: A theoretical study of possible mechansims*, Journal of the American Chemical Society, **124**, pp. 8730-8740.
28. Engel, T. (1993), *The interaction of molecular and atomic oxygen with Si(100) and Si(111)*, Surface Science Reports, **18**, pp. 91-144.
29. Pamungkas, M.A., Joe, M., Kin, B.H., Lee, K.R. (2011), *Reactive molecular dynamics simulation of early stage of dry oxidation of Si(100) surface*, Journal of Applied Physics, **110**, pp. 053513-1-7.

30. Gunst, S., Weinbruch, S., Wentzel, M., Ortner, H.M., Skogstad, A., Hetland, S., Thomassen, Y. (2000), *Chemical composition of individual aerosol particles in workspace air during production of manganese alloys*, Journal of Environmental Monitoring, **2**, pp. 65 - 71.
31. Ulrich, G.D. (1971), *Theory of particle formation and growth in oxide synthesis flames*, Combustion Science and Technology, **4**, pp. 47-57.
32. Lindackers, D., Strecker, M.G.D., Roth, P., Janzen, C., Pratsinis, S.E. (1997), *Fromation and growth of SiO_2 particles in low pressure $H_2/O_2/Ar$ flames doped with SiH_4*, Combustion Science and Technology, **123**, pp. 287 - 315.
33. Ulrich, G.D., & Surbramanian, N.S. (1977), *Particle growth in flames III: Coalescence as a rate-controlling process*, Combustion Science and Technology, **17**, pp. 119-126.
34. Preining, O. (1998), *The physical nature of very, very small particles and its impact on their behaviour*, Journal of Aerosol Science, **29**, pp. 481 - 495.
35. Hildal, K., *Steam explosions during granulation of Si-rich alloys: Effect of Ca- and Al-additions*, 2002, PhD-thesis, Department of Materials Science and Engineering, Norwegian University of Science and Technology (NTNU), Trondheim.
36. Alcock, C.B., & Hooper, G.W. (1960), *Thermodynamics of the gaseous oxides of platinum-group metals*, Reoceedings of the Royal Society of London. Series A, Mathematical and Physical Sciences, **254**, pp. 551 - 561.
37. Fujii, H., & Nogi, K. (2004), *Formation and disappearance of pores in aluminum alloy molten pool under microgravity*, Science and Technology of Advanced Materials, **5**, pp. 219 - 223.
38. Fujii, H., Umakoshi, H., Nogi, K. (2004), *Bubble formation in aluminum alloy during electron beam welding*, Journal of Materials Processing Technology, **155-156**, pp. 1252 - 1255.
39. Copland, E. (2006), *Vapor pressures in the {$Al(l) + Al_2O_3(s)$} system: Reconsidering $Al_2O_3(s)$ condensation*, Journal of Chemical Thermodynamics, **38**, pp. 443 - 449.
40. Pilling, N.B., & Bedworth, R.E. (1923), *The oxidation of metals at high temperatures*, The Journal of the Institute of Metals, **1**, pp. 529 - 591.
41. Xu, C., Gao., W. (2000), *Pilling-Bedworth ratio for oxidation of alloys*, Material Research Innovations, **3**, pp. 231 - 235.
42. Ashrafian, A., Johansen, S.T., Gaal, S., Andresen, B., Klevan, O.S., *A reactor model for ladle refining of silicon melt*, in *6th international Conference on CFD in Oil & Gas, Metallurgical and Process Industries*. 2008: SINTEF/NTNU, Trondheim, Norway.
43. Tang, K., (2007), *Thermodynamic analysis of oxidative ladle refining of silicon melt including models of thermophysical properties of the silicon melt and SiO_2-Al_2O_3-CaO slag*, SINTEF, Report No. F8532, Trondheim.
44. Mori, K. (1988), *Kinetics of fundamental reactions pertinent to steelmaking process*, Transactions of the Iron and Steel Institute of Japan, **28**, pp. 246 - 261.

45. Xie, Y., Orsten, S., Oeters, F. (1992), *Behaviour of bubbles at gas blowing into Wood's metal*, The Iron and Steel Institute of Japan International, **32**, pp. 66 - 75.
46. Mazumdar, D., & Guthrie, R.I.L. (1995), *The physical and mathematical modeling of gas stirred ladle systems*, The Iron and Steel Institute of Japan International, **35**, pp. 1 - 20.
47. Xia, J.L., Ahokainen, T., Holappa, L. (2001), *Analysis of flows in a ladle with gas-stirred melt*, Scandinavian Journal of Metallurgy, **30**, pp. 69 - 76.
48. Johnston, M.D., & Barati, M. (2010), *Distribution of impurity elements in slag-silicon equilibria for oxidative refining of metallurgical silicon for solar cell applications*, Solar Energy Materials & Solar Cells, **94**, pp. 2085 - 2090.
49. Johnston, M.D., & Barati, M. (2011), *Effect of slag basicity and oxygen potential on the distribution of boron and phosporous between slag and silicon*, Journal of Non-Crystalline Solids, **357**, pp. 970 - 975.
50. Wu, J, Ma, W., Yang, B., Dai, Y., Morita, K. (2009), *Boron removal from metallurgical grade silicon by oxidizing refining*, Transactions of Nonferrous Metals Society of China, **19**, pp. 463 - 467.
51. Ikeda, T., & Maeda, M. (1992), *Purification of metallurgical silicon for solar-grade silicon by electron beam button melting*, Iron and Steel Institute of Japan, **32**, pp. 635 - 642.
52. Morita, K., & Miki, T. (2003), *Thermodynamics of solar-grade-silicon refining*, Intermetallics, **11**, pp. 1111 - 1117.
53. Tang, K., Andersson, S. Nordstrand, E., Tangstad, M. (2012), *Removal of boron in silicon by H_2-H_2O gas mixtures*, The Journal of The Minerals, Metals & Materials Society, **64**, pp. 952 - 956.
54. Nordstrand, E.F., & Tangstad, M. (2012), *Removal of boron from silicon by moist hydrogen gas*, Metallurgical and Materials Transactions B, **43**, pp. 814 - 822.
55. Krystad, E., Tang, K., Tranell, G. (2012), *The kinetics of boron transfer in slag refining of silicon*, The Journal of The Minerals, Metals & Materials Society, **64**, pp. 968 - 972.
56. Lynch, D. (2009), *Winning the Global Race for Solar Silicon*, The Journal of The Minerals, Metals & Materials Society, **61**, pp. 41 - 48.
57. Jung, I., Zhang, Y. (2012), *Thermodynamic calculations for the dephosphorization of silicon using molten slag*, The Journal of The Minerals, Metals & Materials Society, **64**, pp. 973 - 981.
58. Garcia, M. & Myrhaug, E.H., (2007), *Revisjon av materialbalanse for sporelementer i Si-ovn basert på målekampanje på Elkem Thamshavn april 2007*, Elkem, Internal Report, , Trondheim.
59. Myrhayg, E.H., & Tveit, H., *Material Balances of Trace Elements in the Ferrosilicon and Silicon Processes*, in *58th Electric Furnace Conference*. 2000: Orlando, FL, USA.

60. Bakke, P., & Klevan, O.S., *Thermodynamics of liquid silicon based alloys*, in *Process Technology Conference. Ladle Processing: Metallurgy and Operations*. 1995: Orlando, Florida, USA.
61. Safarian, J., Kolbeinsen, L., Tangstad, M. (2012), *Thermodynamic activities in silicon binary melts*, Journal of Materials Science, **47**.
62. Online database: *FactSage™* [accessed 15.02.13]; Available from: http://www.crct.polymtl.ca/fact/documentation/.
63. Tang, K., Tranell, G., Øvrelid, E., Tangstad, M., *Thermochemical and Kinetic Databases Designed for the Solar Cell Grade Silicon Materials*. 2009, in Nakajima, K. & Usami, N. (ed.) *Crystal growth of Si for solar cells*, Springer, USA.
64. Gaye, H., Lehman, J., Matsumiya, T., Yamada, W., *A statistical thermodynamics model of slags: Applications to systems containing S, F, P_2O_3 and Cr oxides*, in *4th Interantional Conference on Molten Slags and Fluxes*. 1992, ISIJ: Sendai.
65. Gulbransen, E.A., Andrew, K.F., Brassart, F.A. (1966), *Oxidation of silicon at high temperatures and low perssure under flow conditions and the vapor pressure of silicon*, Journal of the Electrochemical Society, **113**, pp. 834 - 837.
66. *NEO Monitors*. [accessed 21.03.13]; Available from: http://www.neomonitors.biz/solutions/products/dust-in-situ/laserdust/.
67. Karpersen, P., Personal communication., *NEO Monitors*. 2010: Trondheim.
68. Olsen, J.E., Næss, M., Tranell, G., *CFD modeling of silica fume formation during refining of silicon metal*, in *8th International Conference on CFD in Oil & Gas, Metallurgical and Process Industries,* . 2011: SINTEF/NTNU, Trondheim, Norway.
69. Olsen, J.E., Næss, M., Tranell, G., *Understanding fuming during metal refining by CFD*, in *CFD Modeling and Simulation in Materials Processing, TMS Annual Meeting & Exhibition March 3-7, 2012*. 2012: Orlando, FL, USA.
70. Svehla, R.A., (1962), *Estimated viscoisities and thermal conductivities of gases at high temperature*, National Aeronautics and Space Administration (NASA), Technical report no. R-132, Lewis Research Center, Cleveland, Ohio.
71. Darmana, D., (2008), *CFD hydrodynamic validation of a flat bubble column*, SINTEF Materials and Chemistry, Report no. A4383,
72. Díaz, M.E., Iranzo, A., Cuadra, D., Barbero, R., Motes, F.J., Galán, M.A. (2008), *Numerical simulation of the gas-liquid flow in a laboratory scale bubble column. Influence of bubble size distribution and non-drag forces*, Chemical Engineering Journal, **139**, pp. 363 - 379.

PAPERS

PAPER 1

2nd International Symposium on High-Temperature Metallurgical Processing
Edited by: Jiann-Yang Hwang, Jaroslaw Drelich, Jerome Downey, Tao Jiang, and Mark Cooksey
TMS (The Minerals, Metals & Materials Society), 2011

FUGITIVE EMISSIONS RELATED TO OXIDATION OF LIQUID SILICON DURING LADLE REFINING

Mari K. Næss, Gabriella M. Tranell, Nils Eivind Kamfjord

Norwegian University of Science and Technology (NTNU);
Alfred Getz vei 2, NO-7491 Trondheim, Norway.

Keywords: Liquid silicon, oxidation, ladle refining, condensed silica fume, boundary layer

Abstract

In oxidative ladle refining (OLR) of silicon, the metal surface is oxidized resulting in the formation of a condensed silica fume (SiO_2). In the current work, industrial measurement campaigns were performed aiming to measure the fume generation during OLR. A thorough discussion of the possible mechanisms has been included in order to improve our understanding of the $Si_{(l)}$-$O_{2(g)}$ system.

The measurement campaigns were performed at the Elkem Salten plant in Norway. In addition to fume generation from OLR, the metal temperatures and ladle purge gas amount were recorded. The results of this work suggest that fume generation during OLR results from splashing of the metal and/or oxidation of the metal surface, with oxygen transport to the metal surface being the limiting factor. Other mechanisms of SiO_2 formation were investigated, however insignificant.

Introduction

One of the main environmental and economical challenges facing the metallurgical industry is fugitive emissions of both materials and energy. In the production of metallurgical grade silicon (MG-Si), refining of the silicon generally takes place through an oxidative ladle treatment (purging with an air-O_2 mixture). In the refining process, exposure of silicon to air results in the formation of condensed silica fumes (SiO_2) – one of the main sources of fugitive emissions in silicon production plants. The oxidation of liquid silicon, as opposed to solid silicon, has not been widely studied and described in the literature [1], thus a thorough investigation of the oxidation mechanisms, and factors affecting the oxidation reaction rate are essential in order to deal with the problem. In the current work, the rate of liquid silicon oxidation has been studied through industrial measurements of fume generation from refining

ladles, where the purge gas rate and composition have been varied. The results from these measurements were discussed in light of existing models describing the liquid silicon oxidation kinetics.

Theory

The oxidation of liquid silicon is widely accepted as a process consisting of two steps: formation of volatile SiO gas, followed by combustion in air to form SiO_2 [2]:

$$Si_{(l)} + \tfrac{1}{2}O_{2(g)} \rightarrow SiO_{(g)} \quad (1)$$

$$SiO_{(g)} + \tfrac{1}{2}O_{2(g)} \rightarrow SiO_{2(s)} \quad (2)$$

The heterogeneous reaction between oxygen and liquid metal takes place at a phase boundary. As illustrated by Figure 1, the reaction involves mass transport of gaseous or liquid species from the bulk through a boundary layer to the interface, where the reaction takes place. The chemical reaction is generally considered to be very fast due to the high temperature, thus the rate limiting step for the oxidation is mass transfer of reactants *to* the interface and/or reaction product *from* the interface [3]. The process is thus referred to as *diffusion controlled.* In addition, there will be a counter flux of carrier gas (nitrogen in the case of oxidation in air), and also a condensed phase of SiO_2 may be present. All of these species constitute the boundary layer through which the oxygen must diffuse to reach the reaction interface.

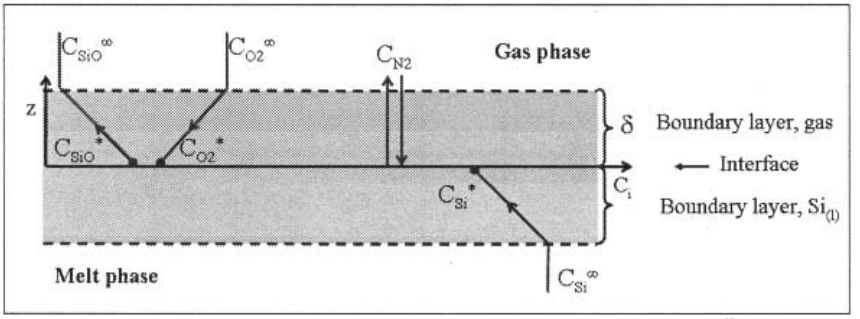

Figure 1: A sketch of the mass transport mechanisms in the system. The C_i^{∞} are the bulk concentrations. The C_i^{*} are the concentrations at the interface, and δ is the thickness of the boundary layer.

The diffusion of $Si_{(l)}$ and $O_{2(g)}$ to the interface will be strongly affected by the chemical reaction (eq. 1); the concentration of silicon and oxygen at the interface will approach zero, due to the rapid reaction between them [4].

Carl Wagner's theory about active and passive oxidation of silicon [5] is well known and widely used and modified in theoretical modeling of the oxidation of liquid metals. At low oxygen partial pressures above the surface, reaction (1) will take place and a partial pressure p_{SiO} is obtained. If the p^{*}_{SiO} at the surface is lower than the equilibrium partial pressure, $p_{SiO(eq)}$, from the reaction:

$$\tfrac{1}{2}Si_{(l)} + \tfrac{1}{2}SiO_{2(s)} \rightleftarrows SiO_{(g)} \tag{3}$$

the surface of the silicon will stay uncovered by SiO_2 and SiO will continue to form. This is the state of *active* oxidation, where the rate of attack is increasing with increasing oxygen partial pressure. When the partial pressure of SiO reaches the $p_{SiO(eq)}$, a layer of SiO_2 may be formed at the surface, and there is a transition from active to passive oxidation.

Wagner makes an important assumption prior to the derivation of the equations for the rate of oxidation; the reaction between Si and O_2 has a low activation energy, thus the reaction is rapid and the partial pressure of oxygen at the surface, $p^{*}_{O_2}$ is low, - much lower than the bulk partial pressure, $p^{\circ}_{O_2}$. The derived equation for the consumption of silicon in gram-atoms per unit area per unit time, j_{Si}, during active oxidation is according to Wagner

$$j_{Si} = \frac{2p_{O_2}{}^{\circ} D_{O_2}}{\delta_{O_2} RT} \tag{4}$$

where D_{O_2} is the diffusion coefficient of oxygen through the boundary layer with thickness δ_{O_2}, R is the gas constant and T is the absolute temperature. The rate of oxidation is determined by the supply of oxygen for the formation of SiO. When $p^{\circ}_{O_2}$ becomes larger than $p^{\circ}_{O_2}(\max)$, the rate of attack becomes

$$j_{Si} = \frac{D_{SiO} p_{SiO}{}^{*}}{\delta_{SiO} RT} = \frac{D_{SiO} K}{(p^{\circ}_{O_2})^{\frac{1}{2}} \delta_{SiO} RT} \tag{5}$$

where D_{SiO} is the diffusion coefficient of SiO molecules, δ_{SiO} is the effective thickness of the boundary layer for diffusion of SiO, p^{*}_{SiO} is the SiO pressure at the surface and K is the equilibrium constant for the reaction in equation (2). The partial pressure of SiO at the surface will increase linearly with $p^{\circ}_{O_2}$, and is equal to the equilibrium partial pressure ($1.5*10^{-2}$ atm, at T = 1410°C) when the oxygen pressure reaches maximum ($6.1*10^{-3}$ atm, at T = 1410°C). Here, the SiO pressure drops to a value eight orders of magnitude lower. As seen in equation (5), the steady state rate of attack is proportional to the surface partial pressure of SiO, thus the rate will drop when the SiO pressure drops [5].

Wagner does not discuss the fate of the SiO gas except when the partial pressure of oxygen reaches the critical point of formation of SiO_2. It might be crucial to take into consideration the counter flux of N_2 and SiO inside the boundary layer, and also the possible presence of SiO_2, which would be a fog of condensed phase – oxidized SiO gas. Hence, the system is probably more complex than pictured by Wagner, and the flux of oxygen is most likely altered by these influences.

Ratto et al. [1] extended Wagner's theory and made it more general. With extensive derivations they took into account the counter flux of SiO-gas and also derived a transport regime with a heterogeneous boundary layer, where condensed SiO_2 was present. They considered the two limiting cases of null reaction and instantaneous reaction in the boundary layer, with local equilibriums. They compared their results to Wagner's results, and found that the fundamental concept is in complete agreement; however, the fluxes of each chemical species in the layer will be entirely different, due to the reactions in the boundary layer [1]. This discrepancy is shown schematically in Figure 2.

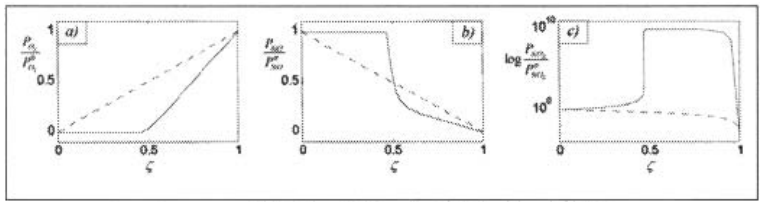

Figure 2: Pressure profiles of the species in a heterogeneous boundary layer. ζ is the non-dimensional distance from the surface; z/δ. Dotted lines = no reactions (Wagner), solid lines = instantaneous reactions in the boundary layer. Modified from Ratto et al.[1].

In the heterogeneous layer with instant reactivity case, i. e. the SiO oxidizes to SiO_2 instantly as it meets oxygen on its way out of the layer, Ratto et al. came to an important conclusion: the oxygen concentration at the surface of the molten silicon will be very low and does not change with increased bulk concentration of oxygen. An increase in the bulk oxygen partial pressure will only increase the oxidation/combustion of the SiO gas. This implies that saturation will never occur and active oxidation will just go on without passivation [1]. The relative pressure profiles of oxygen, SiO and SiO_2 in the heterogeneous system with null and instant reactions can be seen in Figure 2. In Wagner's approach (null reaction, dotted lines) the concentration profiles are linear, and in the case of instantaneous reaction they are strongly non-linear.

In the industrial ladle refining case, more complexity is introduced to the system as an oxygen/air mixture is purged through the metal from the bottom of the ladle. This generates a turbulent environment for the oxidation, combined with the continuous exposure of new silicon surface to the ambient air.

Experimental

Two industrial measurement campaigns were carried out at Elkem Salten in April and August, 2010. The tapping of the silicon was discontinuous during the measurements, in order to record only the fume formed during refining, rather than the fume from the tapping. The rate and composition of the purging gas were varied in order to see whether this would affect the rate of the fume formation.

Videotapes of the refining process, in addition to measurement of the amount of SiO_2 formed, were recorded. The equipment used to measure SiO_2 amounts in the off gas channel was a LaserDust MP with process parameters 200°C, 1013 mbar and 1.2 m measuring path. The apparatus had a relative error of 2 % in the measurements, however it was not calibrated for this kind of fume particles. It is a reasonable assumption that the measurements have an absolute error of 30% [6].

At the time of the measurements, the temperature in the metal was in the range of 1450-1500°C. Gas temperature measured at ~0.5 m above the metal was typically in the range of 370-500°C. Figure 3 shows the location of the LaserDust MP, and how a ladle top/silicon surface typically looks like during refining.

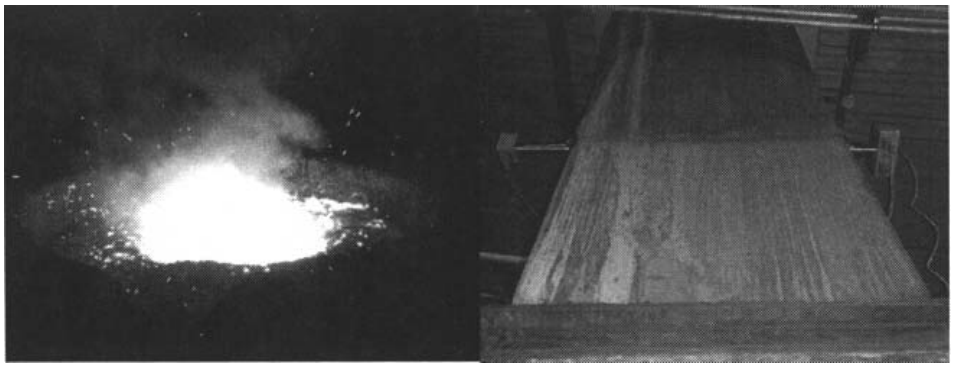

Figure 3: Left: A photo of the top of a ladle with silicon being refined, showing the dynamic nature of the silicon surface and the air above. Right: Photo of the LaserDust MP installed at the off-gas channel.

There is a layer of slag and solidified silicon along the perimeter of the silicon, and the exposed area of liquid silicon was typically in the range 0.3-0.5 m^2, when we take into account that the surface is curved up convexly from the stirring of the refining bubbles.

Results

The average amounts of silica fume measured in the off-gas are shown in Table 1, and plotted against the amount of oxygen and total gas flow in Figure 4. For the varying total gas flows, the measured amounts correspond to 31-71 mg/m^2s of SiO_2 (0.051-0.119 moles/m^2s of SiO_2). It indicates that the rate of oxidation is increased with increasing total gas flow; however, it is neither significantly affected by the concentration of oxygen in the gas nor of the oxygen flow rate.

Table 1: The numerical values from the silica fume measurements, with calculated standard deviations in parentheses. Amount of oxygen and total gas flow rate is also included.

Measurement #	**1**	**2**	**3**	**4**	**5**	**6**
SiO_2, mg/Nm^3	111 (20)	126 (15)	71.9 (9.9)	127 (8.0)	96.9 (8.2)	65.9 (10)
SiO_2, kg/m^2h	14.6 (2.7)	25.6 (3.1)	14.6 (2.0)	21.3 (1.3)	16.2 (1.4)	11.0 (1.7)
Oxygen flow, m^3/h	5	10	5	4	18	4
Total gas flow, m^3/h	15	24	8	21	22	8

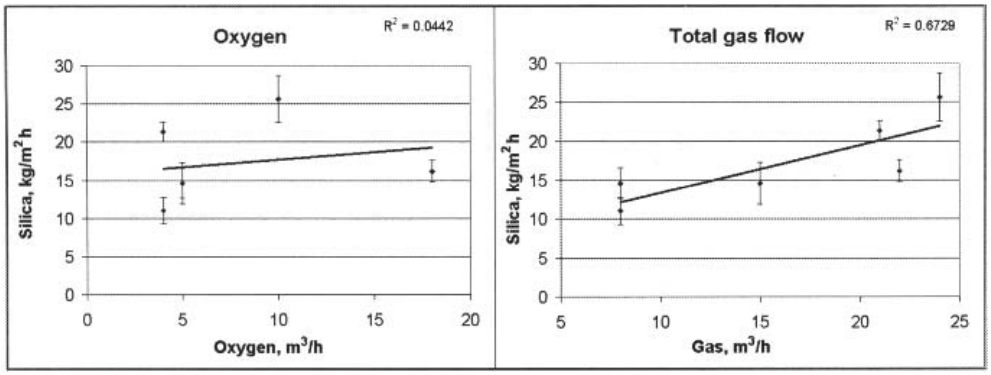

Figure 4: Amount of oxygen and total amount of gas in the refining, plotted against the measured amount of silica fume (kg/m^{2}h).

If we use these values of fume amount, and a diffusion coefficient for oxygen of D_{O_2}=3.84 cm^2/s from Ratto et al. [1], we can calculate the thickness of the boundary layer at 1500°C using Wagner's equation for active oxidation (eq. (4)). The thickness is then in the range 0.93-2.2 cm, assuming that the temperature does not change significantly within the boundary layer (which would affect the diffusion coefficient). The thickness of the boundary layer decreases with higher total gas flow.

In an initial CFD study, it was found that the supply of silicon to the surface was 10 kg/s. This is several orders of magnitude larger than the measured amounts of fume, thus it may be concluded that the availability of silicon is not limiting in this case [7].

Discussion

In the discussion of the formation of condensed silica fume during OLR, it is also important to consider the different paths in which the silica fume formation in the industry may occur. Three different oxidation paths may be envisaged, as outlined in Figure 5. The first scenario is that the SiO-gas formed in the refining bubbles is oxidized as the gas is released at the top. The second possibility, referred to as splashing, is where the bubbles from the purging gas will drag silicon up in the air, in which the droplets will oxidize to SiO_2. The last possibility is the surface oxidation, where the continuous exposed surface of liquid silicon is oxidized by the oxygen in the air above.

As the rate of formation of silica fume is independent on the amount of oxygen in the refining gas, it is probably the dynamic mechanisms in Figure 5b and c which are most dominant.

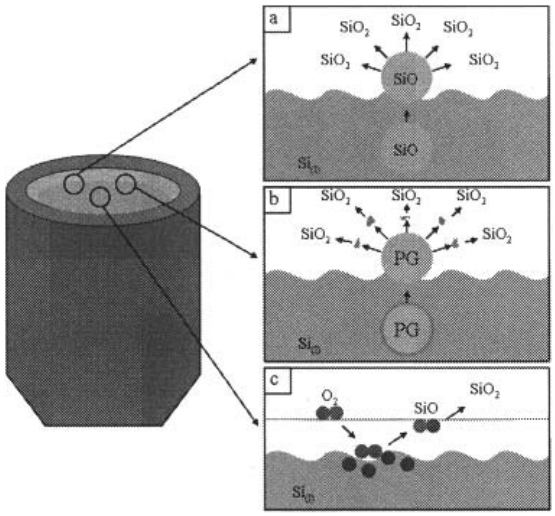

Figure 5: Simple sketch of the possible macroscopic mechanisms in the ladle: a) oxidation of SiO in the bubbles from the refining, b) oxidation from splash of liquid silicon due to the drag of the purge gas (PG) in the bubbles, and c) surface oxidation when in contact with oxygen in air.

In addition to the results from the industrial measuring, the amount of SiO_2 formed due to SiO from the bubbles was estimated using Tang's equation for the SiO-pressure in the bubbles [3]:

$$P(SiO) \approx \sqrt{\frac{\exp(11.13 + 39464/T}{\exp(-23.66 + 113623/T}} \qquad (6)$$

where T is the absolute temperature. The estimated amount from equation (6) was orders of magnitude smaller than the measured amounts of fume, thus found insignificant. This supports our result that the amount of silica fume formation is not significantly affected by the oxygen amount in the purging gas in the present set-up.

Even though we can exclude SiO from the refining bubbles as a dominating macroscopic mechanism, we cannot decide which of the other two dynamic mechanisms is dominating. The splash of metal caused by bubble drag will increase with increasing gas flow rate, however, the surface area of liquid silicon available for oxidation will also increase. Thus we cannot say with certainty which of the two dynamic mechanisms is dominating, and both may contribute to the silica fume formation.

A problem with comparing the models of Wagner and Ratto et al. with the system in a real situation in the ladle is that the silicon surface is turbulent and moving, which leads to active oxidation even though there should have been a passivation, according to Wagner. The complexity of the boundary layer most likely slow down/hinder the oxygen transport to a large extent, making the supply of oxygen to the surface low enough to get active oxidation. Although Ratto et al. operates with much lower bulk oxygen pressures than ambient air in their derivations, it might be that their theory about the heterogeneous layer with instant reactions applies in our system. The oxygen in the air which is transported through the boundary layer meets a flow of SiO and is instantly consumed to such an extent that the true oxygen partial pressure at the silicon surface is in the active oxidation range.

Conclusions

Results from industrial measuring campaigns where oxidation rate have been measured, show that the rate of oxidation of liquid silicon increases with increasing gas flow in the refining process. Theory and preliminary CFD modeling suggests that the rate limiting step in the surface oxidation is the oxygen transport to the surface, however, the dominating dynamic mechanism is not final from these results.

Further evaluation of this system should be considered by doing modeling with CFD and more advanced theoretical calculations. Examination of collected silica fume from the off-gas channel with SEM is planned, in order to investigate the morphology and thus the dynamic mechanisms. In the future we intend to perform small scale laboratory experiments, in order to investigate the system in a more controlled environment.

Acknowledgements

The financing of this work was provided by the Norwegian Research Council and FFF (Ferro Alloys Industries Research Association) through the FUME project (Fugitive emissions of Materials and Energy). We would like to express our appreciation to SINTEF for their contribution to this work, and Elkem for allowing us to carry out the measurements at their plant in Salten. Also we would like to thank Norsk Elektro Optikk AS (NEO) for using their equipment, and for assisting in the technical part of the measurements.

References

1 Ratto, M., Ricci, E., Arato, E. & Costa, P. (2001) Oxidation of metals with highly reactive vapors: Extension of Wagner theory *Metallurgical and Materials Transactions B* **32**, 903-911.

2 Gelain, C., Cassuto, A. & Le Goff, P. (1971) Kinetics and mechanism of low-pressure, high-temperature oxidation of silicon, *Oxidation of metals* **3**, 139-151.

3 Bongiorno, A. & Pasquarello A. (2005) Atomic-scale modelling of kinetic processes occuring during silicon oxidation, *Journal of Physics: Condensed Matter* **17**, 2051-2063.

4 Tang, K. (2008) *Thermodynamic analysis of oxidative ladle refining of silicon melt including models of thermophysical properties of the silicon melt and SiO_2-Al_2O_3-CaO slag*, SINTEF Report

5 Wagner, C. (1958) Passivity during the oxidation of silicon at elevated temperatures, *Journal of Applied Physics* **29**, 1295-1297.

6 Personal communication with Norsk Elektro Optikk AS (NEO), (2010).

7 Olsen, J. E. , (2010), *MEMO: CFD perspective on dusting from Si-ladles,* (Unpublished Work), SINTEF

PAPER 2

Oxid Met (2012) 78:239–251
DOI 10.1007/s11085-012-9303-9

ORIGINAL PAPER

Mechanisms and Kinetics of Liquid Silicon Oxidation During Industrial Refining

Mari K. Næss · Gabriella Tranell · Jan Erik Olsen · Nils Eivind Kamfjord · Kai Tang

Received: 4 August 2011 / Revised: 19 March 2012 / Published online: 22 May 2012

Abstract During oxidative ladle refining (OLR) of silicon, the metal surface is partly oxidized, resulting in the formation of a condensed silica fume (SiO_2). This fugitive emission of silica represents a potential health hazard to the workers in the silicon and ferrosilicon industry. In the current work, industrial measurement campaigns aimed at recording the fume generation during OLR were performed at the Elkem Salten plant in Norway. The measured amounts of silica produced were 2.5–5.1 kg/h, depending on the gas flow rate in the refining process. The rate of silica production correlates with the total flow rate and amount of air in the purge gas, and increases as the flow rate increases. The results of this work suggest that fume generation during OLR primarily results from oxidation of the exposed metal surface, with oxygen transport from the surrounding atmosphere to the metal surface being the limiting factor. Other identified mechanisms of SiO_2 formation were splashing of the metal and/or oxidation of SiO gas carried with the refining purge gas.

Keywords Liquid silicon · Ladle refining · Oxidation mechanism · Kinetics · Condensed silica fume

Introduction

An important step in the production of metallurgical grade silicon (MG-Si) is the oxidative ladle treatment of liquid silicon produced in the carbothermic process,

M. K. Næss (✉) · G. Tranell · N. E. Kamfjord
Norwegian University of Science and Technology (NTNU), Alfred Getz vei 2,
NO-7491 Trondheim, Norway
e-mail: mari.naess@material.ntnu.no

J. E. Olsen · K. Tang
SINTEF Materials and Chemistry, 7465 Trondheim, Norway

with the purpose of purifying the melt from the main impurities, which are aluminum (Al) and calcium (Ca). The treatment is usually performed by purging an air-oxygen mixture through the melt by a nozzle in the bottom of the ladle into which metal is tapped from the electric arc furnace, preferentially oxidizing the impurities into a slag phase [1]. As a result of the contact between liquid silicon and oxygen in the air, silica fume is produced.

While the ladle is under a fume hood, the silica fume formed during refining may be captured. However, when a ladle containing liquid silicon is not kept under a fume hood, or the ladle is transported in the melting hall at the plant, i.e. during casting, the fume is not captured. These fugitive emissions represent a severe indoor environment problem in the silicon and ferrosilicon industry and a potential health hazard for the employees working in the plant [2]. In order to reduce the emissions, a better understanding of the mechanisms and kinetics of the rate of fuming under different conditions, is imperative.

While the oxidation of solid silicon is reasonably well documented due to its importance in the electronic industry, the oxidation behavior of liquid silicon is not widely studied [3]. Wagner [4] studied the phenomenon theoretically in 1958, and presented a well-known theory for the oxidation reaction and its boundary conditions. In 1963, Turkdogan et al. [5] published extensive experimental work on vaporization and oxidation of several liquid metals, and presented a general theory for oxidation of all metals. Wagner and Turkdogan's theories are widely used and modified in later works, however there does not seem to be a consensus about the boundary conditions and reaction scheme in the Si–O system [6]. The present work is aimed at understanding and determining the rate of oxidation in the industrial processing of silicon. The data will be used, together with existing theories, to develop a model of the oxidation of liquid silicon for industrial prediction of silica fuming rate.

The Mechanisms

When the gas mixture is bubbled through the liquid silicon, there are two possible oxidation reactions occurring in the bubble; the direct oxidation of silicon, where a solid or liquid oxide/slag of silica (SiO_2) is produced (passive oxidation, according to Wagner), and the partial oxidation, where the gas silicon monoxide (SiO) is produced (active oxidation, according to Wagner):

$$Si_{(l)} + O_{2(g)} \rightarrow SiO_{2(s/l)} \tag{1}$$

$$2Si_{(l)} + O_{2(g)} \rightarrow 2SiO_{(g)} \tag{2}$$

By assuming that the activities of silicon in the melt, and silica on the melt-gas bubble interphase are close to unity, the equilibrium constants of reaction (1) and (2) can be used to calculate the equilibrium SiO partial pressure, $p_{SiO(eq)}$, inside the bubbles at a given temperature T, using thermodynamic data from the FactSage thermochemical database [7]:

$$p_{\mathrm{SiO}} \approx \sqrt{\frac{\exp(11.13 + 39464/T)}{\exp(-23.66 + 113623/T)}} \tag{3}$$

At a certain critical temperature, T_{crit}, the SiO_2 product becomes unstable, and the only oxidized product is $SiO_{(g)}$ due to the reaction

$$\mathrm{Si}_{(l)} + \mathrm{SiO}_{2(s/l)} \rightarrow 2\mathrm{SiO}_{(g)} \tag{4}$$

The amounts of SiO and SiO_2 formed in and on the bubble, respectively, are expressed in Fig. 1. Above the critical temperature, the only oxidation product is SiO, which leads to no refining and loss of silicon.

In the present case, this critical temperature is only dependent on the amount of oxygen in the purge gas, and increases as the oxygen content in the gas increases. An approximate numerical expression for the critical temperature may be derived from Eq. (3) and the equilibrium constant of reaction (4) [7]:

$$T_{\mathrm{crit}} = 1874.7 + 88.533 \ln(x) \tag{5}$$

where x is the initial molar fraction of oxygen in the purge gas, and the temperature is in degrees Celsius. When the bubbles reach the surface of the silicon in the ladle, they burst and the $SiO_{(g)}$ is released into the air above, where it combusts and oxidizes into $SiO_{2(s)}$. Thus, the factor determining the fuming rate by this mechanism is the O_2 flow rate. There is a possibility of $SiO_{(g)}$ oxidizing to $SiO_{2(g)}$ inside the bubble prior to the burst at the surface, however due to the instability of SiO_2-gas at the temperatures in question, this mechanism has not been considered further.

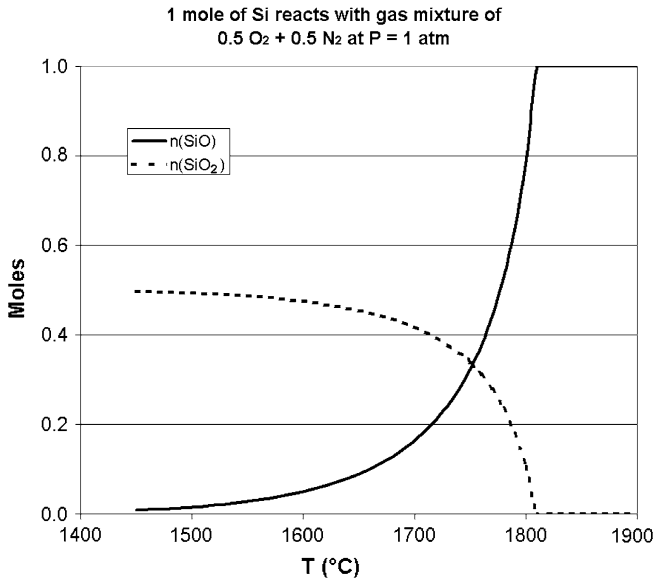

Fig. 1 A schematic display of the number of moles of SiO and SiO_2 formed in the bubble as a function of temperature. In this scenario 1 mol of Si reacts with 0.5 mol of O_2 and the pressure is 1 atm. At the critical temperature, here 1,813 °C, the SiO_2 production ceases and there is pure loss of silicon to SiO production

The actual refining of the silicon takes place with the following exchange reactions

$$3SiO_{2(s,l)} + 4\underline{Al} \rightarrow 2Al_2O_{3(l)} + Si_{(l)} \quad (6)$$

$$SiO_{2(s,l)} + 2\underline{Ca} \rightarrow 2CaO_{(l)} + Si_{(l)} \quad (7)$$

Thus the produced SiO_2 at the bubble–liquid metal interface is partly consumed in the refining process, forming an SiO_2–Al_2O_3–CaO slag. The slag is transported to the surface and mixed with the top slag phase due to the buoyancy of the bubble. The refining will lead to a change in composition of both the slag and the silicon, thus a shift in the equilibrium will take place at both the bubble interface and the top metal-slag-atmosphere interface. The initial concentrations of Al and Ca in the metal are typically 1.5 and 0.5 %, respectively, and the end concentrations 0.7 and 0.04 %, respectively [1]. This shift in the equilibrium conditions for the silicon and the slag is however assumed not to affect the equilibrium between the $SiO_{(g)}$ and the SiO_2 significantly. This assumption is reasonable because there is little Al/Al_2O_3 and Ca/CaO compared to SiO_2 and $SiO_{(g)}$ in the system, and because the SiO-pressure is only dependent on the temperature in the metal.

Another possible mechanism for fume formation is the surface oxidation of the liquid silicon. Fresh silicon surface is constantly exposed to the ambient atmosphere due to the violent stirring of the melt form gas purging. When oxygen from the surrounding atmosphere meets the surface, reaction (2) will take place and the $SiO_{(g)}$ formed is further combusted in air to become $SiO_{2(s)}$ fume. Following Hinze and Graham [8], this reaction may be written:

$$SiO_{(g)} + \frac{1}{2}O_{2(g)} \rightarrow SiO_{2(s)} \quad (8)$$

In order for the active oxidation (Eq. 2) rather than the passive oxidation (Eq. 1) to occur, there has to be, according to Wagner [4], a significantly lower oxygen partial pressure at the gas-metal interface than in the bulk gas phase, which in the industrial case is ambient air. A complex boundary layer in the gas phase near the surface is described by Ratto et al. [3]. The $SiO_{(g)}$ leaving the interface reacts with the oxygen flowing towards the surface. This heterogeneous boundary layer makes it possible to reach a sufficiently low oxygen partial pressure at the surface of the liquid silicon, even though the bulk oxygen pressure is much higher than the maximum bulk oxygen pressure stated by Wagner (6.1×10^{-3} atm at 1,410 °C). This leads to active oxidation being the preferred oxidation reaction, and Ratto et al. [3] states that the oxygen pressure at the surface will not be dependent on the bulk oxygen pressure. An empirical confirmation of active oxidation is the industrial observation of white fume going off the silicon while it is refined. If the passive oxidation was the sole reaction, the SiO_2 produced would be forming a thin layer on the metal surface and it would most likely become a part of the slag phase, and not come off the surface as fume. The rate of silicon surface oxidation with this mechanism will be determined by the rate of oxygen supply to the silicon surface and the size of the exposed melt area.

A third possible mechanism for fume formation is splashing of the metal due to drag from the purge bubbles rising with high velocity towards the surface. Visualizing that the dynamic silicon surface looks like a kettle of fast boiling water,

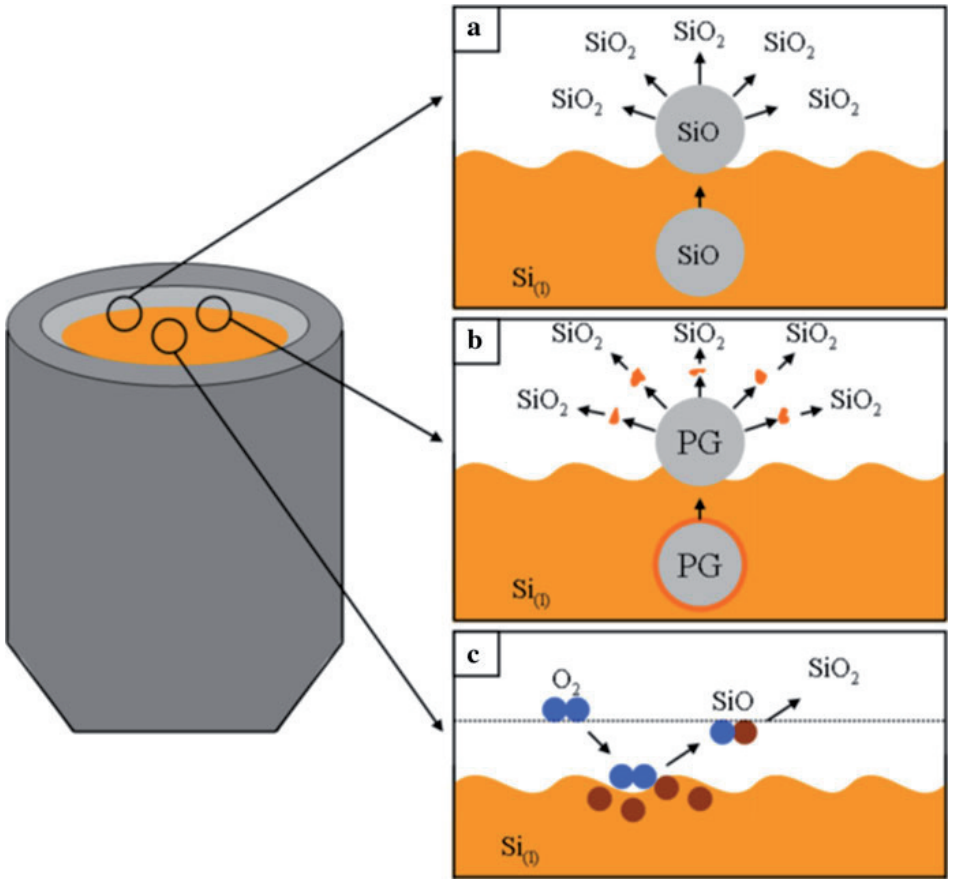

Fig. 2 Simple sketch of the possible macroscopic mechanisms in the ladle: **a** oxidation of SiO from the refining bubbles, **b** fuming from splashing of liquid silicon due to the drag of the purge gas (PG) in the bubbles, and **c** surface oxidation when in contact with oxygen in air

and as with water, some very small droplets of silicon may be ejected from the bulk melt. These small silicon droplets are either oxidized and become a part of the fume, or fall to the ground if they are too big and heavy (this is frequently observed). The three possible mechanisms for fume generation in the OLR are schematically visualized in Fig. 2.

In order to quantify the silica fuming during industrial refining of MG-Si under different operational conditions, an industrial measurement campaign was carried out at Elkem's Salten MG-Si plant in Norway in August 2010. In the present paper, the measurement results from the campaign are presented and discussed in light of existing literature and the presented theories of silica fuming mechanisms.

Experimental

In the measurements it was important to evaluate only the fume formed during the refining of silicon, thus the operationally practiced continuous draining of the

furnace was made discontinuous during the measurements. The ladles being refined were placed under the fume hood in order to collect all of the fume in the off-gas channel where the measuring equipment was placed. The measuring equipment was a LaserDust MP, a commercial apparatus from NEO Monitors (Lørenskog, Norway) [9]. The LaserDust measures the transmission of a laser beam, through for example an off gas duct/channel, and the reduction in the signal will correspond to the amount of fume in the measuring path. This change in signal is dependent on the properties of the particles, primarily the particle size distribution. The LaserDust used was not calibrated particularly for silica fume, however the measurements are evaluated to have a total measuring error of 30 %, which is in the same order of magnitude as the typical standard deviations in the measurements. The measuring path was 1.2 m (the width of the off gas channel). The LaserDust was programmed with the pressure and temperature, which on the day of our measurements was 1,013 mbar and approximately 50 °C (in the off gas channel). The apparatus had a relative error of 2 % in the measurements, and measured the fume amount in the off-gas channel every 5 s [10].

In order to relate the rate of the fume formation to the stirring occurring in the ladle, the rate and composition of the purge gas were varied. A summary of the chosen conditions for the six measurements are shown in Table 1. One of the ladles was refined with a semi-lid in order to see whether this would affect the fume amount (measurements 4–6 in Table 1). The semi lid covered the perimeter of the ladle, and had a hole with a diameter of $\sim$60 cm in the center for practical operational purposes.

The output unit from the LaserDust MP, mg/m^3, was converted to kg/h by implementing the measured temperature ($\sim$50 °C) and the measured volume flow in the pipes (50.000 Nm^3/h). The output in mg/m^3 was multiplied with the calculated factor of 11.2 m^3/s in order to obtain the mass per time unit.

In addition to measurement of the amount of silica, videotapes of the refining process were recorded. At the time of the measurements, the temperature in the melt was in the range of 1,450–1,500 °C. Gas temperature measured at approximately 0.5 m above the silicon was in the range of 370–500 °C. Figure 3 shows how a ladle top (silicon surface) typically looks like during refining, and the location of the

Table 1 Summary of the chosen oxygen and air contents in the purge gas, total purge gas amount, number of measurement points in each measurement, measured temperature in the liquid silicon and calculated critical temperature (Eq. 5)

Measurement #	Oxygen flow, m^3/h	Air flow, m^3/h	Total gas flow, m^3/h	# of measurement points	$T_{\mathrm{Si}(l)}$, °C	Calculated T_{crit}, °C
1	5	10	15	277	1483	1808
2	10	14	24	107	1478	1820
3	5	3	8	114	1468	1844
4	4	17	21	102	1465	1784
5	18	4	22	83	1453	1861
6	4	4	8	106	1450	1830

Fig. 3 *Top*: Photo of the top of a ladle with silicon being refined, showing the dynamic nature of the silicon surface and the air above. *Bottom*: Photo of the LaserDust MP installed at the off-gas channel

LaserDust MP at the off gas channel, approximately 20 m from the ladle top. There is a layer of slag and solidified silicon along the perimeter of the melt, and the exposed area of liquid silicon was typically in the range 0.3–0.5 m^2, when taking into account that the surface is convex from the bubble stirring.

Silica fume was collected in the off-gas channel during tapping and refining with a "cold finger" (a hollow copper tube cooled with water). The fumes were examined using a scanning electron microscope (SEM) and compared to samples of silica taken from the furnace stack. The SEM used was a Zeiss Ultra 55 Limited Edition field emission microscope. The samples were held in place by a carbon tape in order to avoid charging, and the images were recorded at an acceleration voltage of 2–5 kV, with magnifications 2k–50k. From the SEM images, the particle size distribution and mean diameter of the particles were estimated. The SEM apparatus was also used to perform element analysis of the samples with energy dispersive spectroscopy (EDS). The EDS-spectra were recorded at 20 kV.

The fume was also examined with a transmission electron microscope (TEM) in order to confirm that the silica was amorphous and to see if the particles were hollow. The TEM used was a JEOL JEM2010. The samples were dispersed on a Holey Carbon Film 300 mesh Cu from Agar Scientific, and the images were recorded at 200 kV.

The specific surface area of the fume samples were measured with BET (an adsorption theory and method developed by Brunauer, Emmett and Teller) in order to find out whether the particles were porous or not, and to compare the specific surface area to that of the silica samples taken from the furnace stack (this was not possible for the sample collected during refining, due to too small sample size). The samples were degassed over night at 250 °C under vacuum in a VacPrep 061 from Micromeretics, and analyzed with liquid nitrogen in a Tristar™ 3000 from Micromeretics.

Results and Discussion

The calculated average amounts of SiO_2 measured for the different experimental conditions are shown in Table 2. The maximum and minimum amounts were calculated with a combined error function (standard deviation and the total measurement error of 30 % combined). The "macro" area of exposed silicon at the top surface was estimated from the videotapes of the refining, and used to calculate the flux of silica (moles/s m^2). Due to the vigorous stirring, this estimated area is underestimated compared to a true metal-gas surface area, but it gives an indication of the silicon surface area not covered by slag.

Plots of the SiO_2 produced per unit time as a function of total gas flow rate, air and oxygen flow rates are shown in Fig. 4.

The amount of fume formed during refining correlates best with the amount of air in the purge gas, and also adequately with the total amount of purge gas. The difference between the fume amount with (dotted lines, triangles) and without a lid

Table 2 The numerical results from the measurements in the present work, with standard deviations in parentheses

Measurement #	Area of exposed Si (m^2)	SiO_2 (kg/h)	SiO_2 (kg/h m^2)	SiO_2 (moles/s m^2)	Max (kg/h)	Min (kg/h)	Calc. SiO_2 from bubbles (kg/h)
1	0.45	4.4 (0.7)	10 (1)	0.046 (.007)	5.9	3.0	0.082
2	0.31	5.1 (0.6)	16 (2)	0.076 (.009)	6.7	3.4	0.11
3	0.30	2.9 (0.3)	9.5 (0.9)	0.044 (.004)	3.8	2.0	0.020
4	(0.37)	5.1 (0.3)	13.9 (0.9)	0.064 (.004)	6.7	3.6	0.11
5	(0.37)	3.9 (0.3)	10.5(0.8)	0.049 (.004)	5.1	2.7	0.023
6	(0.37)	2.5 (0.2)	6.7 (0.5)	0.031 (.002)	3.2	1.7	0.022

Measurement 4–6 was conducted with a lid, the exposed surface areas were therefore estimated (average of the first three measurements). The maximum and minimum values are calculated from the combined error where both standard deviation and the total measurement error of 30 % are taken into account. The calculated SiO_2 from the bubbles is estimated by Eq. 3 and equations for the equilibrium amounts of SiO and SiO_2 in the bubbles, elaborated in Ashrafian [11]

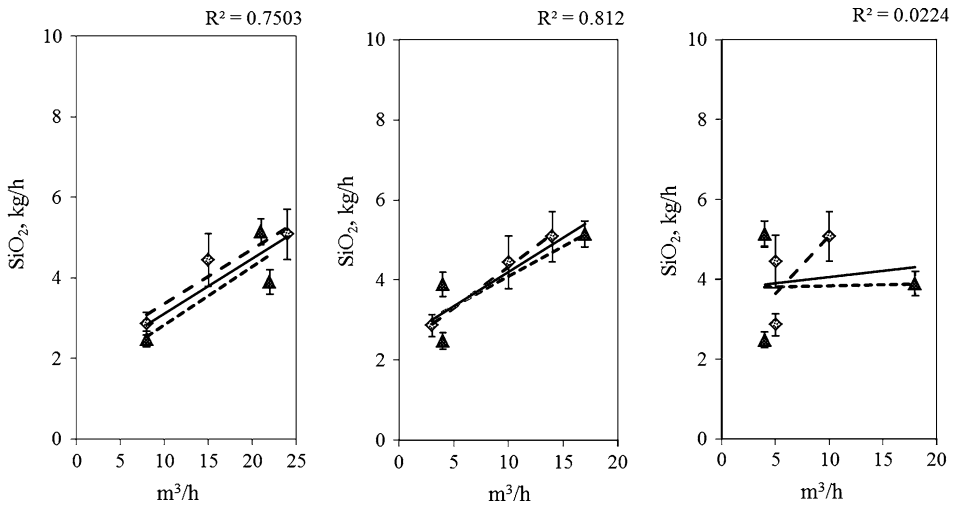

Fig. 4 Plots of the measured amount of silica fume (kg/h) versus the amount of gas total (*left*), air (*middle*) and oxygen (*right*) in m^3/h. The regression lines for all measurements (*solid lines*), and for ladles with lid (*dotted lines*) and without lid (*dashed lines*), are shown. The squared correlations (R^2) for all measurements (*solid lines*) are given in the upper right corner of each graph, and the shape of the points indicates whether a lid (*triangles*) or no lid (*diamonds*) was present

(dashed lines, diamonds) is not significant, thus the amount of oxygen available to the surface in not limited by the lid in the current conditions. The lid only serves to concentrate the fume in order to capture it better with the ventilation off-gas channel. The reason for the increased amount of fume with increasing amount of purge gas is likely due to more stirring and thus a larger area of the surface will be exposed to air, available for oxidation. This effect is observed both with and without a lid, the oxygen availability is thus assumed to be similar in both cases.

The results also indicate that the fuming rate is not dependent on the oxygen content in the purge gas (neither the input amount nor the total amount, which is not shown here). According to Eq. (3), the calculated equilibrium $SiO_{(g)}$ partial pressure in the bubbles corresponds to 0.02–0.11 kg of SiO_2 per hour, using the experimental gas rates and compositions. Compared to the measured total of 2.5–5.1 kg of SiO_2 per hour, it was concluded that oxidation of $SiO_{(g)}$ from the purge gas bubbles is not the dominating mechanism for fume formation during silicon refining.

Gulbransen and Jansson [12] measured a flux of 0.0538 mol/s m^2 at 1,300 °C, $P_{tot} = 1.3 \times 10^{-4}$ atm and with an oxygen flow of 7.0×10^{18} molecules per second (corresponds to $\sim$11.4 L/s, or a flow rate of 21 m/s). Although this was measured on solid silicon, the flux is in the same order of magnitude as the estimated fluxes in this work.

Images from SEM and TEM analysis of silica fume are shown in Fig. 5. The silica from the refining and tapping looked exactly the same as condensed silica fume; the particles are perfect spheres with a size distribution of 0.001–3 μm, with 70–90 % of the particles being <0.05 μm in size. This is somewhat smaller than reported in literature [13]. The particle size distributions for the three different samples are shown in Fig. 6. The TEM (right part of Fig. 5) showed that the

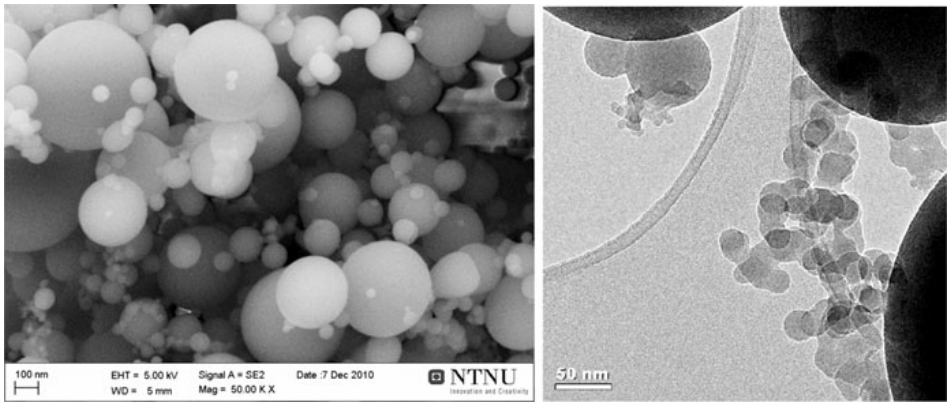

Fig. 5 SEM-image (*left*, 50k magnification) and TEM-image (*right*, 250k magnification) of collected fume from the refining. (The two lines in the TEM image, going from the *middle* in the *top* and out to *left* and *right*, are pores in the carbon film and not a part of the sample)

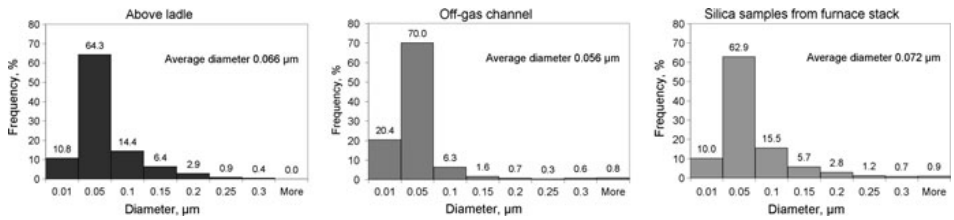

Fig. 6 Particle size distributions of the two collected silica samples and the silica samples taken from the furnace stack, with number average diameter given. In each distribution ∼1,000 particles were measured and counted

particles were amorphous, as expected, and also that they had no pores or were hollow. In the figure it is seen that there is no ordered crystal structure of the atoms in the particles, and the smallest particles are ∼10 nm in diameter.

The particles in the collected samples and the silica samples taken from the furnace stack had very similar particle size distribution. However, the samples collected above the ladle during refining and in the off-gas channel during tapping, contained some few particles with sizes of 20–70 µm. These particles were also spherical, as shown in Fig. 7, however, they contained some iron and aluminum, in addition to silicon, oxygen and carbon. This type of particles was not found in the silica samples taken from the furnace stack. As seen in the upper right inset in Fig. 7, the surface of these large particles had a rough, layered texture, possibly due to oxidation of the surface of a silicon droplet. It is suggested that these large particles are created from splashing of the metal due to bubble drag (mechanism b in Fig. 2). The presence of Fe and Al supports this, as these elements will predominantly follow the metal and not the fume, in addition to the fact that these large particles were not found in the silica samples taken from the furnace stack.

The specific surface area of the samples measured by BET were 17.61 ± 0.05 m^2/g for the silica samples taken from the furnace stack, and 14.90 ± 0.04 m^2/g for silica

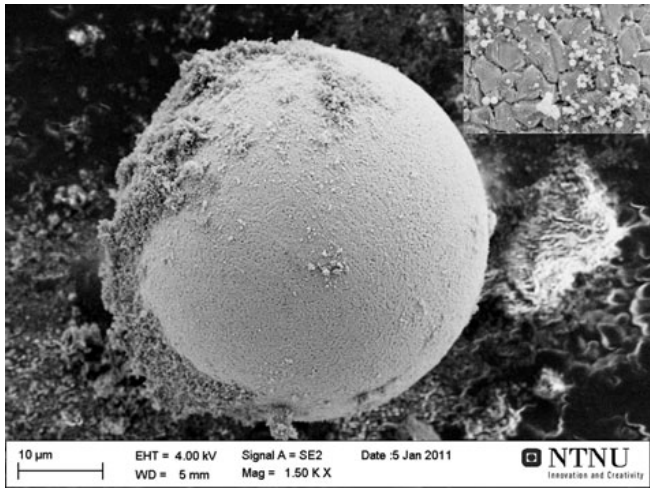

Fig. 7 SEM-image of a large particle found in the fume collected during refining (1.5k magnification), with an inserted image where the surface structure is shown (25k magnification)

fume collected during tapping. These areas are in the same order of magnitude, and the fairly low values signify that the particles are not porous. The similar specific surface area, and similar particle size distribution indicates that the particles in the fume samples from the refining and tapping are generated from the same mechanism as the silica from the furnace stack; $SiO_{(g)}$ oxidation. It is well known that the silica fume from the furnace stack is produced by the combustion of SiO rising up through the furnace into the off-gas channel together with the other gases from the silicon production (CO and small amounts of e.g. SO_2 and NO_x). This supports our theory of the active oxidation on the liquid silicon surface (mechanism c in Fig. 2).

In a Computational Fluid Dynamics (CFD) study, Olsen et al. [14] have modeled the ladle refining and performed a sensitivity study in order to map the factors affecting the fuming rate significantly. They tested temperature, emissivity of the silicon surface, different lid designs and exposed metal surface area. In the study they found that metal temperature is not an important factor, as the temperature effect on diffusion and/or convection will counteract the increased reaction rate. The CFD modeling concluded that exposed surface area was the most significant factor in the fuming rate, and that oxygen availability is the limiting factor in the oxidation [14]. These results support the findings of the present study, as the results suggest surface oxidation to be the dominant oxidation mechanism in OLR.

Conclusions

The amount of silica fume produced during industrial refining of MG-Si has been measured. In order to correlate the fuming rate to stirring in the molten silicon, the gas purging rate and composition were varied. The amount of fume was recorded with a LaserDust MP, which was installed in the off-gas channel. The measurements had an assumed total measurement error of 30 %. Six different measurements were

carried out, with recorded fume amounts of 2.5–5.1 kg of SiO_2 per hour. The results indicate that the fuming rate is correlated with the amount of purge gas.

Three mechanisms for the fume formation were proposed and evaluated (see Fig. 2): Fume produced from oxidation of SiO-gas from the refining bubbles was found to be less significant compared to the recorded amount of fume. Splashing of metal droplets due to bubble drag is a contributing mechanism, however, the dominating mechanism is believed to be the surface oxidation of the molten silicon. Increased amount of purge gas leads to more vigorous stirring and larger exposed surface area available for oxidation with oxygen from the air. The results indicate that refining with and without a semi-lid on the ladle do not affect the amount of fume formed, and a lid will thus not limit the oxygen supply to the surface significantly. Even though the bulk oxygen pressure in air is too high for active oxidation to occur (the Wagner theory), active oxidation would still be possible if a complex heterogeneous boundary layer is present, where most of the oxygen is consumed by oxidation of $SiO_{(g)}$ to SiO_2, prior to the liquid silicon surface.

The primary particles in the fume had a size distribution of 0.01–3 μm, with 70–90 % of the particles being <0.05 μm in diameter. The particles are amorphous and non-porous. The similarity between the particles in the fume samples collected during tapping and refining, and the silica samples collected from the furnace stack, suggest that they are formed from the same mechanism; oxidation of $SiO_{(g)}$. This finding supports the theory of the surface oxidation being the dominant mechanism in the fuming during OLR.

The conclusion that the surface oxidation is the dominating oxidation mechanism is supported by a CFD study performed by Olsen et al. in [14], where it was concluded that the exposed silicon surface area is the most important factor in the fuming rate, and that the oxygen availability is the limiting factor to the oxidation.

The results in this paper have given a better understanding of the mechanism from which the fugitive emissions of silica during OLR are generated. The amounts of silica emitted have been quantified. Further work will be small scale experiments in order to better understand the fundamental mechanism of the oxidation, and in order to better characterize the boundary layer and the boundary conditions for the active oxidation.

Acknowledgments The financing of this work was provided by the Norwegian Research Council and FFF (Ferro Alloys Industries Research Association) through the FUME project (Fugitive emissions of Materials and Energy). We would like to express our appreciation to SINTEF for their contribution to this work, and Elkem for allowing us to carry out the measurements at their plant in Salten. Also we would like to thank Norsk Elektro Optikk AS (NEO) for using their equipment, and for assisting in the technical part of the measurements.

References

1. A. Schei, J. K. Tuset, and H. Tveit, *Production of High Silicon Alloys* (TAPIR forlag, Trondheim) (1998).

2. H. L. Johnsen, *Lung Function, Respiratory Symptoms, and Occupational Exposure. Ph.D. Thesis*. University of Oslo, Oslo (2009).
3. M. Ratto, E. Ricci, E. Arato and P. Costa, Oxidation of metals with highly reactive vapors: Extension of Wagner theory. *Metallurgical and Materials Transactions B* **32**, 903 (2001).
4. C. Wagner, Passivity during the oxidation of silicon at elevated temperatures. *Journal of Applied Physics* **29**, 1295 (1958).
5. E. T. Turkdogan, P. Grieveson and L. S. Darken, Enhancement of diffusion-limited rates of vaporization of metals. *Journal of Physical Chemistry* **67**, 1647 (1963).
6. K. Hildal, (2002). *Steam explosions during granulation of Si-rich alloys: Effect of Ca- and Al-additions. Ph.D. Thesis*. Norwegian University of Science and Technology (NTNU), Trondheim.
7. K. Tang, *Thermodynamic analysis of oxidative ladle refining of silicon melt including models of thermophysical properties of the silicon melt and SiO_2–Al_2O_3–CaO slag*, (SINTEF, Trondheim, 2007).
8. J. W. Hinze and H. C. Graham, The active oxidation of Si and SiC in the viscous gas-flow regime. *Journal of the Electrochemical Society* **123**, 1066 (1976).
9. *NEO Monitors* [Online]. Lørenskog: NEO Monitors. Available: www.neomonitors.com/products/dust-cross-stack/laserdust/ [Accessed 20.02.2012].
10. P. Kaspersen, *Personal Communication*, (*Norsk Elektro Optikk AS* (*NEO*), Lørenskog) (2010).
11. A. Ashrafian, S. T. Johansen, S. Gaal, B. Andresen and O. S. Klevan, A reactor model for ladle refining of silicon melt. *6th international Conference on CFD in Oil and Gas, Metallurgical and Process Industries*, SINTEF/NTNU, Trondheim, Norway, 10–12. June, 2008.
12. E. A. Gulbransen and S. A. Jansson, The high-temperature oxidation, reduction, and volatilization reactions of silicon and silicon carbide. *Oxidation of metals* **4**, 181 (1972).
13. E. Dingsøyr, M. Dåstøl and W. C. Wedberg, Particle size and particle size distribution of Elkem Microsilica and its relevance to technical application. *The 5th European Symposium Particle Characterization*, Nurnberg, Germany, 24–26. March, 1992.
14. J. E. Olsen, M. Næss and G. Tranell, CFD modeling of silica fume formation during refining of silicon metal. *8th International Conference on CFD in Oil and Gas*, *Metallurgical and Process Industries,* SINTEF/NTNU, Trondheim, Norway, 21–23. June 2011.

PAPER 3

Oxid Met (2012) 78:363–376
DOI 10.1007/s11085-012-9312-8

ORIGINAL PAPER

Active Oxidation of Liquid Silicon: Experimental Investigation of Kinetics

Mari K. Næss · David J. Young · Jianqiang Zhang · Jan Erik Olsen · Gabriella Tranell

Received: 2 July 2012 / Revised: 10 August 2012 / Published online: 31 August 2012

Abstract Small scale laboratory experiments on the oxidation of liquid silicon have reproduced important features of the industrial refining of liquid silicon: active oxidation led to the formation of amorphous silica spheres as a reaction product. The boundary condition for active oxidation in terms of maximum oxygen partial pressure in the bulk gas was found to lie between $2{\cdot}10^{-3}$ and $5{\cdot}10^{-3}$ atm at $T = 1{,}500$ °C. The active oxidation of liquid silicon had linear kinetics, and the rate was proportional to bulk oxygen partial pressure and the square root of the linear gas flow rate, consistent with viscous flow mass transfer theory. Classical theory for unconstrained flow over a flat plate led to mass transfer rates for $SiO_{(g)}$ which were 2–3 times slower than observed. However, computational fluid dynamic modeling to take into account the effects of reactor tube walls on flow patterns yielded satisfactory agreement with measured volatilization rates.

Keywords Silicon · Active oxidation · Thermodynamics · Kinetics

Introduction

One of the main environmental and economic challenges facing the metallurgical industry is fugitive emissions of both materials and energy. In the production of

M. K. Næss (✉) · G. Tranell
Department of Materials Science and Engineering, Norwegian University of Science and Technology (NTNU), 7491 Trondheim, Norway
e-mail: mari.naess@material.ntnu.no

M. K. Næss · D. J. Young · J. Zhang
School of Materials Science and Engineering, University of New South Wales, UNSW, Sydney, NSW 2052, Australia

J. E. Olsen
SINTEF Materials and Chemistry, 7465 Trondheim, Norway

metallurgical grade silicon (MG-Si), the tapping and refining processes are generally the biggest sources of fugitive emissions in the plant. Silicon refining is performed in the ladle by purging with an air–O_2 mixture in order to reduce the levels of the main impurities calcium and aluminum. Oxygen in the refining bubbles is consumed through the overall reaction with the melt

$$\mathrm{Si_{(l)}} + \mathrm{O_{2(g)}} \rightarrow \mathrm{SiO_{2(s)}} \tag{1}$$

The refining exchange reactions may be written respectively

$$\begin{aligned} 4\underline{\mathrm{Al}} + 3\mathrm{SiO_2} &\rightarrow 2\mathrm{Al_2O_3} + 3\underline{\mathrm{Si}} \\ 2\underline{\mathrm{Ca}} + \mathrm{SiO_2} &\rightarrow 2\mathrm{CaO} + \underline{\mathrm{Si}} \end{aligned} \tag{2}$$

where underlining denotes solute species. These exchange reactions recycle some of the silicon back to the melt and deplete the silicon of calcium and aluminum [1]. An equilibrium partial pressure of $SiO_{(g)}$ is simultaneously established in the bubbles [2].

In the refining process, exposure of liquid silicon to air results in the formation of large amounts of condensed silica fume (SiO_2)—one of the main sources of fugitive emissions in a silicon production plant. In an earlier study [3], this fume was characterized, and its generation quantified. The fuming mechanism was concluded to be active oxidation of the liquid silicon surface, as described below. The reaction product consisted of spherical, amorphous silica particles with an average diameter of $\sim$60 nm. The flux of silicon in this particular process was found to be 0.031–0.076 mol m^{-2} s^{-1}.

In 1958, Wagner [4] published a theory regarding the active and passive oxidation of liquid silicon, where the active oxidation involves the partial oxidation of silicon to SiO-gas:

$$\mathrm{Si_{(l)}} + \frac{1}{2}\mathrm{O_{2(g)}} \rightarrow \mathrm{SiO_{(g)}} \tag{3}$$

In his paper, Wagner stated that the maximum bulk oxygen partial pressure for active oxidation to occur was $6.1 \cdot 10^{-3}$ atm at 1,410 °C. If the bulk oxygen pressure was higher than this, passivation would occur: an oxide layer would form on the surface, making the production of SiO-gas very slow [4]. However, Wagner did not account for the fate of the $SiO_{(g)}$ formed during active oxidation, and the maximum oxygen pressure he stated for active oxidation was much lower than that in ambient air. Thus this theory does not match the observation of active silicon surface oxidation in the industrial ladle refining process. Accordingly, Ratto et al. [5]. presented a modified theory regarding the occurrence of active oxidation at higher oxygen pressures: If the $SiO_{(g)}$ formed at the silicon surface reacts with incoming oxygen inside the hydrodynamic boundary layer, the oxygen partial pressure at the surface can be low enough for active oxidation to occur. According to their theory of a heterogeneous boundary layer (that is, with condensed matter inside the boundary layer), the surface oxygen pressure is independent of the bulk oxygen pressure. Hence active oxidation of silicon in ambient air is possible.

Hinze and Graham [6] investigated the oxidation mechanism of solid silicon at high temperatures. They used a set of equilibrium equations in the Si–O system to

calculate the possible bulk oxygen partial pressures to obtain active oxidation, and calculated an experimental mass transfer coefficient from their experimental results. The results were in accordance with the theoretical calculations, but the active oxidation of solid silicon had two different stages. The first stage was the "normal" active oxidation with a bare silicon surface, and the second stage showed growth of silica whiskers at the silicon surface, but still at a high rate. Growth of these silica whiskers at the silicon surface was also found by Carter et al. [7] who studied silicon bearing alloys at 1,130 °C. The growth of these structures at the silicon surface is probably not applicable for liquid silicon, as the surface structure is so different. However, Hinze and Graham's [6] technique for evaluating the system and calculating the experimental mass transfer coefficient may be applied to liquid silicon oxidation.

The oxidation of liquid silicon, as opposed to solid silicon, has not been extensively experimentally studied. A thorough investigation of the oxidation mechanisms and factors affecting the oxidation reaction rate is essential in order to obtain a more fundamental understanding of the reactions, and thus arrive at a solution for the fugitive emissions in the industry.

In the current work, the rate of liquid silicon oxidation has been studied through small scale experiments, where the kinetics and boundary conditions have been examined. The aims of this paper are thus to (1) find the rate of active oxidation as a function of oxygen pressure and linear gas velocity and (2) determine the boundary conditions for active oxidation of liquid silicon.

Thermodynamic and Kinetic Calculations

A simple schematic of the system is shown in Fig. 1. Diffusion of gaseous species both inward towards the surface and outward to the bulk gas are expected. Oxygen from the bulk, with partial pressure $p^{\circ}_{O_2}$, diffuses through a boundary layer of thickness δ, and meets the liquid silicon surface with a partial pressure $p^{*}_{O_2}$. This

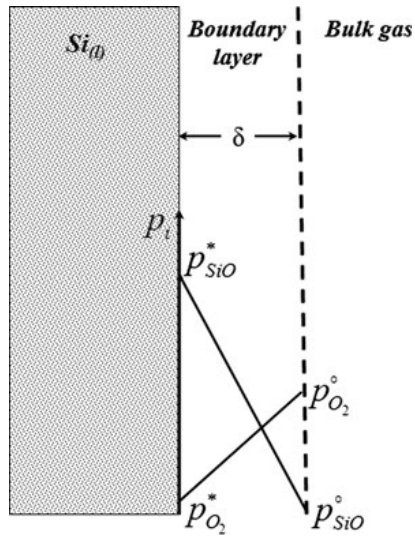

Fig. 1 Schematic of active oxidation in the Si–O system, where oxygen diffuses into the surface and reacts with liquid silicon to form $SiO_{(g)}$, which diffuses out through the boundary layer of thickness δ

value is very low as a result of the rapid consumption of oxygen via the reaction of Eq. (3). The resulting $SiO_{(g)}$, with surface partial pressure p^*_{SiO}, diffuses out of the boundary layer. Its bulk partial pressure $p^\circ_{SiO} \approx 0$, due to the instability of $SiO_{(g)}$ and its prompt oxidation:

$$SiO_{(g)} + \frac{1}{2}O_{2(g)} \rightarrow SiO_{2(s)} \tag{4}$$

These processes generate the concentration gradients of gaseous species within the boundary layer shown schematically in Fig. 1. The diffusion of $SiO_{(g)}$ out to the bulk will be a counter flux to the oxygen coming in, and the production of $SiO_{(g)}$ is controlled by the rate of the oxygen flux. In this discussion, it is assumed that $SiO_{(g)}$ oxidizes to SiO_2 outside the boundary layer.

Thermodynamic equilibrium calculations using HSC Chemistry [8] were used to establish the partial pressure of Si-bearing species at 1,500 °C. The results are shown in Fig. 2, which illustrates the principal features of the Si–O system. The partial pressure of SiO is controlled by the equilibrium of Eq. (3) at oxygen activities too low for solid silica formation.

The variation of p^*_{SiO} with $p^*_{O_2}$ is represented by the solid line in Fig. 2, and reaches a maximum at a surface oxygen pressure of $p^*_{O_2}$ (max) $= 2.86 \cdot 10^{-18}$ atm, where SiO_2 becomes stable. At higher $p^*_{O_2}$ values, the equilibrium in Eq. (1) leads to formation of a stable SiO_2 phase, and passivation of the silicon surface. The maximum oxygen partial pressure in the bulk gas permitting active oxidation, $p^\circ_{O_2}$ (max), is now calculated.

Boundary value gas partial pressures are related to the rate of mass transport across the hydrodynamic boundary layer. Assuming that the melt surface is clean, and $Si_{(l)}$ freely available, then if chemical reaction at the liquid–gas interface is fast

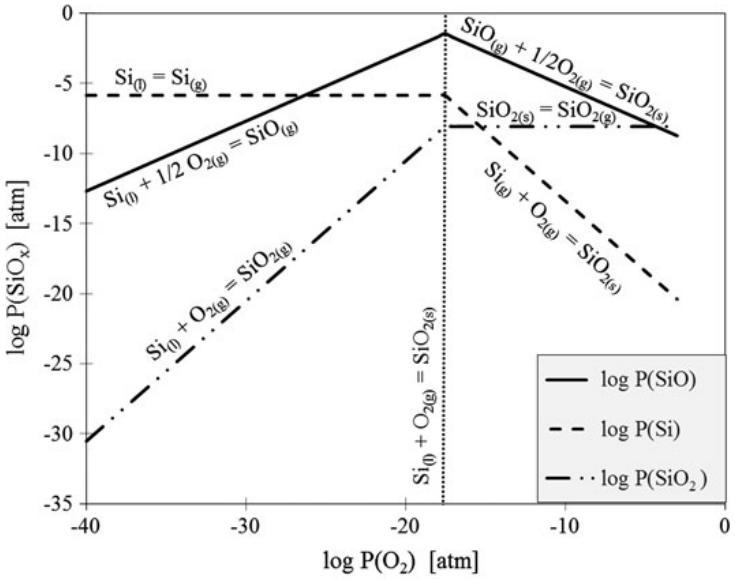

Fig. 2 Thermodynamically calculated partial pressures of $Si_{(g)}$, $SiO_{(g)}$ and $SiO_{2(g)}$ as a function of p_{O_2} at 1,500 °C

enough to establish local equilibrium, the molar flux of $SiO_{(g)}$, J_{SiO}, from the silicon surface can be calculated:

$$2J_{O_2} = J_{SiO} = \frac{k_{SiO}}{RT} \cdot p^*_{SiO} \tag{5}$$

Here k_{SiO} is the mass transfer coefficient for $SiO_{(g)}$ (m s^{-1}), R is the gas constant ($8.21 \cdot 10^{-5}$ m^3 atm K^{-1} mol^{-1}), T is the absolute temperature and the stoichiometric balance between SiO and O_2 fluxes is recognized.

The mass transfer coefficient, k, is calculated from the relationship [6]:

$$k_i = 0.664 \left(\frac{D_i^4}{v_i}\right)^{\frac{1}{6}} \cdot \left(\frac{v_g}{l}\right)^{\frac{1}{2}} \tag{6}$$

where D_i is the diffusion coefficient of species i (m^2 s^{-1}), v_i is the kinematic viscosity (viscosity, μ divided by density, ρ) (m^2 s^{-1}), v_g is the velocity of the gas in the vicinity of the surface (m s^{-1}), and l is the length of the sample (m). A condition [9] for the applicability for Eq. (6), can be expressed in terms of the Schmidt number, Sc,

$$\mathrm{Sc} = \frac{\mu}{\rho D}, \quad 0.6 < \mathrm{Sc} < 50 \tag{7}$$

The diffusion coefficients and viscosities are calculated according to the Chapman–Enskog method, as described by Bird et al. [10]. The Schmidt number for the present conditions is 0.71 for oxygen in argon, thus Eq. (6) is valid.

Experimental conditions were selected to yield the maximum rate of SiO volatilization in order to improve measurement accuracy. For $T = 1{,}500$ °C and $p^*_{O_2} = 1 \cdot 10^{-18}$ atm (just below the maximum $p^*_{O_2}$), p^*_{SiO} is calculated to be $2.1 \cdot 10^{-2}$ atm. This value allows calculation of the outward SiO flux from Eq. (5), as $1.47 \cdot 10^{-3}$ mol m^{-2} s^{-1} at a linear gas velocity of 0.047 m s^{-1}. The stoichiometric equivalent inward flux of oxygen of $7.34 \cdot 10^{-4}$ mol m^{-2} s^{-1} then leads via the mass transfer equation:

$$\frac{1}{2} J_{SiO} = J_{O_2} = \frac{k_{O_2}}{RT} p^\circ_{O_2} \tag{8}$$

to an estimated maximum $p^\circ_{O_2}$ (max) of $8.6 \cdot 10^{-3}$ atm. Higher values of $p^\circ_{O_2}$ are expected to produce faster rates of inward mass transfer and silicon passivation. Lower values of $p^\circ_{O_2}$ would reduce the rate of $SiO_{(g)}$ volatilization. This estimate of the maximum $p^\circ_{O_2}$ is independent of v_g, because both k_{SiO} and k_{O_2} depend in the same way on gas flow rate, and the effects cancel out.

It is of interest that this detailed mass transfer calculation leads to a result similar to that of $6.1 \cdot 10^{-3}$ atm for $T = 1{,}410$ °C, calculated by Wagner [4] using an approximate estimate of mass transfer rates.

Experimental

The material used in the experiments was photovoltaic grade silicon (9 N). The experiments were performed in a resistance heated furnace, fitted with an alumina

Table 1 Experimental matrix, with number of experiments at the different flow rates and oxygen pressures are given

Linear gas flow rate ($m\ s^{-1}$)	$p^{\circ}_{O_2}$ (10^{-3} atm)					
	0.5	1	1.5	2	5	10
0.023	1					
0.047	5	1	1	1	1	1
0.093	1					
0.12	1					
0.14	1					

tube with an inner diameter of 5.2 cm. Silicon charges of about 10 g were placed in pre-fired alumina boats of 9 cm length and 1 cm width and height, inserted parallel to the tube axis. The gas flow was parallel to the silicon surface. During heating and cooling, a gas-mixture of 5 vol.% H_2 in Ar was used to avoid oxidation. The reaction gas used was premixed 1 vol.% O_2 in Ar which was further diluted with high purity Ar in order to obtain the desired bulk oxygen partial pressure. Gas flow rates were controlled by mass flow controllers, and were in the range 0.023–0.14 m s^{-1}, corresponding to Reynolds numbers of 8.5–51, well below the turbulent flow limit of 2,000. All experiments were performed at 1,500 °C. Temperatures in the sample location were uniform within ±3 °C.

Experimental conditions used are summarized in Table 1. The kinetics of $SiO_{(g)}$ volatilization were investigated at $p^{\circ}_{O_2} = 0.5{\cdot}10^{-3}$ atm and $v_g = 0.047$ m s^{-1}. For the other exposure conditions a single reaction time of 16 h was used in each case. Post-melting sample surface areas were measured manually.

Weight changes were measured after each exposure, and the samples were metallographically sectioned and examined by X-ray diffraction (XRD) and scanning electron microscopy (SEM). Silica found deposited on the furnace wall was removed from the alumina tube and examined by XRD and SEM.

Glancing angle XRD on the surface of a passive and an active sample was performed at angles of 2.35° and 5.5°, respectively, using a PANalytical Xpert Materials Research Diffractometer. Conventional XRD on the silica collected from the tube was conducted with a D8 Focus Advance from Bruker.

The SEM used was a Zeiss Ultra 55 Limited Edition field emission microscope, operated at 5 kV.

Results

Initial experiments at $p^{\circ}_{O_2} = 1{\cdot}10^{-2}$ atm resulted in passivation. Oxidation of the Si-surface is clearly shown in the cross section as a thick oxide scale in Fig. 3a. The structure of the surface layer was identified by low angle XRD as a mixture of amorphous silica and the crystalline phase of SiO_2 cristobalite (syn), shown in Fig. 4a. Passivation also resulted at $p^{\circ}_{O_2} = 5{\cdot}10^{-3}$ atm but was avoided at lower oxygen pressures. The samples where active oxidation occurred had a visually clean surface.

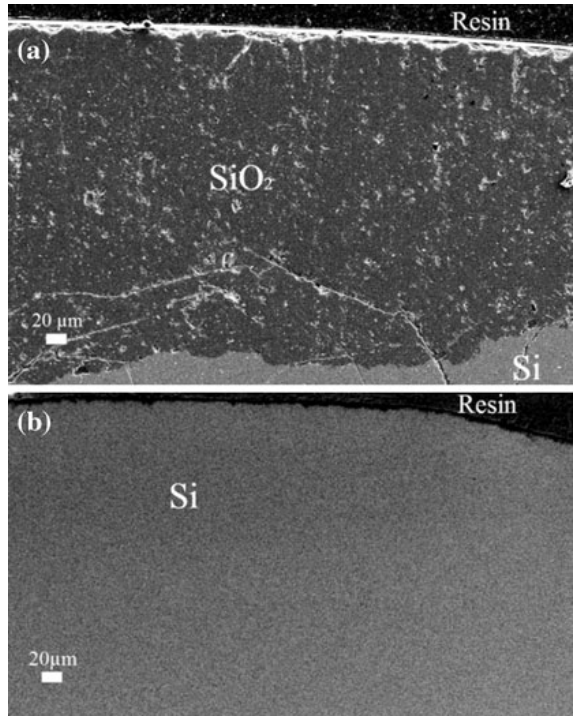

Fig. 3 SEM image of sample cross section after **a** passive and **b** active oxidation. Experimental conditions: **a** $v_g = 9.3$ cm s^{-1}, $t = 16$ h, $p^{\circ}_{O_2} = 1{\cdot}10^{-2}$ atm, **b** $v_g = 4.7$ cm s^{-1}, $t = 16$ h, $p^{\circ}_{O_2} = 0.5{\cdot}10^{-3}$ atm

Cross section analysis by SEM showed no deposits formed on the silicon surface (Fig. 3b), and the low-angle XRD did not detect any silica, only silicon (Fig. 4b). Closer examination of the Si diffraction seen in Fig. 4a and b reveals that the silicon had developed different textures during solidification with and without a silica coating.

Weight loss kinetics are shown in Fig. 5 for $p^{\circ}_{O_2} = 0.5{\cdot}10^{-3}$ atm and $v_g = 0.047$ m s^{-1}. The regression line has an R^2 value of 0.74.

The rate of weight loss (r) as a function of bulk oxygen partial pressure, $p^{\circ}_{O_2}$ at a flow rate of $v_g = 0.047$ m s^{-1} is displayed in Fig. 6, with an R^2 value of the regression line of 0.90.

The linear dependence of rate on $p^{\circ}_{O_2}$ confirms the applicability of Eq. (8). The slope of the curve is related through Eq. (9) to the mass transfer coefficient for oxygen, k_{O_2}:

$$\frac{d|r|}{dP^{\circ}_{O_2}} = \frac{2k_{O_2}}{RT} \tag{9}$$

The experimental mass transfer coefficient estimated this way is $k^{ex}_{O_2} = 3.06$ cm s^{-1} for a linear velocity of 0.047 m s^{-1} and $T = 1{,}500$ °C. The variations in the rate of weight loss with $(v_g/l)^{0.5}$ [see Eq. (6)] is shown in Fig. 7, where the linear dependency is apparent. The R^2 value for the linear regression in Fig. 7 is 0.73.

The experiments which gave active oxidation produced a silica layer deposited on the tube wall. The XRD spectrum of this deposit is presented in Fig. 8, and an

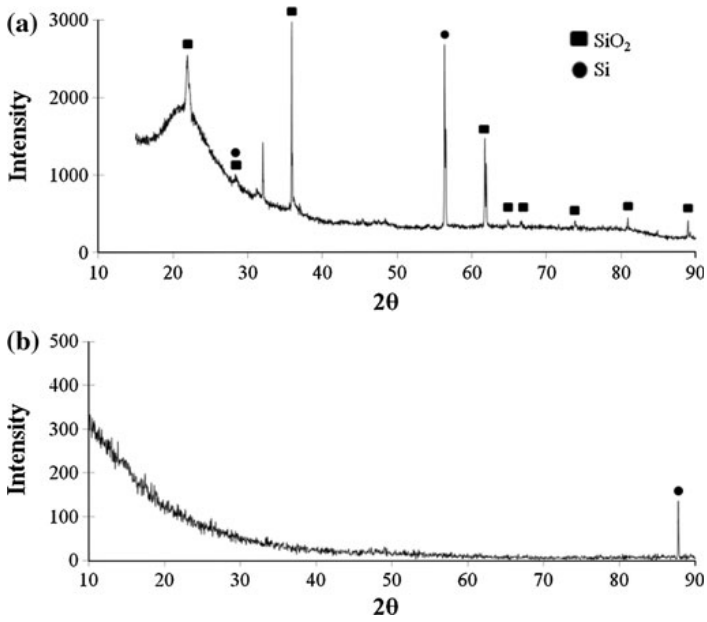

Fig. 4 Glancing XRD diffraction patterns of the surface of a passive sample (**a**) and an active sample (**b**). Experimental conditions: **a** $v_g = 9.3$ cm s^{-1}, $t = 16$ h, $p^{\circ}_{O_2} = 1{\cdot}10^{-2}$ atm, **b** $v_g = 4.7$ cm s^{-1}, $t = 16$ h, $p^{\circ}_{O_2} = 1{\cdot}10^{-3}$ atm

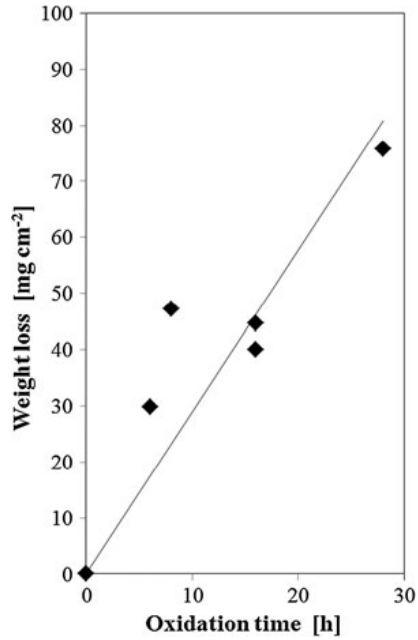

Fig. 5 Weight loss kinetics at $T = 1{,}500$ °C, $p^{\circ}_{O_2} = 0.5{\cdot}10^{-3}$ atm and $v_g = 0.047$ m s^{-1}. Regression line has an R^2 value of 0.74

SEM image of the fume particles is shown in Fig. 9. It is shown that the deposit is amorphous silica particles in the shape of spheres with a rather uniform size of 50–200 nm.

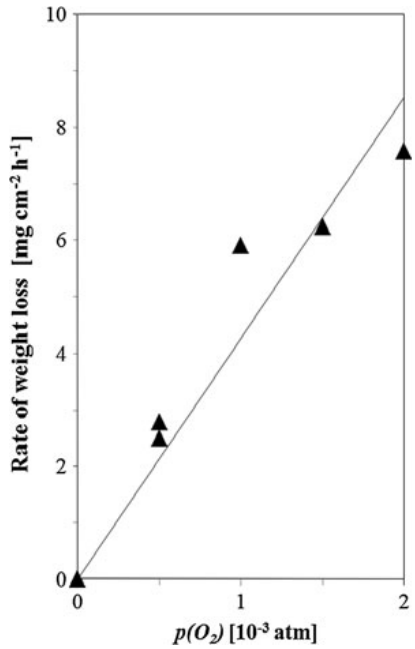

Fig. 6 Rate of weight loss, r, as a function of bulk oxygen pressure at 1,500 °C and $v_g = 0.047$ m s^{-1}

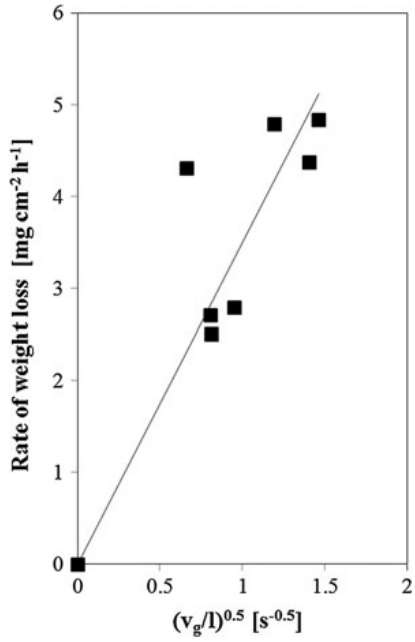

Fig. 7 Rate of weight loss as a function of the square root of linear velocity divided by sample length, measured at $T = 1{,}500$ °C and $p^{\circ}_{O_2} = 0.5{\cdot}10^{-3}$ atm

Discussion

Experiments performed at $5{\cdot}10^{-3}$ and $10{\cdot}10^{-3}$ atm bulk oxygen pressures led to passive oxidation of the liquid silicon surface (Fig. 3a). This was observed as an apparently glassy layer, identified as a mixture of amorphous silica and cristobalite by XRD (Fig. 4a).

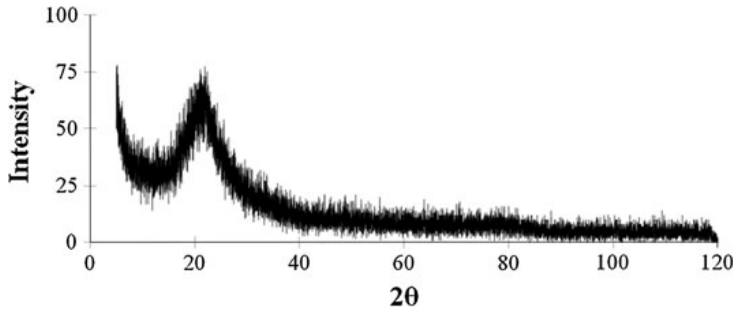

Fig. 8 XRD-pattern from fume deposits collected from inside the furnace tube

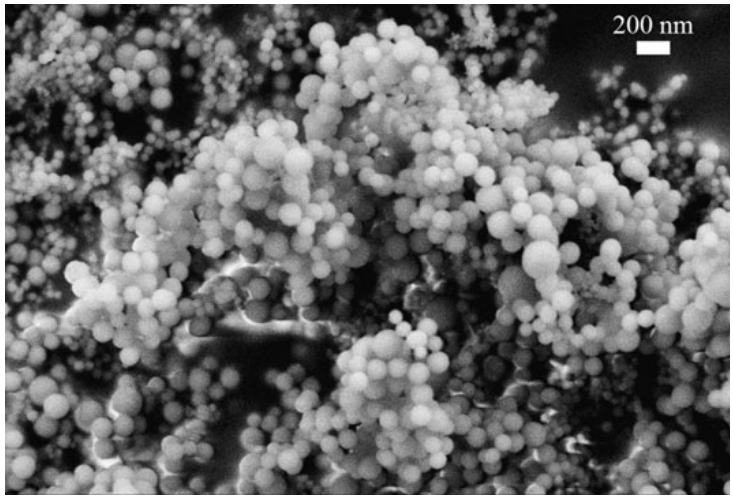

Fig. 9 SEM image of the fume deposits collected from inside the tube

At oxygen partial pressures of $2{\cdot}10^{-3}$ atm and lower, the active oxidation regime was obtained, as evidenced by the clean silicon surface (Fig. 3b), absence of crystalline oxide detectable by glancing angle XRD (Fig. 4b) and linear oxidation kinetics. Thus the critical value for the active–passive transition, $p^{\circ}_{O_2}$ (max), was between $2{\cdot}10^{-3}$ and $5{\cdot}10^{-3}$ atm. Active oxidation rates were proportional to $p^{\circ}_{O_2}$ and $(v_g/l)^{0.5}$, in agreement with the viscous flow regime mass transfer Eqs. (6) and (8). However, the critical value $p^{\circ}_{O_2}$ (max) calculated from this theory was $8.6{\cdot}10^{-3}$ atm, approximately twice the experimental value. Reasons for this quantitative failure are investigated first.

In an evaluation of mass transfer, the boundary layer thickness, δ, is an important factor. The elementary mass transfer theory described earlier applies to boundary layer flow over a flat plate in an otherwise unconstrained space. However, the experiments were performed in a tubular furnace where the velocity profile is not accurately predicted by the boundary layer theory, because δ is significant compared to the tube cross-section. For a proper assessment of the experiments, it is therefore necessary to employ computational fluid mechanics (CFD).

Mathematical modeling of the experiments was performed using the CFD-software ANSYS/Fluent 13.0. The experimental geometry and conditions were simulated as isothermal laminar gas flow with species tracking of Ar, $SiO_{(g)}$ and O_2. Gas properties were specified as described above at the experimental temperature of 1,500 °C. At the tube inlet, velocity and gas composition are set by the experimental conditions. At the metal surface, all O_2 is assumed to be consumed and a $SiO_{(g)}$ concentration is specified. Calculations of flow field and mass transfer coefficient are not sensitive to the chosen $SiO_{(g)}$ surface concentration. All simulations were carried out with higher order numerical schemes and showed good convergence.

Results of interest are the velocity field and calculations of the overall mass transfer coefficient. The mass transfer coefficient is given by the flux of O_2 and the concentration difference of O_2 between the surface and the bulk gas (inlet value). These values can be extracted from the CFD simulations. The mass transfer coefficient results are discussed below. A typical flow field is seen in Fig. 10, where the average linear gas velocity is 4.7 cm s^{-1}. The mathematical assessment shows that the flow profile deviates from that of simple boundary layer theory, but that the flow is laminar for all experimental settings.

Mass transfer coefficients extracted from the CFD modeling, $k_{O_2}^{CFD}$, are compared to values calculated from Eqs. (6) and (8), $k_{O_2}^{th}$, in Fig. 11. The CFD results are seen to be consistently higher than those calculated for unconstrained flow over a flat plate. The difference increases with gas velocity, but is not large in the region examined. At $v_g = 4.7$ cm s^{-1}, $k_{O_2}^{CFD} \approx 3.9$ cm s^{-1}. Use of this higher value in Eq. (8) leads to a prediction of $p_{O_2}^{\circ}(\max) \approx 3{\cdot}10^{-3}$ atm, in satisfactory agreement with the experimental finding of $2–5{\cdot}10^{-3}$ atm.

The experimental mass transfer coefficient, $k_{O_2}^{ex}$, deduced from Fig. 6 is shown as a single point on Fig. 11. The three different mass transfer coefficients are in the same order of magnitude at 0.047 m s^{-1} gas flow rate. However it is seen that $k_{O_2}^{ex}$ (=3.06 cm s^{-1}) is better predicted from $k_{O_2}^{CFD}$ (=3.93 cm s^{-1}) than from the classical flat plate flow model, $k_{O_2}^{th}$ (=1.24 cm s^{-1}).

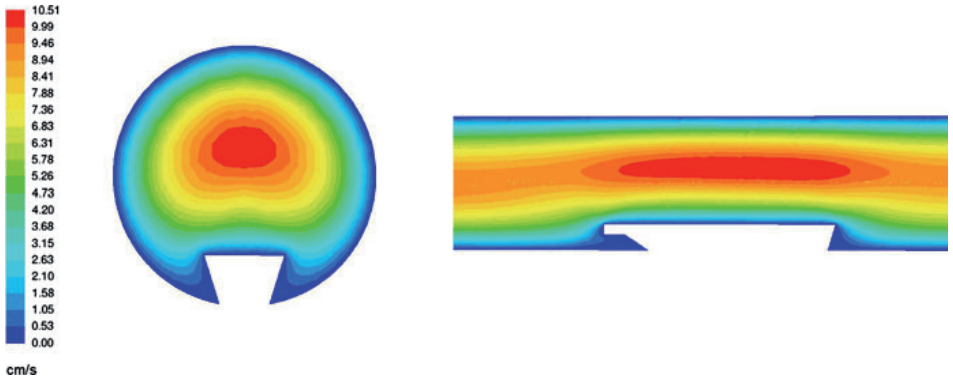

Fig. 10 Flow pattern in a tube modeled with CFD. Linear velocity color codes shown in cm s^{-1}. The average linear velocity of the gas is 4.7 cm s^{-1}

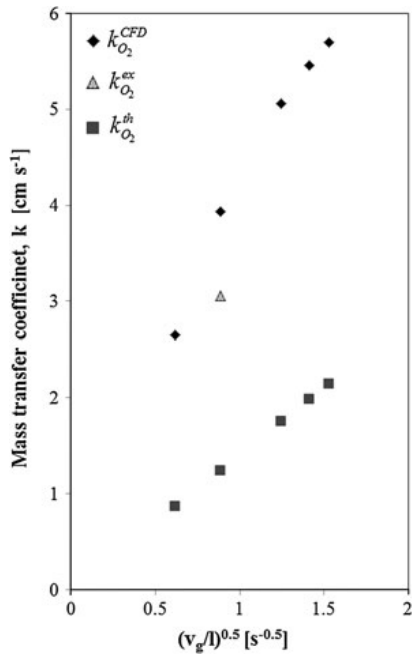

Fig. 11 Mass transfer coefficients estimated from classical theory (*square*) and from CFD modeling (*diamond*), compared to the experimentally measured mass transfer coefficient (*triangle*). $l = 6$ cm was used

The similarity between $k_{O_2}^{ex}$ and $k_{O_2}^{CFD}$ is significant, as it indicates that the flow in the tube was indeed laminar and that the simple mathematical model of Eqs. (6) and (8) describes reasonably well the common laboratory experiments conducted at low flow rates in tube furnaces. Nonetheless, maximum gas velocities are accelerated by the formation of a hydrodynamic layer attached to the tube wall, and in the present case the rate of silicon oxidation is thereby increased.

With this information it is possible to predict changes in the system as the temperature varies. In Table 2, the calculated $SiO_{(g)}$ pressure and flux plus theoretical mass transfer coefficients for oxygen temperatures are shown for three different temperatures. The minor differences in the values demonstrate that temperature is not an important factor in this system, provided that the conditions for active oxidation are achieved.

The formation of an oxidation product made up of fine, amorphous, spherical silica particles can be understood in light of the strongly exothermic nature of $SiO_{(g)}$ oxidation:

$$SiO_{(g)} + \frac{1}{2}O_{2(g)} = SiO_{2(s)}, \quad \Delta H_1 = -773.21\,\text{kJ/mol at } 1,500\,^{\circ}\text{C} \tag{10}$$

Table 2 Gas phase properties at $p_{O_2} = 1{\cdot}10^{-3}$ atm and a linear gas velocity of 0.047 m s^{-1} (where applicable)

T (°C)	1,450	1,500	1,650
p^*_{SiO} (atm)	$2.30{\cdot}10^{-3}$	$2.43{\cdot}10^{-3}$	$2.45{\cdot}10^{-3}$
J_{SiO} (mol m^{-2} s^{-1})	$1.65{\cdot}10^{-4}$	$1.71{\cdot}10^{-4}$	$1.72{\cdot}10^{-4}$
$k^{th}_{O_2}$ (cm s^{-1})	1.17	1.24	1.36

An adiabatic temperature rise calculation is performed using heat capacities and phase change enthalpies from HSC Chemistry [8] to show that the silica particles have been formed via the liquid state of SiO_2, hence the spherical shape:

$$SiO_{2(s)}(1500\,^{\circ}C) \rightarrow SiO_{2(s)}(1713\,^{\circ}C), \quad \Delta H_2 = \int C_{p(s)}dT = 17.58\ \text{kJ/mol} \quad (11)$$

$$SiO_{2(s)} \rightarrow SiO_{2(l)}, \quad \Delta H_3 = -1.31\ \text{kJ/mol at } 1713\,^{\circ}C \quad (12)$$

$$SiO_{2(l)}(1713\,^{\circ}C) \rightarrow SiO_{2(l)}(2950\,^{\circ}C), \quad \Delta H_4 = \int C_{p(l)}dT = 106.10\ \text{kJ/mol} \quad (13)$$

$$SiO_{2(l)} \rightarrow SiO_{2(g)}, \quad \Delta H_5 = 527.65\ \text{kJ/mol at } 2950\,^{\circ}C \quad (14)$$

$$SiO_{2(g)}(2950\,^{\circ}C) \rightarrow SiO_{2(g)}(4935\,^{\circ}C), \quad \Delta H_6 = \int C_{p(g)}dT = 123.18\ \text{kJ/mol} \quad (15)$$

A final gas temperature of 4,935 °C is calculated from the heat balance

$$\Delta H_1 = -(\Delta H_2 + \Delta H_3 + \Delta H_4 + \Delta H_5 + \Delta H_6) \quad (16)$$

and it is recognized that the product is silica vapor. Rapid cooling and condensation leads to formation of liquid droplets, which grow until they ultimately solidify. This accounts for the spherical shape of the particles. Their near uniformity of size can be explained by particle growth theory [11].

Summary and Conclusions

Active oxidation of liquid silicon surfaces to produce very fine spherical particles of amorphous silica was observed in small scale laboratory experiments, successfully reproducing the essential features of fuming in the industrial oxidative ladle refining of metallurgical grade silicon.

The rate of active oxidation was controlled by gas phase mass transfer, as evidenced by the linear kinetics and the dependence of the rate on both oxygen pressure and the square root of linear gas velocity. Classical theory for mass transfer in the viscous flow regime above a flat plate yielded order of magnitude agreement with observed rates and the critical value for oxygen pressure separating active and passive oxidation regimes.

An improved description of mass transfer was provided by CFD-modeling which took into account the constraints of the reactor tube wall on gas flow. Formation of a boundary layer attached to the tube wall accelerates linear gas flow in the tube interior. This has the effect of increasing the mass transfer coefficient relative to that calculated from classical theory for unconstrained flow over a flat plate.

Calculations showed that temperature is not an important factor in determining the thermodynamics and kinetics of $SiO_{(g)}$ volatilization at temperatures of 1,450–1,650 °C, and laboratory flow conditions.

Acknowledgments The experimental work presented in this paper was performed at the School of Materials Science and Engineering at The University of New South Wales in Sydney, Australia. The

funding was provided by Norwegian Research Council and FFF (Ferro Alloys Industries Research Association) through the FUME project (Fugitive emissions of Materials and Energy). The funding for the research exchange was provided by UNIFOR, Elkem's research fund and Norsk Hydro's research fund.

References

1. A. Schei, J. K. Tuset, and H. Tveit, *Production of High Silicon Alloys* (Tapir Forlag, Trondheim, 1998).
2. A. Ashrafian, S. T. Johansen, S. Gaal, B. Andresen, and O. S. Klevan, in *6th international Conference on CFD in Oil & Gas, Metallurgical and Process Industries* (SINTEF/NTNU, Trondheim, Norway, 10–12 June, 2008).
3. M. K. Næss, G. Tranell, J. E. Olsen, N. E. Kamfjord and K. Tang, *Oxidation of Metals*, doi: 10.1007/s11085-012-9303-9 (2012).
4. C. Wagner, *Journal of Applied Physics* **29**, 1295 (1958).
5. M. Ratto, E. Ricci, E. Arato, and P. Costa, *Metallurgical and Materials Transactions B* **32**, 903 (2001).
6. J. W. Hinze, and H. C. Graham, *Journal of the Electrochemical Society* **123**, 1066 (1976).
7. P. Carter, B. Gleeson, and D. J. Young, *Oxidation of Metals* **56**, 375 (2001).
8. HSC Chemistry 7.0, Outotec. Research Oy, Helsinki (2009).
9. D. J. Young, and B. A. Pint, *Oxidation of Metals* **66**, 137 (2006).
10. R. B. Bird, W. E. Stewart and E. N. Lightfoot, *Transport Phenomena*, Chaps. 1 & 17 (Wiley, New York, ISBN 0-471-41077-2 2002).
11. N. E. Kamfjord, H. Tveit, M. K. Næss and E. H. Myrhaug, in *TMS* (The Minerals, Metals & Materials Society, March 11–15, Walt Disney World, Orlando, FL, USA, 2012).

PAPER 4

EXPERIMENTAL STUDY OF RATE OF SILICA FUME FORMATION FROM ACTIVE OXIDATION OF LIQUID SILICON

Mari K. Næss[1], Nicholas Smith[1], Gabriella Tranell[1], Jan Erik Olsen[2]

[1]Norwegian University of Science and Technology (NTNU);
Alfred Getz vei 2, NO-7491 Trondheim, Norway.
[2] SINTEF Materials and Chemistry, 7465 Trondheim, Norway.

ABSTRACT

In the silicon and ferrosilicon industry there are several environmental challenges, one of them being diffuse emissions of fume. Fume emissions in the plant are often poorly captured, and thus contribute to making the indoor environment harmful for the workers. On-going research into solutions to reduce the emissions is hence vital.

In earlier studies, the main source of fugitive emissions - amorphous silica fume formation - was established; oxidation of liquid silicon during tapping and refining. The limiting factor for the fuming rate was found to be the oxygen availability at the liquid silicon surface, and a silica flux was estimated from measurements.

In order to better understand the mechanisms behind industrially observed fuming rates, experiments performed in a 75 kW induction furnace were carried out, and the rate of fume formation as a function of gas composition and flow velocity was measured. The particle size of fume particles, formed due to active oxidation of a moving liquid silicon surface, was also determined as a function of gas flow rate, and gas composition. The fume was collected in an industrial type filter, and all equipment was weighted before and after each experiment in order to monitor the weight loss/gain.

The results of the experimental study showed that the flux of silica increased with increased gas velocity above the liquid surface, and was found to correlate well with mass transfer rates calculated from impinging jet theory. The size of the particles was also found to be dependent on the gas flow rate.

The findings are discussed in light of recent measurements and modeling of Si oxidation rate in industrial and small scale.

Key words: Diffuse emissions, liquid silicon, oxidation rate, amorphous silica fume.

INTRODUCTION

In recent years, the restrictions enforced by authorities on the working environment for operators in the Norwegian ferroalloy industry have become stricter. As a consequence, there has been increased attention to monitoring the fugitive emissions which have an impact on this environment, and attempts to quantify the emissions have been made[1].

The fume emitted to the indoor environment is a possible threat to the health of the workers at the plant[2], in addition to being a direct loss of silicon, which in turn has economic consequences. In a typical silicon plant there are large fugitive emissions of fumed silica related to the tapping, refining and casting processes, and fume hoods are not always adequate to capture all of the fume. In some cases it will not even be possible to capture the fume, for example during moving of the ladle in the hall of the plant.

In an earlier work, the fugitive emissions of fume during refining of metallurgical grade silicon were quantified[1]. It was found that the flux of fume is linearly correlated to the purging rate of the refining gas which is purged through the melt from a nozzle in the bottom of the ladle. When the purging increases, there will be more rigorous stirring and a larger and more dynamic surface available to the air. The amount of fume going off during refining was approximately 1 kg SiO_2 per ton of Si produced, equivalent to 75 tons of silica per year.

The major mechanism behind the fume formation was also established; active oxidation of the liquid silicon surface. The silicon is first partially oxidized to SiO gas (Eq. 1) which escapes the surface and is subsequently combusted to become SiO_2 fume (Eq. 2). The fume consists of small, amorphous spheres of glassy silica[1, 3].

$$Si_{(l)} + \tfrac{1}{2} O_{2(g)} \rightarrow SiO_{(g)} \quad (1)$$

$$SiO_{(g)} + \tfrac{1}{2} O_{2(g)} \rightarrow SiO_{2(l/s)} \quad (2)$$

If the oxygen partial pressure in the bulk gas above a stagnant silicon surface is increased above a certain maximum pressure ($6.1 \cdot 10^{-3}$ atm at 1410°C according to Wagner[3]), passivation of the surface will occur; a layer of oxide will form on the silicon surface (Eq. 3), inhibiting further oxidation:

$$Si_{(l)} + O_{2(g)} \rightarrow SiO_{2(l/s)} \quad (3)$$

The rate of the active oxidation of liquid silicon has recently been investigated with small scale experiments, where a laminar flow of different Ar-O_2 mixtures was carried over a stagnant silicon surface. The reaction mechanism and reaction product found in the industry were reproduced, but not the rate of fume production or the oxidation conditions (oxygen partial pressure and a dynamic silicon surface)[4]. A comparison of the industrial measurements and the small scale experiments is shown in Figure 1.

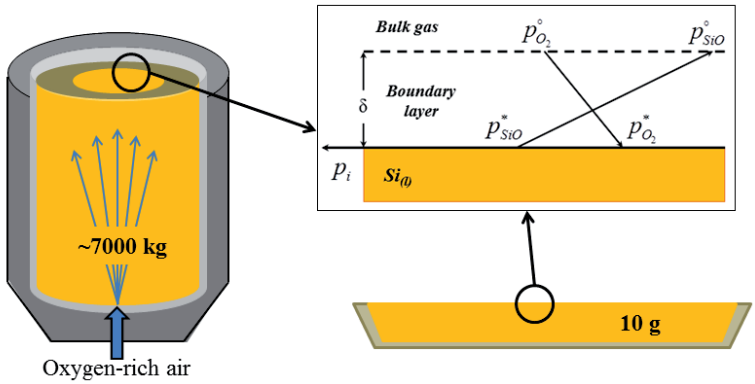

Industrial Measurements	**Small scale experiments**
Turbulent, moving Si surface	Stagnant Si surface
Turbulent natural convection in air above silicon surface	Forced, laminar flow of Ar-O_2 above silicon surface
$p^{\circ}_{O_2} = 0.21$ atm	$p^{\circ}_{O_2} = 2 \cdot 10^{-3}$ atm
$J_{Si} = 0.018$ - 0.037 mole/m²s	$J_{Si} = 2.5 \cdot 10^{-4}$ - $7.5 \cdot 10^{-4}$ mole/m²s

Figure 1: Comparison of the conditions and results from industrial measurements of fume formation and fundamental small scale experiments.

As the results from the investigation in industrial and small scale are not in order of magnitude agreement in terms of oxidation rate per unit exposed silicon area, the key question of which main factors determine the rate of fume formation in the industry, still remain. In this work, the situation of the oxidation in industry is attempted reproduced in terms of oxygen partial pressure

(air) and a moving silicon surface. However, gas is introduced on top of the silicon surface rather than through the melt.

The molecular reaction mechanism for the active oxidation is not yet fully understood, but it is generally accepted[5] that the chemical reaction is fast due to the high temperature and that the transport of reactant and product are the rate limiting steps. The diffusion of oxygen towards the silicon surface, and SiO away from the surface is linear according to Fick's law[6];

$$\tfrac{1}{2} J_{SiO} = J_{O_2} = \frac{k_{O_2}}{RT} p^{\circ}_{O_2} = \tfrac{1}{2} \frac{k_{SiO}}{RT} \cdot p^{*}_{SiO} \tag{4}$$

Here k_i is the mass transfer coefficient for species i [m/s], R is the gas constant, T is the absolute temperature and the stoichiometric balance between SiO and O_2 fluxes is recognized. In the classical flat plate theory, the mass transfer coefficient is a function of the square root of the linear gas velocity in vicinity of the surface, $\sqrt{v_g}$ [6]. However, in the theory for an impinging laminar jet the mass transfer coefficient is, according to Scholtz (1970)[7], a function of the linear gas velocity to the power of ¾, $v_g^{\frac{3}{4}}$:

$$\mathrm{Sh} = 0.5071 \mathrm{Re}^{\frac{3}{4}} \cdot \left(\frac{x}{R} \right)^{-\frac{5}{4}} \cdot 0.1955 \ \mathrm{Sc} \tag{5}$$

where

$$\mathrm{Sh} = \frac{k_i l}{D} \ , \ \mathrm{Re} = \frac{\rho v_g l}{\mu} \ , \ \mathrm{Sc} = \frac{\mu}{\rho D} \tag{6}$$

Sh denotes Sherwood number, Re the Reynolds number and Sc the Schmidt number. x is the distance from the stagnation zone (in the center of the surface), R is radius of the jet nozzle, l is the characteristic length (in this case the nozzle diameter), D is the diffusion coefficient, ρ is the density, μ is the viscosity and v_g is the linear gas velocity. Using this relation it is possible to relate the measured flux of silica to the linear gas velocity in the impinging jet system.

In this work the moving silicon surface was obtained with an induction furnace, and a laminar impinging jet was used to mimic the natural convection of air above the melt. The turbulent Si surface caused by gas bubbling in industrial refining was not reproduced as the aim was to obtain a better understanding of the fundamental factors determining the rate of silica formation on the silicon *surface* in the industrial refining of silicon.

METHOD

The experiments were performed in a 75 kW induction furnace from Inductotherm Europe Ltd. The silicon was melted in a graphite crucible, and the typical sample batch was 1750 g of refined metallurgical grade silicon (99 % Si). The crucible was covered with a specially designed lid with three holes; one for the graphite thermowell where an S-type thermocouple was placed, one for the graphite lance and one for the exhaust port with a cooler and a filter attached. The experimental setup is shown in Figure 2. The filter used was an industrial filter of the type Gore Acid Resistant Fiberglass. The cooling system was applied due to the maximum working temperature of the filter of 280°C.

The lance was connected to a mass flow meter which was connected to synthetic air (5.5N). In order to avoid oxidation of the inside of the graphite lance, an alumina tube was placed inside the graphite tube.

The silicon was heated to 1550 ±11 °C, and kept at this temperature during the blowing. After the synthetic air was set to the desired flow rate, the lance was lowered so that the tip was situated

2.5 cm above the silicon melt surface. The experiments at 16, 21 and 26 m/s gas velocity at the lance exit were held for 30 minutes, and the experiments at 5 m/s gas velocity at the lance exit were held for 60 minutes.

In addition, an experiment with humid air was performed. The synthetic air was bubbled through a water bath at 23.5°C, obtaining a partial pressure of water of 0.03 atm. The humid air experiments were performed at 16 m/s gas velocity at nozzle exit, and held for 20 minutes.

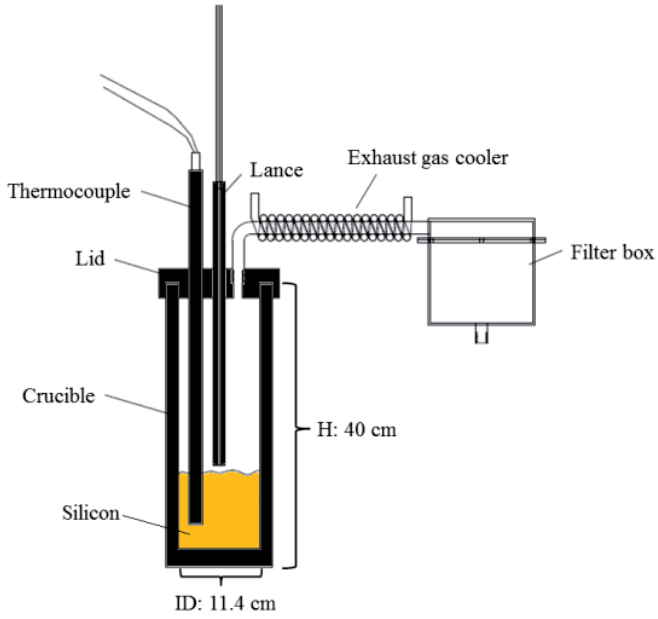

Figure 2: Sketch of experimental setup.

In order to determine whether the increased amount of oxygen introduced to the surface per time or the increased gas velocity itself was the factor for increased silica production with increased gas flow, a diluted air experiment was also performed. The synthetic air was diluted 1:4 with Ar, obtaining the same amount of oxygen delivered to the surface per unit time as that of the 5 m/s-experiment, and the same gas velocity as in the 26 m/s-experiments. These experiments were held for 20 minutes.

To monitor the amount of silica produced, all parts of the experimental equipment were weighed before and after each experiment, and the weight gain was summed up to be the total amount of silica.

The experimental matrix is shown in Table 1, where the number of experiments at each flow rate and gas composition is indicated.

The amount of silica in grams was used to calculate the average flux of SiO_2 in moles/m^2s, assuming a flat silicon surface of 102 cm^2.

Table 1: The experimental matrix with number of experiments performed at each condition is indicated.

Type of air	Linear gas velocity at lance tip, m/s			
	5	16	21	26
Dry	2	2	2	2
Wet		2		
Diluted				2

Fume samples from the experiments were examined in a Scanning Electron Microscope (SEM). The equipment used was a Zeiss Ultra 55 Limited Edition field emission microscope. The samples were held in place by a carbon tape in order to avoid charging, and the images were recorded at an acceleration voltage of 5 kV, with magnifications 2 k - 50 k.

The specific surface area of the fume samples were measured with BET to find the average particle diameter. The samples were degassed over night at 250°C under vacuum in a VacPrep 061 from Micromeretics, and analyzed with liquid nitrogen in a Tristar™3000 from Micromeretics.

In order to evaluate the flow fields at the different gas velocities, CFD modeling was performed. CFD (i.e. computational fluid dynamics) calculates flow field from differential equations expressing conservation of mass and momentum. Conservation of atomic species and reaction mechanics may also be included to study reactive phenomena[7]. The gas velocity was extracted at ¼ r, ½ r and ¾ r (where r is the radius of the silicon surface, 5.7 cm) and 0 - 20 mm from the surface.

RESULTS & DISCUSSION

The measured flux of SiO_2 as a function of $v_g^{\frac{3}{4}}$ is plotted in Figure 3. The fluxes were calculated from the surface area of the silicon, measured weight of silica produced and blowing time. Two parallels at each flow rate and gas composition were performed, and the variation between parallels was 3 – 37 %. When the flux was plotted in the same manner as a function of $v_g^{\frac{1}{2}}$ in accordance with the flat plate theory, the regression line for the dry air points had an R^2 value of 0.76, which is a little bit lower than the impinging jet plot in Figure 3.

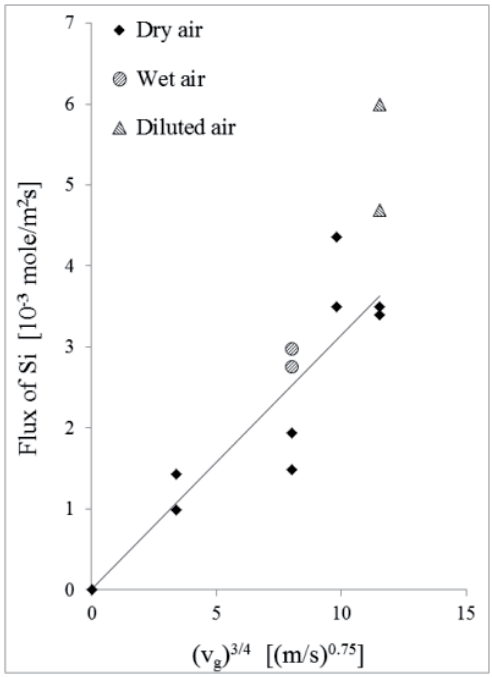

Figure 3: Measured flux of Si as a function of $v_g^{\frac{3}{4}}$. The diamonds (♦) are for dry synthetic air, and the sphere (●) is water saturated synthetic air, and the triangle (▲) is for diluted air. The regression line is for the dry air points only, with an R^2 value of 0.80.

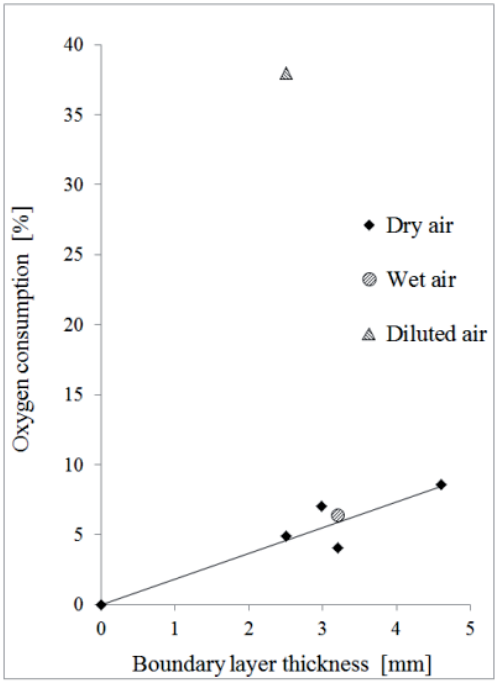

Figure 4: The average oxygen consumption as a function of average boundary layer thickness from CFD modeling. The diamonds (♦) are for dry synthetic air, and the square (●) is water saturated synthetic air, and the triangle (▲) is for diluted air. The regression line is for the dry air points only, and the R^2 value is 0.86.

The fluxes measured in the present setup are still one order of magnitude lower than that measured in the industry. The reason for this is unclear, however the movement of the Si surface in industry is turbulent and fast, compared to the calm stirring in an induction furnace. This may be a factor affecting the rate of fume formation and should be investigated further.

The experiment with humid air gave an absolute increase in the flux of 68 % as compared to dry air, thus water may have an important effect in the fuming rate in industry. However, looking at the statistics, the flux is still within the experimental error, and when calculating the oxygen consumption, this was only increased from 4 % with dry air to 6 % with wet air.

The relative consumption of available oxygen as a function of boundary layer thickness is shown in Figure 4. The boundary layer thickness was found from the CFD modeling, where the boundary layer thickness at the three distances from the center was set to be at the point with max velocity, as shown in Figure 5. The distances were averaged and set as the boundary layer thickness for that particular flow rate. This approximation is reasonable, since the boundary layer is not discrete. The CFD model confirmed that the flow was laminar in all experiments, and that there is a linear relation between the gas velocity at the lance tip and along the surface at all flow rates.

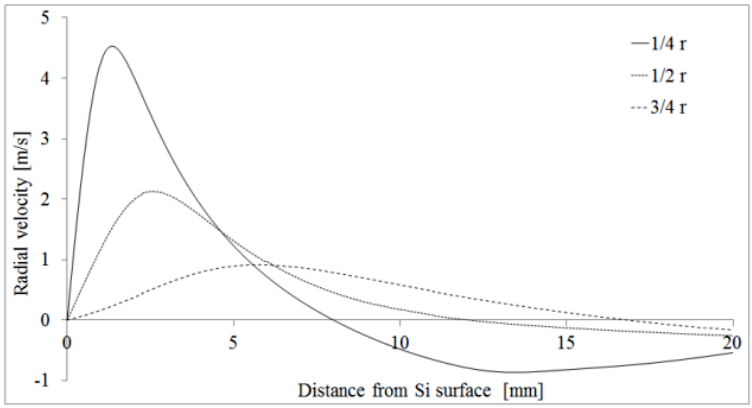

Figure 5: CFD modeled radial gas velocities above the silicon surface at three different radial positions.

The fact that the consumption of oxygen or "oxygen efficiency" decreases with increased gas flow rate tells us that the decrease in the boundary layer thickness is not proportional to the increase in amount of oxygen delivered per unit time. In fact there is a linear decrease in the oxygen efficiency as the boundary layer thickness becomes thinner (Figure 4). At 5 m/s, the flux of SiO_2 was $1.2 \cdot 10^{-3}$ mole/m^{2}s, and at 26 m/s it was $3.5 \cdot 10^{-3}$ mole/m^{2}s. If the oxygen efficiency was the same, the flux would have to be five-fold, however the measured increase in flux was only a factor of 2.9, which reflects the decrease in oxygen consumption from 9 % at 5 m/s to 5 % at 26 m/s. The explanation for this is likely that the transport of oxygen towards the silicon surface is too slow to exploit the increased oxygen amount, and thus it is not consumed.

The experiment performed with 1:4 air:Ar gave a large increase in the flux. The oxygen consumption went from 9 % at 5 m/s air, to 38 % at 26 m/s air-Ar mixture. This indicates that the gas flow rate, and thus the boundary layer thickness is more important to increase the flux of silica, than the oxygen partial pressure. The transport of oxygen from the bulk to the silicon surface is the factor limiting the rate of oxidation of the silicon. This is also reflected in the fact that there is no accumulation of SiO close to the surface as the gas velocity increase; an experimental p_{SiO} was calculated with the mass transfer coefficient found with the impinging jet theory and it was found that the partial pressure of SiO was principally the same for all gas flow rates (0.0037 - 0.0068 atm), with only 25 % standard deviation. This implies that the transport of SiO away from the surface is not rate limiting, as there is no accumulation of SiO at the surface with a higher rate of oxygen coming in. The sole factor limiting the oxidation rate is thus the transport of oxygen. Comparing the diffusion coefficients of SiO ($D_{SiO-N_2} = 3.9 \cdot 10^{-4}$ m^2/s at 1550°C) and O_2 ($D_{O_2-N_2} = 4.7 \cdot 10^{-4}$ m^2/s at

1550°C) shows that the transport of SiO should have been slightly slower than that oxygen, however, when we take into account that the SiO gas is consumed quite fast in the combustion to become $SiO_{2(g)}$ and later grow into silica particles, the transport of SiO will most probably be enhanced.

The product in the reaction was confirmed to be the same as the silica found in industry[1] and small scale experiments[4]; small, spherical particles of amorphous silica, shown in Figure 6. The BET analysis showed that the particles formed at a lower gas flow rate had a significantly larger average particle diameter (91 nm) than the silica formed at higher gas flow rates (66 nm). The average particle sizes are presented in Table 2. The reason may be that the retention time for nucleated SiO_2 particles in the hot gas at low flow rate is longer, thus the particles have the time to grow larger. This is in agreement with Ulrich et al.'s (1977)[8] theory of silica particle growth. The average particles size is similar to that found in silica samples from the refining process in industry, which had an average particle size of 56 – 66 nm.

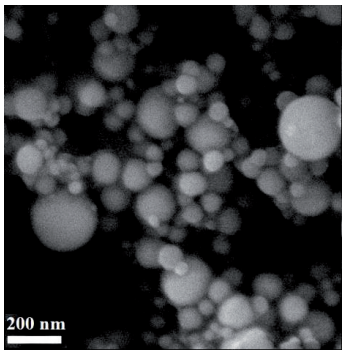

Figure 6: SEM image of the silica collected in the filter.

Table 2: Average particle diameter of the silica produced in the experiments, measured with BET.

Gas flow and composition	5 m/s air	16 m/s air	21 m/s air	26 m/s air	16 m/s wet air	26 m/s diluted air
Average particle diameter	91 nm	63 nm	72 nm	66 nm	57 nm	40 nm

If the mass transfer coefficient found by using Scholtz' equation (Eq. 5) and a sticking coefficient of 0.01 (probability of O_2 to stick to the Si surface) as proposed by Lander and Morrison (1962)[9] is used to calculate the flux of Si with Fick's law, the fluxes obtained by theoretical calculations are in the same order of magnitude as the measured fluxes, as can be seen in Table 3. The sticking coefficient was found by measuring pressure drop due to consumption of oxygen in the reaction with solid silicon at 875°C. Lander and Morrison[9] found that the sticking coefficient was not strongly temperature dependent, and thus concluded that the activation energy for active oxidation was low.

Table 3. Comparison of measured flux of Si and theoretical flux of Si, calculated with mass transfer coefficient from laminar impinging jet theory, and using a sticking coefficient of 0.01.

Gas velocity at nozzle exit	5 m/s	16 m/s	21 m/s	26 m/s
Measured J_{Si}, 10^{-3} mole/m^{2}s	1.2	1.7	3.9	3.5
Theoretical J_{Si}, 10^{-3} mole/m^{2}s	1.0	2.3	2.9	3.4

The similarity of measured and theoretically calculated flux of silicon signifies that the theoretical calculation of a mass transfer coefficient for oxygen works, assuming that the sticking coefficient is correct.

CONCLUSIONS

In this work, the conditions for fume formation in industry have been reproduced; a moving silicon surface with air being the oxidative gas. The measured flux of silica is a linear function of the gas velocity to the power of ¾, in agreement with impinging jet theory.

The rate of fume formation was not reproduced, being one order of magnitude lower than the flux pleasured in the industrial silicon refining process. The reaction product was the same as found in industry; spherical amorphous silica particles with average particle size similar to the one found in industry.

To establish whether the increased amount of oxygen introduced to the surface per unit time or the increased gas velocity itself was the determining factor for increased silica production with increased gas flow, a diluted experiment was carried out. It was found that the transport of oxygen from bulk gas to the silicon surface is the rate determining step for the silica formation, and that there is no accumulation of SiO at the surface with increased oxygen flux to the surface. The effect of dilution gave interesting results which will be investigated further in future studies.

The theoretical calculation of a mass transfer coefficient for oxygen to the silicon surface in the impinging jet system is in general agreement with measured oxidation rates, if a Lander-Morrison O_2 sticking coefficient of 0.01 for oxygen is applied.

ACKNOWLEDGEMENTS

This work was funded by the Norwegian Research Council and FFF (The Norwegian Ferroalloy Producers Research Association) through the FUME project (Fugitive Emissions of Materials and Energy). We would like to express our appreciation to Elkem Thamshavn for providing silicon for the experiments.

REFERENCES

1 Næss, M.K., Tranell, G., Olsen, J.E., Kamfjord, N.E., Tang, K. (2012), Mechanisms and Kinetics of Liquid Silicon Oxidation During Industrial Refining. *Oxidation of Metals,* **78,** pp. 239 - 251.

2 Johnsen, H.L. (2009), *Lung Function, Respiratory Symptoms, and Occupational Exposure.* PhD-thesis, University of Oslo.

3 Wagner, C. (1958), Passivity during the oxidation of silicon at elevated temperatures. *Journal of Applied Physics,* **29,** pp. 1295-1297.

4 Næss, M.K, Young, D.J., Zhang, J., Olsen, J.E., Tranell, G. (2012), Active Oxidation of Liquid Silicon: Experimental Investigation of Kinetics. *Oxidation of Metals,* **78,** pp: 363 - 376, DOI: 10.1007/s11085-012-9312-8.

5 Ratto, M., Ricci, E., Arato, E., Costa, P. (2001), Oxidation of metals with highly reactive vapors: Extension of Wagner theory *Metallurgical and Materials Transactions B,* **32,** pp. 903-911.

6 Hinze, J.W. & Graham, H.C. (1976), The active oxidation of Si and SiC in the viscous gas-flow regime. *Journal of the Electrochemical Society: Solid State Science and Technology,* **123,** pp. 1066-1073.

7 Olsen, J.E., Næss, M., Tranell, G. (2012), Understanding fuming during metal refining by CFD. *TMS Annual Meeting & Exhibition March 3-7, 2012*, Orlando, FL, USA.

8 Ulrich, G.D., & Surbramanian, N.S. (1977), Particle growth in flames III: Coalescence as a rate-controlling process. *Combustion Science and Technology,* **17,** pp. 119-126.

9 Lander, J.J. & Morrison, J. (1962), Low voltage electron diffraction study of the oxidation and reduction of silicon. *Journal of Applied Physics,* **33,** pp. 2089-2092.

PAPER 5

A new method for estimation of emissions and sources of measurements error in the silicon refining process

Mari K. Næss,[a] Ida Kero[a] and Gabriella Tranell[a]

[a] Department of Materials Science and Engineering, Norwegian University of Science and Technology, Alfred Getz vei 2, NO-7491 Trondheim, Norway. Tel: +47 73594881; E-mail: mari.k.naess@ntnu.no

Abstract

In the production of metallurgical grade silicon (MG-Si), fugitive emissions are a serious concern due to the health risks associated with the fumes formed in different parts of the production. The fumes are also a potential environmental hazard. Yet, the chemical composition of the fumes from most process steps in the silicon plant, such as oxidative refining ladle (ORL), remains unknown. This in turn constitutes a problem with respect to the correct assessment of the environmental impact and working conditions. A comprehensive industrial measurement campaign was performed at the Elkem Salten MG-Si production plant in Norway. Samples of the in- and outgoing mass flows were analyzed by High-Resolution Inductively Coupled Plasma Mass Spectrometry (HR-ICP-MS), with respect to 62 elements. In every step of the sampling and sample treatment processes, possible sources of error have been identified and quantified; including process variation, mass measurement accuracy and contamination risk. Total measurement errors for all elements in all phases are established. The method is applied to estimate the order of magnitude of the elemental emissions via the fumes from the tapping and refining processes, with respect to production mass and year. The elements with higher concentrations in the fume than slag and refined silicon include Ag, Bi, Cd, Cu, In, K, Mg, Na, Pb, Rb, Se, Sn, Tl, and Zn: all being present in the ppm range. This work constitutes new and vital information to enable the correct assessment of the environmental impact and working conditions at an MG-Si plant.

Introduction

One of the main environmental challenges facing the metallurgical industry is fugitive emissions of gas and dust. In the production of metallurgical grade silicon (MG-Si), fugitive emissions are a serious concern. The industry is subjected to extensive regulations with regards to these emissions -both in terms of outdoor and indoor environment- and in particular emissions containing toxic compounds, heavy metals or greenhouse gases [1, 2]. Furthermore, the health risks associated with the dust and fumes from the smelting and foundry industries in general, and the silicon and ferro-silicon industry in particular, is well documented [3-7]. The adverse health effects caused by long term exposure and inhalation of fume are numerous and the workers are at risk of developing respiratory problems, including chronic obstruction pulmonary disease (COPD) [8-12]. For that reason the use of dust masks are mandatory in exposed areas in most silicon plants in Norway.

Today's environmental authority reporting from the ferroalloys industry is primarily based on overall tapped material compositions and standard calculations of the distribution of major elements between products, solid waste and fugitive emissions, in addition to ad-hoc industrial measuring campaigns. For most major elements, the reporting accuracy for a plant would be in the order of thousands of kilograms while for some toxic elements like mercury, cadmium etc., accuracies in the range of kilograms are expected. Stricter emission regulations are to be expected in the future and hence, it will become important to have a full understanding of where elements entering the metallurgical plant - including those in very low concentration in the tapped material charge - will end up. It will also be of crucial importance to understand to which accuracy it is possible to measure and analyze trace elements in different phases, and the errors and uncertainties involved in both sampling and analysis of emissions, products and wastes. To date, no one has described the limits for how accurately emissions can be estimated for reporting purposes.

In the past, the fumes in a number of metallurgical processes have been studied, but often with less attention to the chemical composition and reactivity of the particles than to the particle sizes and distributions [1, 13, 14]. The fuming mechanisms in silicon production have been studied [15, 16] and some problems of the fugitive emissions have been documented with respect to the plant and local community [17].

The elemental distributions in silicon and ferrosilicon production have been previously studied with respect to the electric furnace operation [18, 19]. Although the furnace is an important source of fumes from a

silicon plant, the fugitive emissions are not exclusively originating from the furnace. Fumes are produced in virtually every production step and 40-80 % of the fugitive emissions of fume originate from the process steps where molten silicon is in contact with air [13, 20, 21]. The refining process is an important step in the chain of silicon production operations and the analysis of the element distribution in the oxidative ladle refining process will be published separately [22]. The method in itself is of general interest as it may be adapted and implemented for other process steps, as demonstrated by Myrhaug et al. [18, 19] for the electric arc furnace process.

The composition of exhaust gases from the silicon industry have been subject to several investigations as the volatile compounds need to be trapped in different kinds of ventilation and filter systems and many of these gases are potentially harmful to people and nature [23-26]. However, the chemical composition of the condensed particulate matter (CPM) and the variations of the CPM's originating from various process steps in the silicon plant remains unknown. This in turn constitutes a problem with respect to the correct assessment of environmental impact and working conditions, not only for the industry itself but also for the regulatory authorities.

This paper describes the possibilities and limitations for making accurate estimations of element concentrations in the different material flows of the refining ladle and to estimate the total measurement error for each element. The aim of this paper is twofold: 1) Establish a new method for evaluating the accuracy of the elemental analysis of all phases in the refining ladle, and 2) apply said method for estimation of fugitive emissions of main and trace elements (e.g. heavy metals) from an MG-Si plant.

Methods

A comprehensive industrial measurement campaign was performed at the Elkem Salten MG-Si plant in Norway. The main focus was to study the elemental distribution between the different phases in the refining ladle, thus samples from all ingoing and outgoing matter in the ladle was collected. Eight different ladles were investigated, and the amount of fume was measured with a LaserDust MP from Norwegian Electro Optics (NEO [27]) installed in the off-gas channel. The LaserDust measures the transmission of a laser beam, and the reduction in the signal will correspond to the amount of fume in the measuring path. Samples of silicon, slag and

fume were taken from eight refining ladles with standard purge gas mixture and flow rate conditions. At the time of the sampling, the temperature in the Si was in the range of 1446-1677°C. Samples from the tapped Si were taken from the tapping jet. A sample of the fully refined Si was collected just before casting. Slag samples were gathered from the bottom of the ladle, from the side (freeze lining) and from the top layer. Fume samples were collected with a "cold finger" (a water cooled copper tube) placed in the exhaust gas channel during tapping. The ladle and sampling locations are shown schematically in Figure 1.

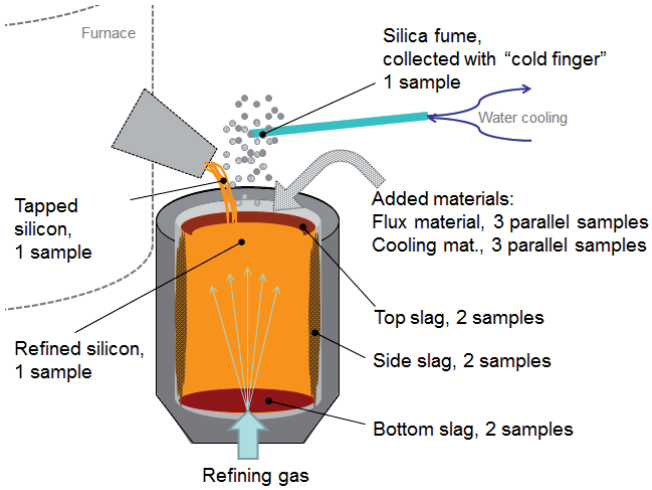

Fig 1 Schematic of the ladle with the sampling of the in- and out-going phases indicated.

In the sampling and sample treatment processes, the possible sources of error in each step have been identified. An overview is provided in Figure 2 and Table 1. For each element considered, all of these sources of error and uncertainties are given either a measured or calculated/estimated value.

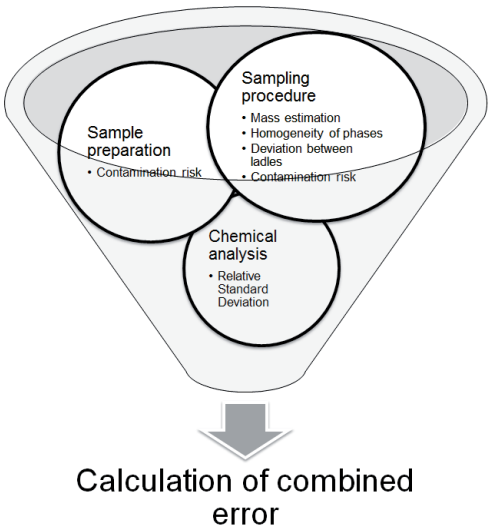

Fig. 2 The major error sources and uncertainties associated with each step of the experimental method.

Table 1: Major error sources in mass flows into and out of the ladle.

Error parameter	*Tapped & refined Si*	*Slag*	*Fume*
a	St. dev. between ladles	St. dev. between ladles	St. dev. between ladles
b	Sample representativity	Sample representativity	Sample representativity
c	Mass measurement	Mass measurement	Mass estimated from measurement
d	Contamination	Contamination	Contamination
e	Analysis (ICP-MS RSD)	Analysis (ICP-MS RSD)	Analysis (ICP-MS RSD)

Finally, a combined measurement error for each element is estimated using equation (1) [28]:

$$X_{\varphi}^{El} = \sqrt{a_{\varphi}^{El\ 2} + b_{\varphi}^{2} + c^{2} + d_{\varphi}^{El\ 2} + e_{\varphi}^{El\ 2}} \quad (1)$$

where X_{φ}^{El} is the total/combined measurement error for element *El* in phase φ, and *a, b,….e* are the calculated measurement errors in each step of the sampling process and samples preparation, as indicated in Table 1. These errors may be specific for elements, and are then marked with a superscript *El*, or they are the same for all elements (e.g. error in mass estimation).

Recovery calculations for each element have been carried out according to:

$$\%R_i = 100 \cdot \left(\frac{m_{i,out}}{m_{i,in}} \right) \tag{2}$$

where $\%R_i$ is the recovery in %, $m_{i,out}$ and $m_{i,in}$ are the total masses of element *i* flowing out of and into the ladle, respectively. Out-going mass flow is the sum of the produced Si, the slag and the fume. In-going mass flow is the sum of the tapped Si, the cooling material and the flux material.

Some potential sources of contamination are not taken into account in this paper; these are for example the use of steel lances and bullets for opening the tapping hole of the furnace, and fractioning of the ladle lining upon slag removal. They are estimated to have comparatively small influences on the overall element concentration and distribution.

In the following sections, the measurement errors in each step in the sampling and sample treatment processes are described.

Sampling procedure

The tapped silicon was sampled directly as tapped from the furnace. The samples of tapped silicon may not be entirely representative for the whole bulk of tapped silicon, due to inhomogeneous silicon in the furnace. As the tapped silicon sample is collected by a small crucible on a stick and cast in a holder, there will be little or no contamination in the sampling process. The measurement error due to process variation is however taken into account through the standard deviation between the eight sampled ladles for all elements (error type *a*).

Due to the vigorous stirring produced by the refining gas introduced from the bottom of the ladle, the refined silicon sample is relatively homogenous which enables representative samples. Also here, the process variation is taken into account for all elements by calculating the standard deviation between the eight samples.

The slag consists of the top slag, the bottom slag and the freeze lining, each of which are inhomogeneous phases which poses practical sampling problems in terms of the samples being representative for the bulk phase. Most slag tapped from the furnace is expected to end up in the bottom slag. Therefore, the slag samples may not be entirely representative for all the elements analyzed. In the estimation of the combined error for elements in the slag the standard deviation between the slag samples in each ladle is taken into account (error type *b*), in addition to the process variation (error type *a*).

The fume samples were collected with a "cold finger" (water cooled Cu tube) in the ventilation hood above the ladle. The fumes discussed here are therefore only the condensed components of the fume. Some volatile compounds (for example H_2S, NO_x, CO_x, SO_2, O_2 and H_2) are known to occur in the off-gas [24-26] but were not collected by the "cold finger", which may affect the recovery of certain elements. The "cold finger" was placed in the ventilation hood for approximately 30 min during tapping, while the whole tapping and refining process lasts for approximately 2 - 2.5 h for each ladle. The fume samples collected were considered representative for all the fume produced during the tapping. The degree of contamination of the fume samples during sampling is likely to be within standard deviation for all elements except copper (Cu). The "cold finger" used to collect the fume was made from copper, and there was a distinct contamination of copper in all the fume samples. As the true copper concentration in the fume thereby remains unknown, a recovery value of 100 % was given to all fume samples.

Mass estimation

The estimation of the mass of the in- and outgoing phases is represented by error type c in Eq. 1, and is the same for all elements. The mass flux of fume was measured with the LaserDust MP for three ladles and based on these measurements, estimated for the remaining five ladles. The standard deviation in the fume measurements were approximately 50 %, due to variations in the amount of fume during the tapping process. This high value for the error in the mass estimation of fume is assumed to include the error due to estimation of fume amount for the five ladles where the fume was not measured.

The amount of tapped silicon is measured by weighing the ladle before and after tapping. The amount of refined silicon produced in a ladle is measured by weighing the ladle before and after casting. The accuracy

of the scale is ± 10 kg, which corresponds to an average error of 0.14 % for the tapped silicon and 0.17 % for the refined silicon. The amount of slag is correspondingly measured by weighing the ladle before tapping and after casting. The calculated mass measurement error for slag is 5.4 %

Sample preparation

A total of 105 samples were collected. The solid bulk samples were crushed to a powder in a steel mill for 30 seconds. This steel mill is known to contaminate samples with Fe, Cr, W, Co, Mn, Ni, B and V (experimentally determined amounts) [29]. Where these contaminations were considered large enough (more than half of the RSD for said elements in each sample), they were included in the calculations of combined error as the elemental specific error type d.

For the HR-ICP-MS analysis 25-35 mg of each sample was used. The silicon samples were dissolved in 0.5 mL concentrated HF and 1.5 mL concentrated HNO_3 and digested at room temperature. The fume, slag and flux samples were dissolved in 0.5 mL concentrated HF, 0.5 mL concentrated HNO_3 and 0.5 mL concentrated H_2SO_4 and digested in an UltraClave from Milestone. The load pressure was 50 bar and the samples were heated to 250°C and held for 20 min. This treatment of the slag-, flux- and fume samples was performed due to earlier difficulties dissolving them at ambient temperature and pressure. Three blank samples were run at the same time as the samples in order to subtract the contamination from dissolving process and/or the chemicals used. After digestion all samples were diluted to 250 mL and run through the HR-ICP-MS.

Element analysis by HR-ICP-MS

The instrument used was an ELEMENT 2 from Thermo Electronics. This instrument will have an instrumental detection limit (IDL) for each element, determined by the blanks and by the concentration of the element. Thus, e.g. silicon had a very high IDL due to its high concentration in the samples. Elements readily found in nature like K, Na, Ca and Mg, will also have high IDL's, due to standard instrumental settings. In the cases were the concentration of an element was below its respective IDL (or had a negative concentration due to high blank concentration), half the IDL was set to represent the concentration in that sample. As an error margin of IDL/2 is generally acceptable, this approach is widely used [19].

When the samples are analyzed in the HR-ICP-MS, each sample is run three times, thus a relative standard deviation (RSD) from the ICP-MS analysis itself is obtained. The RSD is usually low, and an element analysis with an RSD < 5 % is considered as good/reliable. An RSD above 10 % is considered not very reliable. This is usually the case when elements are present in concentrations close to or below the IDL. The average RSD for all elements in all phases are included in the combined error estimation as error type e.

Estimation of combined error

When all measurement errors and calculated errors caused by variations in process and composition were identified, a combined error was calculated using Equation 1. Consider for example, the combined error of the lead (Pb) concentration in the fume.

The calculated standard deviation between the eight different fume samples is for Pb, a_{Fume}^{Pb} = 76 %. The fume samples were assumed to be representative for the whole bulk of fume produced during tapping, thus b_{Fume} = 0 % is used. The mass measurement of the fume, has an uncertainty of c_{Fume} =50 %. No Pb contamination is suspected, thus d_{Fume}^{Pb} = 0 % is used. The average RSD for Pb in the fume e_{Fume}^{Pb} was 1.8 %. The combined error for Pb in the fume (X_{Fume}^{Pb}) is then 91 %. If a concentration of 10 ppm Pb in the fume is assumed (this is a typical value), the standard deviation is 9.1 ppmw. These estimates may be used to calculate a mass range of 0.008 - 0.17 g Pb in the fume per tonne produced silicon. The annual “loss” of Pb to fume will hence for an annual production volume of 75000 tonnes silicon be 0.59 - 12 kg per year.

This method is used to calculate the combined errors for all elements in all phases, and the amount of each element in the fume per tonne silicon produced and per year has been estimated. Some errors will become seemingly high, like the 91 % in the case of lead; however, the order of magnitude will be reliable. These values may be used to estimate the amount of each element which may escape from the plant as fugitive emissions and they indicate how accurately the emission of each element can be estimated and reported with the present method. In some cases it is evident that new and more suitable methods may need developing for environmental reporting purposes.

Results & Discussion

Measurements accuracy and uncertainty

The numerical IDL and combined errors for each element in all major phases in the refining ladle are found in Table 2. Recovery ranges were calculated for all elements (Eq. 2), based on the calculated concentration intervals, the concentration intervals of elements in the fume phase can be found in table 3 in the appendix. 100 % recovery was within the range for all elements which confirms the applicability of the method. The total errors for each phase have been calculated assuming an increased risk of contamination of Cu in the fume. Increased risks of contamination from the mill (B, Cr, W, Mn, Fe, Co and Ni) have been included for the tapped Si, the refined Si and the slag.

The ICP-MS results for some of the elements (Se, Cd, In, Ir, Pt, Bi, S, Ag, Hg, Na, K, Cs, Tl and Rb), are not considered reliable. These elements were either present in concentrations below the instrumental detection limit or the relative standard deviation of the resulting values was larger than 10 %. In fact, many elements in this category were affected by both of these errors. One set of elements (Se, Cd, In, Bi, Tl, Na, Rb, Ag and K) has high instrumental/analytical errors in the silicon (and some also the slag) samples but the fume concentrations were reliable and accepted.

Note that the RSD values are included in Equation 1 and will therefore influence the combined error values. The IDL values do not influence the combined errors but may be used to assess whether the ICP-MS is a reliable tool for evaluation of any particular element. The IDL is low or very low for most elements in silicon, with some exceptions: Na, K and S have high IDL's. As these elements are present in relatively large amounts but most often have concentrations below their IDL, the interpretation of these numbers is inconclusive. As, in addition, the RSD for S is higher than 10%, any results regarding sulphur are deemed unreliable. Other elements with relatively high IDL's are Ca, P and B but since they are present in concentrations higher than the IDL in all phases, their evaluation is not affected in this case.

Table 2: Instrumental detection limits for all elements, and calculated combined errors, in percent (%) for the tapped Si, the refined Si the slag and the fume.

Element	IDL, (ppmw)	Tapp. Si (%)	Slag (%)	Ref. Si (%)	Fume (%)
Ag	0.125	†	†	†	96
Al	1.25	13	69	29	73
As	0.15625	19	44	28	75
Au	0.00125	35	54	44	80
B	0.5	9	21	12	58
Ba	0.08125	34	93	115	100
Be	0.03125	25	89	63	95
Bi	0.00625	†	†	†	96
Ca	12.5	32	104	72	68
Cd	0.0125	†	†	†	106
Ce	0.00125	12	82	23	108
Co	0.025	7	64	11	106
Cr	0.03125	54	40	63	72
Cs	0.003125	†	†	†	†
Cu	0.1875	14	60	18	71*
Dy	0.0125	15	75	32	113
Er	0.001875	18	85	42	111
Fe	0.125	9	79	7	142
Ga	0.04375	17	75	31	62
Ge	0.125	19	66	16	64
Hf	0.0063	11	36	9	125
Hg	0.00625	†	†	†	†
Ho	0.00125	17	81	39	112
In	0.003125	†	†	†	66
Ir	0.003125	†	†	†	†
K	31.25	†	112	†	60
La	0.0125	15	85	45	107
Li	0.1875	15	79	49	57
Lu	0.00125	19	98	56	108
Mg	0.625	8	84	52	64
Mn	0.0375	8	93	12	96
Mo	0.125	11	37	23	86
Na	62.5	†	115	†	55
Nb	0.1563	9	48	12	114
Nd	0.00125	12	81	21	113
Ni	0.08125	10	58	12	79
P	2.5	12	62	13	201
Pb	0.00125	76	111	74	91
Pr	0.001875	11	84	21	113
Pt	0.00625	†	†	†	†
Rb	0.075	†	138	†	62
S	125	†	†	†	†
Sb	0.0125	36	46	36	217
Sc	0.025	17	70	27	101
Se	0.3125	†	†	†	95
Sm	0.003125	13	70	44	120
Sn	0.00625	78	69	26	116
Sr	0.15625	36	96	104	82
Ta	0.00125	9	57	9	111
Tb	0.00125	16	71	30	113
Th	0.003125	15	73	18	112
Ti	0.125	7	64	10	103
Tl	0.005625	†	†	†	102
Tm	0.003125	18	89	47	111
U	0.0015625	9	77	10	126
V	0.01875	7	63	10	105
W	0.00625	98	101	79	108

Y	0.0025	22	104	73	106
Yb	0.0025	17	92	73	88
Zn	0.15625	78	129	66	69
Zr	0.15625	7	66	9	125

* Cu content in fume was estimated due to contamination
† No value due to concentration lower than IDL or too high RSD.

The major source of variation was found to be the process variation (standard deviation between the ladles). Another important source of uncertainty is the inhomogeneity of the phases sampled, most notably the slag. The inhomogeneity for all slag types is large which makes sampling difficult in terms of obtaining representative samples. Representative values can therefore be obtained by increasing the number of samples. The combined error values for the fume are generally higher than for the other phases and this is associated with the difficulties of proper assessment of the fume mass.

Elements which have a large deviation between the ladles are prone to vary greatly with the process. Elements which are more constant with respect to process must be evaluated with greater attention to analytical errors. The tapped silicon is inhomogeneous in the furnace and the composition may vary with tapping time. The furnace operation is close to a slag-free process, however due to impurities in the quartz and carbonaceous materials, some slag is formed and tapped with the silicon. The amount of slag varies greatly; some tapped material had a considerable amount of slag phase while others had virtually none. This process variation, caused by slag accumulation in the furnace, is difficult to quantify and the operation of the furnace lies outside the scope of this paper. However, as the furnace slag enters the ladle, it is incorporated in the much larger mass of ladle slag; therefore this phenomenon is included in the error estimations of the ladle slag values. While the composition of the side and bottom slags are quite similar, the top slag is different. The top slag has a much higher concentration of silicon than the other slag types which affects the slag average concentration.

Emissions estimation

Figures 2 and 3 shows the mass of each element lost to the fume, based on annual production and silicon tonnage, respectively. The values are also included in Table 3 in the appendix. Since the order of magnitude varies greatly between the elements, a logarithmic y-scale is used. Please note that no negative or zero values can be displayed on a logarithmic scale and therefore some elements appear to have no lower error bounds.

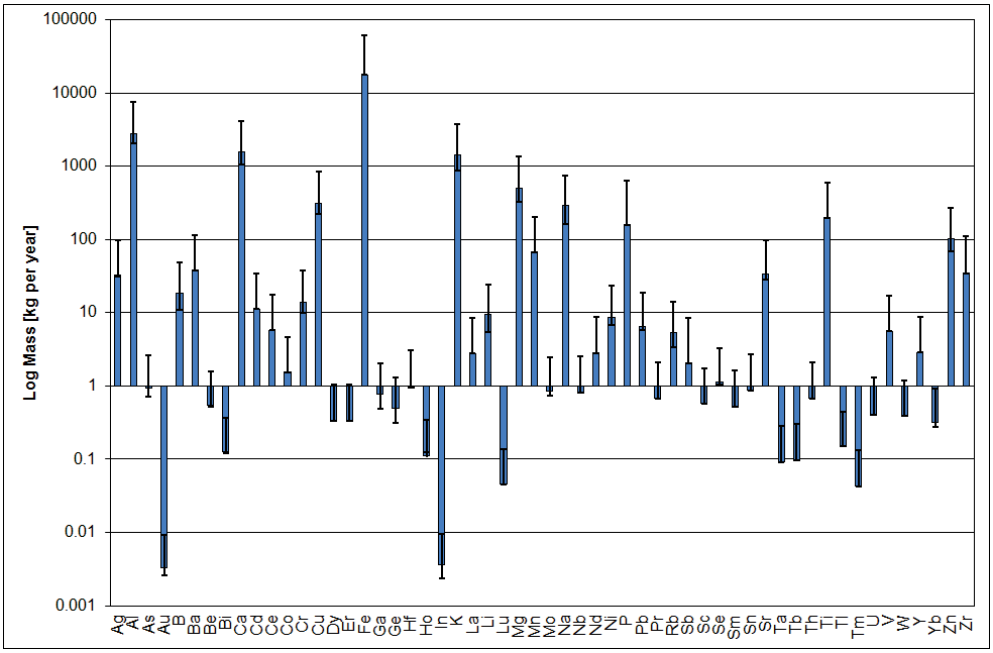

Fig. 2 The annual loss of elements to the fume. Note the logarithmic scale of the y-axis.

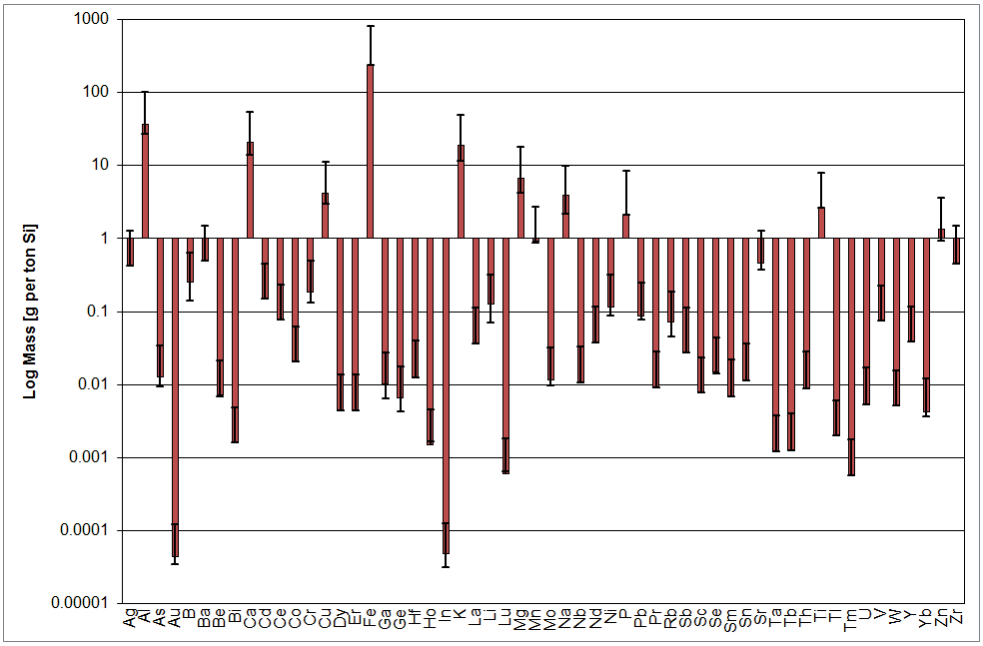

Fig. 3 Loss of elements to the fume per tonne refined silicon. Note the logarithmic scale of the y-axis.

Some of the heavy metals constitute particular risks if released to the environment. As can be seen from Figures 2 and 3 (and Table 3 in the Appendix), the fume is rich in some of the most problematic heavy metals, such as Pb, Cu, Cr, Ni, V. Other elements of special interest are the highly toxic beryllium and arsenic [30, 31]. Both As and Be have relatively high concentrations in fume. Consequently, fume collection and elimination of fugitive emissions are crucial to protect public health and to reduce the environmental impact of the plant.

Based on the error estimations and the fuming rates displayed in Figures 2 and 3 (and Table 4 in the appendix), the fugitive emissions for every element can be calculated. To correctly estimate the amount of fume which may escape a silicon plant is complex and clearly outside the scope of this paper. However, if we assume that 15 % of the fume from the tapping and refining process is released to the environment, the results in Figures 2 and 3 (and Table 4 in the appendix) can be used to calculate the annual emissions for every element via the fume. For example, the annual emission of Pb would then be < 1.9 kg.

Conclusions

The total errors of the concentrations and distributions of 62 elements in the OLR process for Si have been estimated. The elemental mass loss to the fume was estimated with respect to production mass and year, and a concentration range for all elements in the fume is given. Fume collection and mass estimation were significant error sources in these calculations. Other important error sources are the process variation and the inhomogeneity of the slag. Different slag types also have different chemical composition which complicates the slag average interpretation. A thorough understanding of the entire furnace and ladle processes is crucial to optimize the sampling procedure with respect to obtaining representative samples

The instrumental detection limit and the relative standard deviation of the ICP-MS analysis may be used to assess how appropriate the analysis method is for individual elements in each phase and to evaluate the accuracy of each measurement. Certain results are not reliable, this mainly concerns elements present in very low concentrations in the samples (such as Pt, Ir, Au, Bi, Hg, etc.). In some cases however, most notably if Na, K and S are of vital importance, other analysis methods ought to be considered.

This work is the first in its kind to publish a method for estimation of the error sources and uncertainties associated with the assessment of the elemental distributions in the mass flows into and out of the refining ladle. The method can be used to assess the annual emissions of trace elements for reporting purposes. Special emphasis was put on the fume concentrations and both major and trace elements are evaluated. As the fumes from tapping and refining are the main source for fugitive emissions from a silicon plant, this work may be used to improve emission estimates and to assess the credibility of previously reported emissions.

Acknowledgements

The financing of this work was provided by the Norwegian Research Council and The Norwegian Ferroalloy Producers Research Association (FFF) through the FUME project (Fugitive Emissions of Materials and Energy). The authors would like to express appreciation to SINTEF for contributing to this work, and to Elkem for allowing the measurements at their plant in Salten. We are especially grateful to Vegar Andersen and Halvard Tveit for their assistance. The authors would also like to thank Norsk Elektro Optikk AS (NEO) for use of their equipment, and for assistance with technical measurement issues.

References

1. Boullemant, A., Journal of the Air and Waste Management Association, 2011. **61**: p. 311-318.
2. Bartosova, M., A. Pribulova, and P. Gengel, *Influence of foundry industry on the environment*, in *8th International Conference SGEM*. 2008: Albena, Bulgaria. p. 121-128.
3. Hobbesland, Å., H. Kjuus, and D.S. Thelle, Scandinavian Journal of Work, Environment and Health, 2012. **23**(5): p. 342-350.
4. Vincent, J.H. and C.F. Clement, Philosophical Transactions: Mathematical, Physical and Engineering Sciences, 2000. **358**(1775): p. 2673-2682.
5. Laier Johnsen, H., V. Søyseth, and S.M. Hetland, International Archives of Occupational and Environmental Health. **81**: p. 451-459.
6. Bennett, C.M., P. Simpson, J. Raven, B. Skoric, J. Powell, R. Wolfe, E.H. Walters, and M.J. Abramson, Journal of Toxicology and Environmental Health, Part A: Current Issues, 2007. **70**(19): p. 1613-1618.
7. Roman, H.A., K.D. Walker, T.L. Walsh, L. Conner, H.M. Richmond, B.J. Hubbell, and P.L. Kinney, Environmental Science and Technology, 2008. **42**: p. 2268-2274.
8. Lison, D., C. Lardot, F. Huaux, G. Zanetti, and B. Fubini, Arch. Toxicol., 1997(71): p. 725-729.
9. Yuan, H., F. Gao, Z. Zhang, L. Miao, R. Yu, H. Zhao, and M. Lan, Journal of Health Science, 2010. **56**(6): p. 632-640.
10. Englert, N., Toxicology Letters, 2004. **149**: p. 235-242.

11. Kappos, A.D., P. Bruckmann, T. Eikmann, N. Englert, U. Heinrich, P. Höppe, E. Koch, G.H.M. Krause, W.G. Kreyling, K. Rauchfuss, P. Rombout, V. Schulz-Klemp, T.R. Wolf, and H.-E. Wichmann, International Journal of Hygiene and Environmental Health, 2004. **207**: p. 399-407.
12. Oberdörster, G., International Archives of Occupational and Environmental Health, 2000. **74**(1): p. 1-8.
13. Gunst, S., S. Weinbruch, M. Wentzel, H.M. Ortner, A. Skogstad, S. Hetland, and Y. Thomassen, Journal of Environmental Monitoring, 2000. **2**: p. 65-71.
14. Dingsøyr, E., M. Dåstøl, and W.C. Wedberg, in *The 5th European Symposium on Particle Characterization*. 1992. Nurnberg, Germany.
15. Næss, M.K., G. Tranell, J.E. Olsen, N.E. Kamfjord, and K. Tang, Oxidation of metals, 2012(78): p. 239-251.
16. Olsen, J.E., N. Mari, and G. Tranell, in *8th International Conference on CFD in Oil & Gas - Metallurgical and Process Industries* 2011. SINTEF/NTNU, Trondheim, Norway.
17. Nestaas, I. and E.G. Hunnes. De Norske Veritas (DNV) & Molab AS: Mo i Rana, Norway. Official government report, 2009.
18. Myrhaug, E.H. and H. Tveit, in *58th Electric Furnace Conference*. 2000. Orlando, FL.
19. Garcia, M. and E.H. Myrhaug. Elkem Silicon: Oslo, Norway. Elkem Report, 2007.
20. Midtdal, H.F. and N.E. Kamfjord. Sintef Materialer og Kjemi: Trondheim, Norway. Project report, 2010.
21. Kamfjord, N.E., *Mass and energy balances of the silicon process. - Improved emission standards*, in *Department of materials science and engineering*. 2012, Norwegian University of Science and Technology: Trondheim, Norway.
22. Næss, M.K., I. Kero, G. Tranell, K. Tang, and H. Tveit. Norwegian University of Science and Technology: Trondheim, Norway. To be published, 2013.
23. Nygjelten, E. Sintef Materialer og Kjemi: Trondheim. Project report, 2008.
24. Johansen, S.T., H. Tveit, S. Grådahl, A. Valderhaug, and J.Å. Byberg, *Environmental aspects of ferro-silicon furnace operations - an investigation of waste gas dynamics*, in *Infacon 8*. 1998, China Science and Technology Press: Beijing, China. p. 59-63.
25. Kamfjord, N.E., H. Tveit, and I. Solheim, in *3rd international symposia on high-temperature metallurgical processing*. 2012. Orlando, Florida, U.S.A.: Wiley & TMS.
26. Kamfjord, N.E., H. Tveit, M.K. Næss, and E.H. Myrhaug, in *3rd international symposia on high-temperature metallurgical processing*. 2012. Orlando, Florida, U.S.A.: Wiley & TMS.
27. Lørenskog, *NEO monitors available* www.neomonitors.biz/solutions/products/dust-in-situ/laserdust/. Accessed [2013 May 3].
28. Ghilani, C.D., *Adjustment Computations - Spatial Data Analysis*. 5th ed. John Wiley & Sons: 2010.
29. Buhle, S.X., Process Metallurgy and Electrolysis (course TMT 5500). Norwegian University of Science and Technology: Trondheim, Norway. Student report, 2010.
30. Chou, S., C. Harper, L. Ingerman, F. Llados, J. Colman, L. Chappell, M. Osier, M. Odin, and G. Sage. Agency for Toxic Substances and Disease Registry: Atlanta, GA. Public Health Service Report, 2007.
31. Smith, C., L. Ingerman, and R. Amata. Agency for Toxic Substances and Disease Registry: Atlanta, Georgia, U.S.A. Public Health Service Report, 2002.

Appendix

Table 3 Maximum and minimum mass of each element in the fume per year and per tonne silicon produced, and the concentration range of elements in the fume. The amounts with a "less than" sign (<) have a calculated combined error larger than 100 %.

Element	Mass / year (kg)	Mass / tonne Si (g)	Concentration in fume (ppmw)
Ag	1.2-65	0.016-0.86	1-500
Al	747-4827	10-64	1000-10^4
As	0.23-1.7	0.0031-0.022	0.1-5
Au	$6.4\cdot10^{-4}$-0.0059	$8.6\cdot10^{-6}$-$7.9\cdot10^{-5}$	0.001-0.01
B	7.9-30	0.11-0.39	10-50
Ba	<76	<1.0	<500
Be	0.027-1.1	$3.6\cdot10^{-4}$-0.014	0.01-5
Bi	0.0054-0.24	$7.2\cdot10^{-5}$-0.0033	0.01-0.5
Ca	499-2598	6.7-35	500-5000
Cd	<23	<0.31	<50
Ce	<12	<0.16	<50
Co	<3.2	<0.042	<10
Cr	3.8-24	0.050-0.32	5-50
Cs	†	†	†
Cu*	93-539	1.2-7.2	100-1000
Dy	<0.71	<0.0094	<5
Er	<0.70	<0.0094	<5
Fe	$<4.3\cdot10^4$	<571	$<10^5$
Ga	0.29-1.3	0.0039-0.017	0.1-5
Ge	0.18-0.81	0.0024-0.011	0.1-5
Hf	<2.1	<0.028	<5
Hg	†	†	†
Ho	<0.24	<0.0031	<0.5
In	0.0012-0.0059	$1.6\cdot10^{-5}$-$7.9\cdot10^{-5}$	0.001-0.01
Ir	†	†	†
K	570-2302	7.6-31	500-5000
La	<5.7	<0.077	<10
Li	4.0-15	0.054-0.20	5-50
Lu	<0.094	<0.0013	<0.5
Mg	185-832	2.5-11	100-5000
Mn	2.5-134	0.033-1.8	1-500
Mo	0.12-1.6	0.0016-0.021	0.1-5
Na	133-460	1.8-6.1	100-1000
Nb	<1.7	<0.023	<5
Nd	<6.0	<0.081	<10
Ni	1.8-15	0.024-0.20	1-50
P	<475	<6.3	<1000
Pb	0.59-12	0.0078-0.16	0.5-50
Pr	<1.4	<0.019	<5
Pt	†	†	†
Rb	2.1-8.8	0.027-0.12	1-50
S	†	†	†
Sb	<6.5	<0.086	<50
Sc	<1.2	<0.015	<5
Se	0.057-2.2	$7.6\cdot10^{-4}$-0.029	0.01-5
Sm	<1.1	<0.015	<5
Sn	<1.9	<0.025	<5
Sr	6.2-62	0.082-0.83	5-100
Ta	<0.19	<0.0026	<0.5
Tb	<0.20	<0.0027	<0.5
Th	<1.4	<0.019	<5
Ti	<401	<5.3	<1000

Tl	<0.30	<0.0040	<0.5
Tm	<0.091	<0.0012	<0.5
U	<0.90	<0.012	<5
V	<11	<0.15	<50
W	<0.8	<0.011	<5
Y	<5.9	<0.079	<10
Yb	0.038-0.59	$5.1 \cdot 10^{-4}$-0.0079	0.05-1
Zn	31-171	0.42-2.3	10-500
Zr	<78	<1.0	<500

* Estimated value due to Cu contamination from the «cold finger».

† No value due to concentration below IDL or too high RSD.

PAPER 6

Is not included due to copyright